

THE REMOVAL OF ARSENIC AND ANTIMONY
FROM COMPLEX LEAD BULLION
VIA VACUUM DISTILLATION

by

Evody Tshijik Karumb

Copyright by Evody Tshijik Karumb 2019

All Rights Reserved

A thesis submitted to the Faculty and the Board of Trustees of the Colorado School of Mines in the partial fulfilment of the requirements for the degree of Doctor of Philosophy in (Metallurgical & Materials Engineering).

Golden, Colorado

Date _____

Signed: _____
Evody Tshijik Karumb

Signed: _____
Dr. Patrick R. Taylor
Thesis Advisor

Golden Colorado,

Date _____

Signed: _____
Dr. Angus Rockett
Professor and Department Head
Department of Metallurgical and
Materials Engineering

ABSTRACT

Vacuum distillation is based on the selective evaporation of volatile impurities from liquid melts and has been extensively studied. It is known to provide better operation conditions and a better control of product composition. In order to understand the thermodynamics of vacuum distillation, it is essential to know the activity coefficient of the impurity in the melt. In this research, three thermodynamic models were used to calculate the activity coefficient. The models are the molecular interaction volume model (MIVM), the Wilson equation, and the non-random two liquids (NRTL) model. The research focused on the determination of binary parameters for the Pb-As and the Pb-Sb binary systems and the prediction of vapor-liquid (VLE) necessary to understand the removal of arsenic and antimony from their binary lead alloys under reduced pressure. Vacuum distillation experiments were conducted on Pb-As and Pb-Sb alloys by varying distillation pressure, temperature, time, and the alloy composition.

It was discovered that the removal of arsenic increased with a decrease in distillation pressure, and an increase in distillation time and temperature. The removal was a strong function of temperature; at 5 Pa, 650 °C and 45 min, 79.2wt. % removal extent was achieved, and arsenic content decreased from 2.46 wt. % to 0.53 wt. %. It was discovered that antimony removal also increased with a decrease in distillation pressure, and an increase in distillation time, and temperature. At 5 Pa, 700°C, and 90 minutes, 38.6 % antimony was removed, and its content was decreased from 3.5 wt.% to 2.2 wt. %. It is noted however, that antimony removal required higher temperatures processing time for its removal compared to arsenic. The research main's contribution to vacuum distillation is the VLE prediction for the removal of arsenic.

TABLE OF CONTENTS

ABSTRACT	iii
LIST OF FIGURES	vii
LIST OF TABLES	xi
ACKNOWLEDGMENT	xiii
CHAPTER ONE	INTRODUCTION	1
1.1	Background Information	1
1.2	Justification for research	2
CHAPTER TWO	LITERATURE SURVEY	4
2.1	Primary and Secondary Production of Lead	5
2.2	Lead Refining	7
2.2.1	Thermal Processes	8
2.2.2	Electrolytic Refining	14
2.3	Applications of Lead Metal and Compounds	16
2.4	Lead Recycling	20
CHAPTER THREE	THERMODYNAMIC MODELS FOR THE CALCULATION	22
	OF THE ACTIVITY COEFFICIENT	22
3.1	Thermodynamics of Vacuum Distillation	22
3.2	Thermodynamic Models for Prediction of the Activity Coefficient	31
3.2.1	The Molecular Interaction Volume Model (MIVM)	31
3.2.2	The Wilson Equation	34
3.2.3	The Non-Random Two Liquid Model (NRTL)	37
3.3	Calculated Binary Parameters for the Pb-As, Pb-Sb, and As-Sb Binary Systems	39

CHAPTER FOUR	PROCESS DEVELOPMENT AND EXPERIMENTATION	44
4.1	Vacuum Distillation Reactor Design and Setup	44
4.1.1	Design Considerations	44
4.1.2	SolidWorks Design Considerations	46
4.1.3	Experimental Setup Assembly	50
4.2	Alloy Preparation and Casting	55
4.2.1	Alloy Preparation	57
4.2.2	Alloy Casting	59
4.3	Chemical Analysis	61
4.3.1	Sample Preparation and dilution	61
4.3.2	Arc Spark Optical Spectroscopy (Arc Spark OES)	63
4.3.3	Flame Atomic Absorption Spectroscopy (FAAS)	66
4.3.4	Inductively Coupled Plasma Mass Spectrometry (ICP-MS)	67
CHAPTER FIVE	VAPOR LIQUID EQUILIBRIUM PREDICITONS	68
5.1	The Pb- As Binary system	68
5.1.1	VLE Temperature - Composition Diagram	68
5.1.2	VLE Composition Diagram for Arsenic	73
5.2	The Pb-Sb Binary System	75
5.2.1	VLE Temperature – Composition Diagram	75
5.2.2	VLE Composition Diagram for Antimony	79
CHAPTER SIX	RESULTS AND DISCUSSION	80
6.1	The Pb-As Binary System	80
6.1.1	Lead-Arsenic Binary Alloys	80
6.1.2	Effect of Time	88
6.1.3	Effect of Pressure	94

	6.1.4	Effect of Temperature	98
	6.1.5	Effect of Initial Arsenic Content in the Feed	103
	6.1.6	Considerations for the Adjustment of the Binary Parameters for the Pb-As System	106
6.2		The Pb-Sb Binary System.....	107
	6.2.1	Lead-Antimony Binary Alloys	107
	6.2.2	Effect of Time	109
	6.2.3	Effect of Pressure	116
	6.2.4	Effect of Temperature	121
	6.2.5	Effect of Initial Arsenic Content in the Feed	127
CHAPTER SEVEN		CONCLUSIONS	134
CHAPTER EIGHT		RECOMMENDATIONS AND FUTURE WORK	136
	8.1	Effect of Melt Agitation.....	136
	8.2	Multicomponent Systems VLE.....	137
	8.3	Kinetics Vacuum Distillation.....	145
REFERENCES		148
APPENDIX A		SAMPLE BOAT VOLUME CALCULATIONS	151
APPENDIX B		SUPPLEMENTAL INFORMATION ON THE RESULTS FOR THE PB-AS AND PB-SB BINARY SYSTEMS	152

LIST OF FIGURES

Figure 2.1	Schematic of a typical lead ore beneficiation process	6
Figure 2.2	Generalized thermal refining process for lead (Sinclair, 2010)	9
Figure 2.3	Typical electrolytic process for refining lead (Sinclair, 2010).....	15
Figure 2.4	Lead end use recorded from 1975 to 2005 in the United States (Kelly et al., 2005)	16
Figure 2.5	Illustration of the construction of an automotive lead-acid battery (Sinclair, 2010)	18
Figure 2.6	Specifications of soft lead for use in VRLA batteries (Rice and Manders, 1997)	20
Figure 3.1	Saturation vapor pressure of pure metals	30
Figure 4.1	Schematic of the designed vacuum distillation reactor.	47
Figure 4.2	Section view of the condensation unit.....	48
Figure 4.3	Illustration of the sample boat (a) and the casting mold (b).....	49
Figure 4.4	Illustration of the assembled vacuum distillation reactor.....	51
Figure 4.5	Alloy preparation and casting setup.	56
Figure 4.6	Sandwich configuration of the batch alloy	58
Figure 4.7	Remodeling of the lead melting pot for the casting process	60
Figure 4.8	Schematic of a hybrid optics arc/spark OES (Spectrolab, 2016)	63
Figure 5.1	T-x-y diagram for the Pb-As system using MIVM between 5 and 20 Pa	70
Figure 5.2	T-x-y diagram for the Pb-As system using Wilson equation between 5 and 20 Pa.....	71
Figure 5.3	T-x-y diagram for the Pb-As system using the NRTL model between 5 and 20 Pa.....	72

Figure 5.4	VLE composition for the Pb-As binary system at 5 Pa in the temperature range of 340 and 440 °C	74
Figure 5.5	T-x-y diagram for the Pb-Sb system using MIVM between 5 and 20 Pa	76
Figure 5.6	T-x-y diagram for the Pb-Sb system using Wilson equation between 5 and 20 Pa.....	77
Figure 5.7	T-x-y diagram for the Pb-Sb system using NRTL model between 5 and 20 Pa ...	78
Figure 6.1	First alloy preparation trial; a) melting pot setup, b) trial 1 product	81
Figure 6.2	Effect of distillation time on the arsenic content in the distillate fraction; experiments conducted at 5 Pa and 550 °C.....	90
Figure 6.3	Effect of distillation time on the arsenic removal extent; experiments conducted at 5 Pa, and 550 °C.	91
Figure 6.5	Effect of distillation time on the content of lead in the feed samples as well as the product sample; experiments conducted at 5 Pa and 550 °C	93
Figure 6.6	Effect of distillation pressure on arsenic content in the distillate fraction; experiments conducted at 550°C and 45 minutes	95
Figure 6.7	Effect of distillation pressure on arsenic removal extent; experiments conducted at 550°C and 45 minutes	96
Figure 6.8	Effect of distillation pressure on the arsenic content in both the feed and product samples; experiments conducted at 550°C and 45 minutes.....	97
Figure 6.9	Effect of distillation pressure on the lead content in both the feed and product samples; experiments conducted at 550°C and 45 minutes	98
Figure 6.10	Effect of distillation temperature on arsenic content in distillate; experiments conducted at 5 Pa and 45 minutes.....	99
Figure 6.11	Effect of distillation temperature on arsenic removal extent; experiments conducted at 5 Pa and 45 minutes.....	100
Figure 6.12	Effect of distillation temperature on arsenic content in both the feed and the product samples; experiments conducted at 5 Pa and for 45 minutes	101
Figure 6.13	Effect of distillation temperature on lead content in both the feed and the product samples; experiments conducted at 5 Pa and for 45 minutes	102

Figure 6.14	Effect of initial arsenic content on the arsenic content in both the feed and the product samples; experiments conducted at 5 Pa, 550 °C, and for 45 minutes ..	104
Figure 6.15	Effect of initial arsenic content on the lead content in both the feed and the product samples; experiments conducted at 5 Pa, 550 °C, and for 45 minutes ..	105
Figure 6.16	Effect of distillation time on the antimony content in the distillate fraction, experiments conducted at 5 Pa and 550°C.....	112
Figure 6.17	Effect of distillation time on the removal extent of antimony, experiments conducted at 5Pa and 700°C	113
Figure 6.18	Effect of distillation time on the antimony content in both the feed and product samples, experiments conducted at 5 Pa and 700°C	114
Figure 6.19	Effect of distillation time on lead content in both the feed and the product sample, experiments conducted at 5 Pa and 700°C	115
Figure 6.20	Effect of distillation pressure on antimony content in the distillate fraction, experiments conducted at 700° for 30 minutes.....	117
Figure 6.21	Effect of distillation pressure on antimony removal extent, experiments conducted at 700°C for 30 minutes.....	118
Figure 6.22	Effect of distillation pressure on antimony content in both the feed and product fraction, experiments conducted at 700°C for 45 minutes	119
Figure 6.23	Effect of distillation pressure on lead content in both the feed and the product fractions, experiments conducted at 700°C for 45 minutes	120
Figure 6.24	Effect of distillation temperature on antimony content in the distillate fraction, experiments conducted at 5 Pa for 30 minutes	123
Figure 6.25	Effect of distillation temperature on the removal extent of antimony, experiments conducted at 5 Pa for 30 minutes	124
Figure 6.26	Effect of distillation temperature on antimony content in both the feed and product samples, experiments conducted at 5 Pa for 30 minutes	125
Figure 6.27	Effect of distillation temperature on lead content in both the feed and product samples, experiments conducted at 5 Pa for 30 minutes	126
Figure 6.28	Effect of initial antimony content in the feed sample on antimony content in the distillate fraction, experiments conducted at 5 Pa, 700°, and for 45 minutes	129

Figure 6.29	Effect of initial antimony concentration in the feed sample on antimony removal extent, experiments conducted at 5 Pa, 700°C and for 45 minutes.	130
Figure 6.30	Effect of initial antimony initial concentration on antimony content in both the feed and product sample, experiments conducted at 5 Pa, 700°C, and for 45 minutes.....	131
Figure 6.31	Effect of initial antimony initial concentration on lead content in both the feed and product sample, experiments conducted at 5 Pa, 700°C, and for 45 minutes.....	132
Figure B.1	Effect of distillation time on lead content in the distillate fraction, experiments conducted at 5 Pa and 550 °C.....	152
Figure B.2	Effect of distillation pressure on lead content in the distillate fraction experiments conducted at 550°C and for 45 minutes.....	153
Figure B.3	Effect of distillate temperature on lead content in the distillate fraction; experiments conducted at 5 Pa and for 45 minutes.....	154
Figure B.4	Effect of initial arsenic content in the feed samples on the lead content in the distillate fraction, experiments conducted at 5 Pa, 550°C, and 45 minutes.....	155
Figure B.5	Effect of distillation time on lead content in the distillation fraction, experiments conducted at 5 Pa and 700 °C.....	156
Figure B.6	Effect of distillation pressure on lead content in the distillate fraction, experiments conducted at 700°C for 30 minutes.....	157
Figure B.7	Effect of distillation temperature on lead content in the distillate fraction, experiments conducted at 5 Pa for 30 minutes.....	158
Figure B.8	Effect of initial antimony concentration in the feed sample on lead content in the distillate fraction, experiments conducted at 5 Pa, 700°C, and for 45 minutes.....	159

LIST OF TABLES

Table 2.1	Composition of a typical lead bullion.....	8
Table 3.1	History of research on vacuum distillation of metals presented by Westerheide.....	23
Table 3.2	Vapor pressure coefficients for the calculation of saturated vapor pressure of pure metals (Kubachewski, 1979).....	29
Table 3.3	Illustration of binary parameters from the proposed activity coefficient models	39
Table 3.4	Thermochemistry data for lead, arsenic and antimony	40
Table 3.5	Coordination numbers for the Pb-As, Pb-Sb, and As-Sb systems.....	41
Table 3.6	Calculated binary parameters for Pb-As, Pb-Sb, and As-Sb binary systems	42
Table 4.2	Pure metals used for the preparation of synthetic alloy samples	58
Table 5.1	Boiling point of lead and arsenic as a function of pressure	69
Table 6.2	Chemical composition of Pb-As alloys batch 1 by CSM	83
Table 6.3	Chemical composition of Pb-As alloys batch 1 by Sponsor.....	85
Table 6.4	Pb-As alloy preparation weights from trial 2 to trial 4	86
Table 6.4	Comparison between analysis from CSM and sponsor	86
Table 6.5	Chemical analysis of Pb-As alloys batch 2.....	87
Table 6.6	Chemical analysis of Pb-As alloys batch 3.....	87
Table 6.7	Experimental matrix for the Pb-As binary system.....	88
Table 6.8	Effect of distillation time on the removal of arsenic	89
Table 6.9	Effect of distillation pressure on the removal of arsenic	94
Table 6.10	Effect of distillation temperature on the removal of arsenic	99
Table 6.11	Effect of arsenic initial composition on the removal of arsenic	103

Table 6.12	Chemical analysis of batch 1 of Pb-Sb feed samples	108
Table 6.13	Chemical analysis of batch 2 of Pb-Sb samples	108
Table 6.14	Experimental matrix for Pb-Sb binary system.....	109
Table 6.15	Effect of distillation time on the removal of antimony.....	110
Table 6.16.	Equilibrium partial pressures for distillation at 700 °C	110
Table 6.17	Effect of distillation pressure on the removal of antimony	116
Table 6.18	Effect of distillation temperature on the removal of antimony.....	122
Table 6.19	Effect of initial antimony content on the removal of antimony.....	127
Table 8.1	MIVM Binary parameters for lead and seven of its most common impurities. .	138
Table 8.2	MIVM coordination numbers at experimental activity temperatures.....	140
Table 8.3	Wilson Equation Binary parameters for lead and seven of its common impurities	141
Table 8.4	NRTL Binary parameters for lead and seven of its common impurities	143
Table A.1	Calculations for the vacuum distillation sample boat.....	151

ACKNOWLEDGMENT

I would like to extend my humble gratitude to Dr. Patrick R. Taylor, my advisor and mentor for steadfastly guiding me while I carried on with this work; his support, advices, reprimands, and guidance have sharpen my focus even more so then when I concluded my Master's thesis work. I would like to extend my gratitude to the other members of my committee, namely Dr. Corby G. Anderson, Dr. Roderick Eggert, Dr. Emmanuel De Moor, and Dr. Sridhar Seetharaman whose concrete support and constructive criticism has help shape the work that is hereby presented.

My special gratitude goes to the Center for Resource Recovery and Recycling (CR³) for funding this project, and my focus group members for their guidance and feedback. I would like to also thank the Kroll Institute of Extractive Metallurgy (KIEM) for having provided extra funding which has helped me achieved more toward the thesis.

I would not have completed this work so fashionably without the support, encouragement, and help from my fellow "Krollers". I am ever so grateful that you guys have been there for me when I needed you.

Emotional drainage has been my constant companion, especially towards the finish line. I would like to thank my family and friends who have supported me with advices and encouragement during that time. I hold you dear to my heart.

Above all else, I am forever grateful to the almighty GOD in heaven saw me through the entire PhD life, and has shown me the way while strengthening me when I needed it.

To my parents Dieudonne Nduwa Mudikita and Marie Tshikas Karaj

CHAPTER ONE

INTRODUCTION

Chapter one presents an overview of lead metal, its origin, properties, occurrence and abundance in the earth, and historical fact; it also mentions the scope of the present research as well as a justification for its undertaking.

1.1 Background Information

Lead is the 14th element in the transition metals class. It is a soft and malleable metal that has a low melting point and high boiling point, which explains its application in the solder industry. Lead has a high density, reason why it is used as a shielding material in nuclear applications; its electrochemical properties afford its use in storage batteries. It is also recognized to exhibit a good corrosion resistance hence its use in applications of exposed environments (Thorton et al., 2001) Lead has been known to man and used by men since the early ages, with a high use by the romans to make pipes for their water channels (Grant, 2003). The aristocracy has also used it as a cosmetic powder in the 18th century (Sims, 2015).

Lead's abundance in the earth crust is estimated at 14 ppm (Knowledge Door, 2019), and its most important mined mineral is galena (PbS), followed by anglesite (PbSO₄), and cerusite (PbSO₃) (Thornton, Rautiu and Brush, 2001; Grant, 2003; Sinclair, 2010). Galena is mostly associated with sphalerite (ZnS), a zinc sulfide from which it is separated by beneficiation means such as flotation; other associations include pyrite (FeS) and chalcopyrite (CuFeS₂). Owing to their similarity in chemical behaviors with lead and zinc, impurities such as silver (Ag), indium

(In), tellurium (Te), cadmium (Cd), arsenic (As), tin (Sn), bismuth (Bi), antimony (Sb), gallium (Ga), Germanium (Ge), gold (Au), and mercury (Hg) are often present in concentrates of lead and zinc. The presence of precious metal such as silver has a positive effect on the price of lead concentrate because it allows offsetting the operating cost of smelting operations. Bismuth however presents a cost penalty because of the difficulty of its removal during the refining of lead bullion (Sinclair, 2010). Lead's path from mineral to metal will be discussed in chapter two; however, the author feels that this is a good place to bring to the reader's attention that the present thesis will be concerned with the removal of some of the impurities reporting to the hard lead bullion during smelting. The term "hard" emanates from the fact that the presence of impurities renders an extra hardness to lead that is otherwise very soft in pure form.

1.2 Justification for research

In the US, lead production comes primarily from secondary production; per the USGS commodities summary of 2019, an estimated 1.3 million tons of lead was produced from recycling in 2018, and nearly all of it from secondary production (mostly from lead/acid batteries). A reported 85% of lead consumption that year came from lead produced by processing of lead/acid batteries. Lead secondary production does not require beneficiation such as flotation and roasting as would primary production; however, alloying elements found in the recycled batteries need to be removed by refining processes. It is clear to see that secondary refining processes are important to the US when talking about lead production.

An extensive amount of research has been conducted on the refining of lead bullion, namely, to improve the energy consumption in electrorefining, to understand the thermodynamics and kinetics of lead softening, to optimize softening reagents usage. Recently,

there has been an ever-increasing interest in investigating other methods of refining lead bullion; one that resurfaces a lot is vacuum distillation. Most of the vacuum distillation work related to lead bullion has been conducted at the National Engineering Laboratory for Vacuum Metallurgy at the Kunming University of Science and Technology in China. Suffice it to say that the laboratory's list of research is quite extensive including predictions of vapor-liquid equilibrium in binary and multi-component systems of Pb-X where X is Sb, Sn, Cu, Ag, Bi, Ag, etc. that are usually found in lead bullion. One of the scientists at this laboratory also developed a model for the calculation of the activity coefficients in binary and multi-component systems, which chapter three will detail. One area that is yet to be studied by this lab or other laboratories, to the author's knowledge, is the predictions of the Pb-As system.

The focus of the present research will be answering the following two questions: 1) Can we predict the vapor-liquid equilibrium of the Pb-As system accurately? 2) Can we remove arsenic from lead bullion; if yes, what parameters might affect the process? The success of the present research is dependent on the answers to these questions. To assess the success of the study, the research team also looked at the Pb-Sb binary system, which is well documented in literature (see chapter three for more details).

CHAPTER TWO

LITERATURE SURVEY

Chapter 2 will be the focus of the lead industry. Section 2.1 will give an overview of the production of lead, whether primary or secondary. Section 2.2 will present a detailed survey of lead refining by thermal process (softening), and electrolytic (electrorefining) process. Section 2.3 will talk about the numerous applications of lead as a metal and/ or alloys Section 2.4 will present information about lead recycling, and its place in the US lead industry. As mentioned in section 1.2, the majority of literature survey about vacuum distillation of lead is tied to the use of thermodynamic models. Because it is an important part of the thesis, it was in the author's view to dedicate a chapter to this portion of the literature review.

Aside from information gathered from the United States Geological Survey (USGS), there are five other publications which the author deemed adequate as literature survey source. The publications are Sinclair's book titled "*The extractive Metallurgy of Lead*" (Sinclair, 2010), Thornton and coworkers book titled "*Lead: the Facts*" (Thornton, Rautiu and Brush, 2001), Grant's publication titled "Lead production" which is part of a book titled "*Encyclopedia of Materials: Science and Technology*" (Grant, 2003), Hayes and coworkers' publication titled "lead Smelter Surveys" present at the "*Lead-Zinc 2010 Symposium, Held in Conjunction with COM 2010*" in Vancouver, Canada (Hayes et al., 2010), and the Department of Energy's publication titled "*Mining industry of the Future: Energy and Environmental Profile of the US. Mining Industry*"(US-DOE, 2002). Unless otherwise stated, information presented in this chapter

was extracted from these publications; it is in the author's opinion though that Sinclair provided a more extensive review of lead production, both primary and secondary.

2.1 Primary and Secondary Production of Lead

Primary production of lead includes the processing of zinc lead ores. According to Thornton et al., China, Australia, USA, Canada and Mexico are the lead in the production of mined lead ores was there quarters of world production in 2001. To achieve the smelter's required concentrations of zinc and lead, the mined ores have to undergo some sort of beneficiation process (pre-concentration). Across the literature review, lead and zinc ores beneficiation processes include the typical steps shown in figure 2.1. The mined ore undergoes primary crushing at the mine site, then it is subjected to secondary crushing and grinding. The ground ore is sent to selective flotation where galena is first floated while sphalerite is depressed. Afterward, sphalerite is activated and floated. Grant reported that the particle size of the ore going to flotation was between 7 and 10 μm (Grant, 2003). Sinclair reported however that one of the issues of processing lead ores was the formation of slimes; therefore, the particle size of the crushed ore is controlled closely. Between Sinclair and Grant, Lead-zinc ores produced have a lead concentration in the range of 50 to 78 wt. %. According to the USGS, the production of recoverable lead from mine production in the US was 360,000 metric tons (Guberman, 2017), and according to its 2019 mineral industry survey, of lead for the month of July, 21900 tons of recoverable mined lead was produced in July 2019 which was reported to be 8 % less than the production last year.

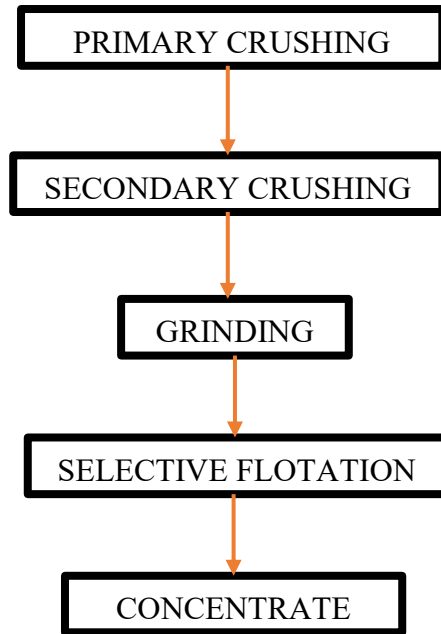


Figure 2.1 Schematic of a typical lead ore beneficiation process

Primary and secondary production of lead is mostly carried using a pyrometallurgical route. When processing lead concentrates from mine ores, the first step is the smelting process through which lead bullion is produced. In the first step of the process, the fine particles of lead concentrate go through the sintering process to make large lumps of ore particles. The goal of the sintering process is to produce particles that are cohesive and strong enough to be used in the blast furnace. The dust generated from the process are mixed with fluxes and returned as feed material. The sulfur dioxide produced can be used to produce sulphuric acid. The second stage is roasting where lead oxide is produced using coke as both a reducing agent and heat source. Limestone is commonly used as a flux with coke; other fluxes such as silica and iron oxide are also used. Molten lead and the slag collect in the hearth region and lead bullion is tapped from the bottom. Lead blast furnace slags are of the type $\text{CaO}:\text{FeO}:\text{SiO}_2$, sometime with addition of ZnO , Al_2O_3 , Fe_2O_3 , and MgO . Sinclair suggests that reasonable and practical melting temperature ranges are achieved with 30 to 40 wt. % SiO_2 , 35 to 45 wt. % FeO , and 20 to 30 wt. % CaO .

An alternative to the sintering-blast furnace production of lead bullion is the Imperial Smelting Furnace (ISF). ISF allows for lead and zinc simultaneous production; lead is tapped while zinc is removed via distillation. Other direct smelting processes known to be used in the processing of lead concentrates include the Swedish Kaldo furnace a.k.a. top-blown rotary converter (TBRC) which operates in batch mode, the Queneau-Schuhmann-Lurgi (QSL) process which takes place in a cylindrical kiln shaped vessel, Isasmelt and Ausmelt which are a version of the Siromelt process and use vertical submerged lance in a cylindrical smelting vessel. Environmental issues associated with two-stage processes includes the production of fumes which requires extensive gas cleaning equipment, and the energy consumption associated with its operation. Lead bullion is a good solvent for impurities such as silver, antimony, sulfur, copper, etc. depending of the feed material; high levels of impurities result in a molten lead usually referred to as “hard,” or “crude” lead.

2.2 Lead Refining

A typical lead bullion contains impurities such as As, Ag, Cu, Zn, Fe, Bi, Sb, and Sn as shown in table 2.1. The concentration of these impurities is dependent on the feed material that was processed in the blast furnace; lead refining processes usually takes place in kettles. Refining is undertaken either via thermal processes after smelting (softening) or electrolytic processes both of which are discussed sections 2.2.1 and 2.2.2.

Table 2.1 Composition of a typical lead bullion

Element	Concentration (wt. %) Ref.1	Concentration (wt. %) Ref.2
Ag	0.05-0.5	0.13-0.31
Au (g/ton)	0 - 3	1.6-3.1
As	0.3 – 2.0	0.7-1.1
Bi	0.01 – 0.03	0.01-0.03
Cu	1.0 – 4.0	1.0-2.5
Fe	0.6 – 0.8	0.6-0.8
S	0.2 – 0.4	0.25
Sb	1.0 – 1.75	1.0-1.75
Sn	0 – 1.0	Tr.
Zn	0 – 0.5	Tr.
Pb	Balance	Balance

Ref:1 (Grant, 2003), Ref.2: EPA 1980

2.2.1 Thermal Processes

Figure 2.2 shows a typical thermal refining process for hot lead bullion. The reader is advised to keep in mind that the process may involve additional stages, or omit others depending on the presence of impurities and their respective levels in the bullion. As shown in the figure, lead bullion from the smelting processes undergoes a series of processes to remove the impurities present. Typical impurities found in hard lead are: Cu, As, Zn, Sb, Ag, Bi, Sn, and S. The sequence in the refining process will usually involve the removal of Cu, and S by drossing (formation of a matte), the removal of As, Sb, and Sn by preferential oxidation (the softening or the Harris process process), the removal of Ag by addition of zinc, the removal the Zn enriched bullion under vacuum, the removal of Bi (e.g. the Kroll Betterton process).

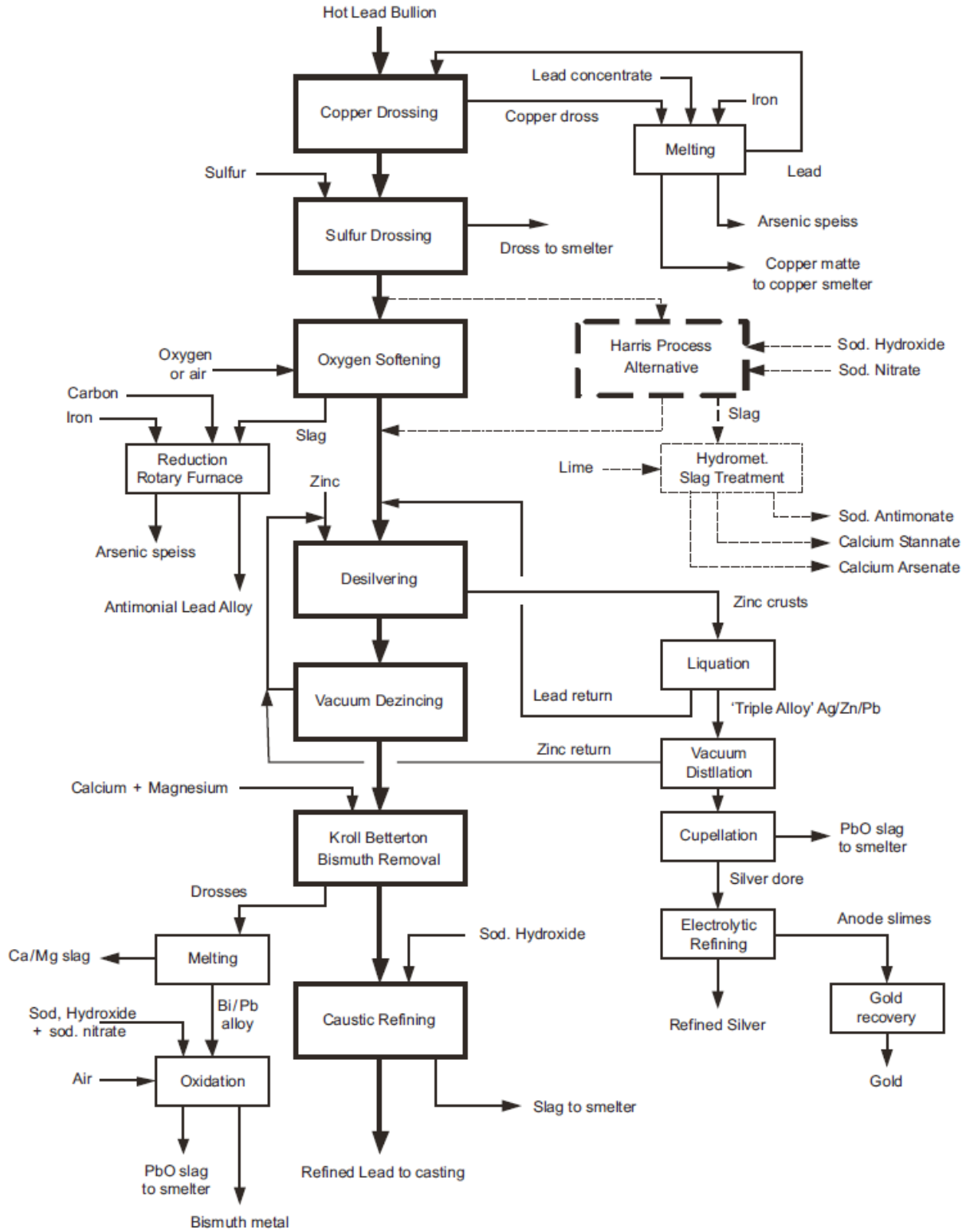


Figure 2.2 Generalized thermal refining process for lead (Sinclair, 2010)

Copper Removal

Depending on the composition of the ore, copper can be present in lead bullion in the range of 1-3 wt. %; the goal is to reduce its concentration below 0.01 wt. % so as to facilitate the desilverizing stage downstream. One way of achieving such a goal is to heat up the bullion just above melting temperature, then cooling it to reduce copper's solubility. From this stage, a mixture of PbS-Cu₂S and α -Cu matte is formed using the dissolved sulfur. As sulfur's content decreases, Cu₃As, Cu₃Sn, and Cu₂Sb can potentially precipitate as well. Sometimes sulfur is added to the bullion to aid the removal by decreasing copper content down to 0.005 wt. %; iron and pyrites can also be added to the bullion as the sulfur source, though the resulting matte's purity in copper will decrease due to iron.

Depending on the smelting process used to produce the bullion, the sulfur content will vary, thus varying the concentration of metallic copper in the dross. With low sulfur content in the dross, the formation of α -Cu result in considerable Pb entrainment; these drosses will require more extensive further processing to produce a salable copper matte. The treatment of the dross usually involves re-melting and addition of PbS to convert metallic copper to matte and forming lead metal. Addition of iron turnings binds the arsenic as a speiss. An alternative process is to treat the matte with sodium (Na) metal; Na will react with PbS resulting in Na₂S and Pb. At 650°C, sodium sulfide is a liquid matte with approximately 30 wt. % Cu which is a better candidate as a salable product for smelters.

Arsenic, Antimony, and Tin Removal

Compared to As, Sn, and Sb, Pb is nobler; therefore, these elements can be removed by preferential oxidation which is carried out either by the oxygen softening process or the Harris process. Oxygen or air, or a mixture of the two (the more enrichment, the better the process) is blown into the bullion at high enough temperatures, PbO is formed; by the nobility of Pb, cementation following thus forming oxides of Sb (antimonites), As (arsenates), and Sn (stannates). It has been found that with oxygen softening, the removal efficiency follows the As (98%)> Sb (90%)> Sn (extraction not mentioned) order. Depending on the degree of oxygen enrichment of the air blown in the furnace, the level of impurities in the bullion, and the selected temperature of treatment, the softening process will vary from 8 to 20 hours in batch mode. The end of the softening process is decided based on the level of Sb in the bullion (0.05 wt. % required). The slags formed during the softening process are generally treated in a rotary furnace by addition of coke or char from which a Sb-rich Pb alloy (typically 30 wt. %) is produced. The slag formed is enriched in arsenic; iron is added to form a speiss containing 30 wt. % arsenic.

The Harris process is the oxidation whereby molten sodium nitrate and sodium hydroxide as oxidants. From this sodium arsenates, antimonite, and stannate are produced and form a molten salt solution in excess sodium hydroxide. By the Harris process, the removal efficiency also follows the same rank as the oxygen softening process; the process being diffusion controlled, vigorous agitation is required for better mass transfer. Above 450°C, and with a residence time of 12 hours, Sb is reduced to 0.0005 wt. % which marks the end of the process.

Slags from the Harris process are treated via a hydrometallurgical route. Water is used to leach the excess NaOH and NaCl; when the initial concentration of excess NaOH is above 35 wt.

%, it was shown that As, Sb, and Sn are insoluble and recovered in the leach residue. However, tin and arsenic are slightly soluble below 35 wt. % NaOH while antimony is completely insoluble. Sodium stannate is hydrated and form $\text{Na}_2\text{SNO}_3 \cdot 3\text{H}_2\text{O}$. The excess NaOH-NaCl is evaporated to form their crystals, and they are recycled to the Harris process. Arsenic and tin are leached from the residue by a water leach leaving behind sodium antimonate.

Silver Removal

Silver was originally removed by cupellation whereby the bullion was completely oxidized to PbO leaving behind silver and gold if present. The PbO-rich slag would have had to be re-melted and refined to produce soft lead. This process was however only feasible for high silver content bullion. The Pattinson process took advantage of the eutectic formation of the silver and lead system at 305 °C and about 2 % silver. The bullion would be fed to a series of kettles and allowed to cool to that temperature such that lead crystals formed. At the end of the process, a soft lead was obtained on one end while the other end was a silver rich lead alloy. This alloy would then undergo a cupellation process.

More recently, silver is removed from lead bullion by adding zinc. Precious metals such as silver and gold would form high melting point intermetallics (e.g. AgZn_m) with zinc; this is the principle of the Parkes process. An additional advantaged of the Parkes process is that above 420°C, zinc and lead form two distinctive liquid phase until they form a single liquid around 798 °C; this ensures that the only solid phase to form are the intermetallics of silver and zinc. Using the Parkes process, the silver content is usually reduced to 0.0005 wt. %. The Ag-Zn alloy is heated under pressure to volatilize zinc which is recycled to the desilverising step. The resulting impure silver is further refined to make pure silver.

Zinc Removal

After the desilverizing process, the zinc content in the bullion is 0.5-0.7 wt. %. Vacuum distillation has widely been used to remove zinc from lead because of the large difference in their vapor pressures at low temperatures (see figure 3.1), and the increased mass transfer under low pressures. It has been shown that vacuum distillation removed more than 90 % of zinc reducing its content in the bullion down to 0.05 wt. %. Additional zinc removal can be achieved by two processes. First, zinc can be oxidized under air or enriched oxygen, and captured by sodium hydroxide. Second, chlorine can be injected in the melt to form a zinc chloride slag. The slag can be skimmed from the surface of lead. The second process poses a problem due to handling and storage of chlorine gas, thus it is not used on a large scale.

Bismuth Removal

Bismuth usually occurs at very low percentage in molten lead, although instances of high bismuth lead concentrate have been reported (e. g. ore found in Canada). According to Sinclair, bismuth levels in the range of 0.005-0.03 wt. % are acceptable in the lead battery business. No further processing of the bullion is required should bismuth content fall in that range. On the other hand, additions of calcium and magnesium has been shown to remove bismuth by the formation of Ca_3Bi_2 , Mg_3Bi_2 , and their ternary phase $3\text{CaMg}_2\text{Bi}_2$ which have high melting points. This treatment is known as the Kroll-Betterton process. Antimony is sometimes added to the process to achieve low residual content of bismuth in lead (0.005 wt. %).

The last stage in refining is oxidation with sodium hydroxide often with the addition of sodium nitrate. Through this process, residual zinc, antimony, calcium, magnesium, and bismuth

are removed from the bullion. This caustic refining process is usually applied in the range 450-580°C for about 6-12 hours of batch run.

2.2.2 Electrolytic Refining

An alternative process for the refining of lead is the Betts process which uses fluorosilicate electrolytes; figure 2.3 shows a typical electrolytic lead refining process. The size of the electrolytic cell normally depends on the size of the electrode and the anodes used. Anodes have the following typical dimensions: 1120 mm length, 1020 mm immersed depth, 780 mm width, 30 mm thickness, 1.59 m² immersed surface area, and 300 kg weight. When the process is initiated, the anode is dissolved and pure lead deposits at the cathode while the impurities collect at the bottom of the tank as slimes. Grant mentioned that the electrolyte of choice is hydrofluorosilic acid (H₂SiF₆) at 90-130 g/L. Lead is present at 70 -100 g/L, and the process is conducted at 40°C. Alternative electrolytes are sulfamic acid (HSO₃.NH₂) and fluoroboric acid (HBF₄); Sinclair also mentions the use of dithionic acid (H₂S₂O₆). According to Sinclair, there are underlying issues associated with the use of dithionic acid and sulfamic acid; the former decomposes to H₂SO₄ which will precipitate lead and SO₂ which will be reduced at the cathode as H₂S and precipitate PbS. The latter is unstable at high current densities and tends to break down to form ammonium sulfate which in turn will precipitate lead sulfate. As seen in figure 2.3, the Betts process does not completely replace the softening process, as the latter still needs to be performed until arsenic, antimony, and tin are removed. Advantages of using the electrolytic refining process include the effective removal of bismuth, higher purities of lead, and environmental safety of the operation compared to the softening process. Disadvantages includes the cost associated with it which is higher than the pyrometallurgical softening process, the

requirement of separate thermal processes, and the disposal of solutions which are rich in impurities.

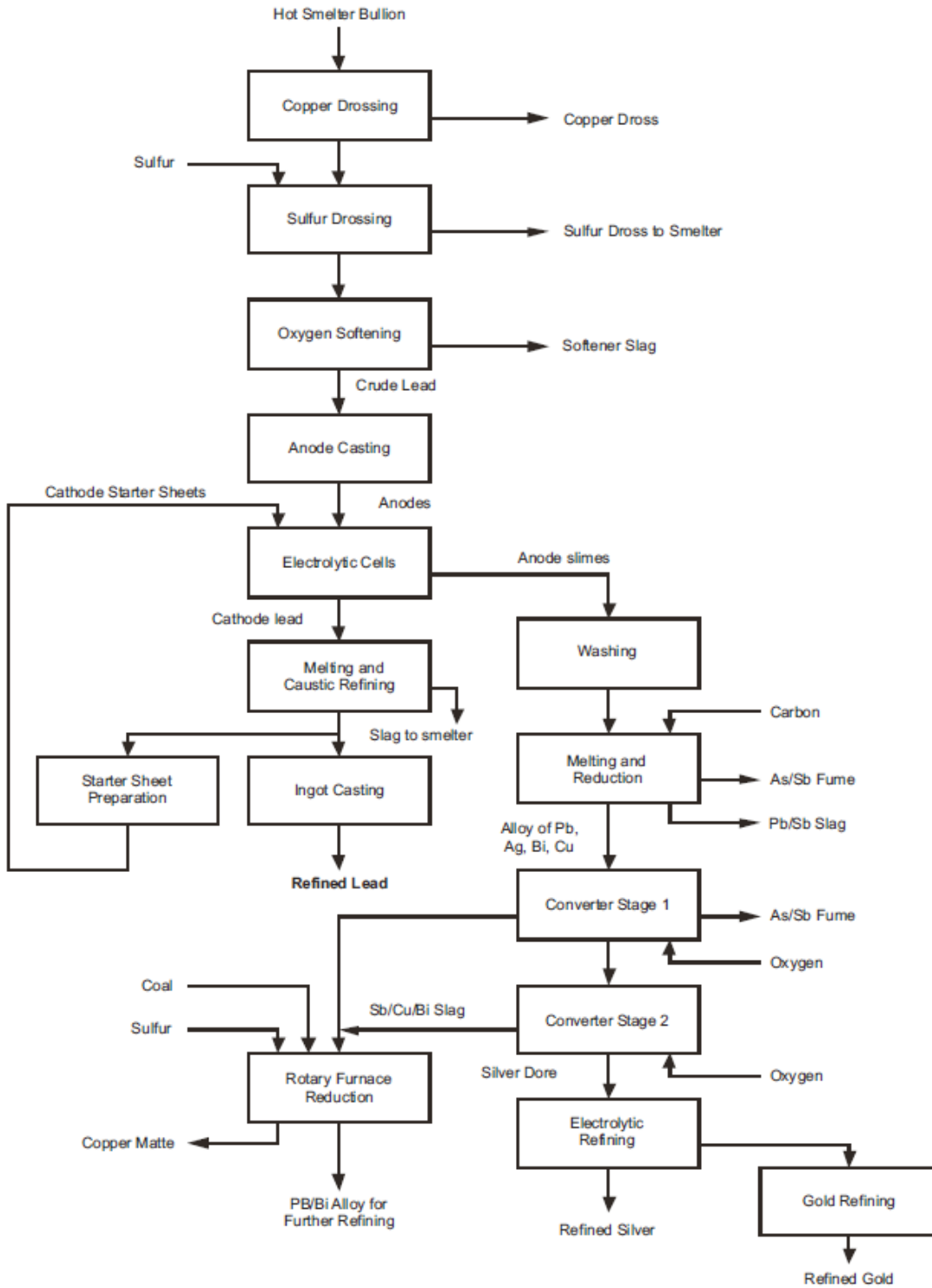


Figure 2.3 Typical electrolytic process for refining lead (Sinclair, 2010)

2.3 Applications of Lead Metal and Compounds

Lead application in society dates back to ancient Egyptian times. Lead has a wide range of applications spanning from piping to nuclear shielding, including solder alloys. Figure 2.4 shows lead's end uses from 1975 to 2005 (Kelly et al., 2005). As a sheet, lead is used primarily in the construction industry with higher demands in Europe. Due to its durability and malleability, lead sheet is used in roofing, and it represented 85 % of lead sheet demand. Lead sheet use in Europe is still prominent because of its durability and the fact that almost all of it comes from secondary production. A small fraction of lead sheet is used radiation shielding and noise attenuation. In the U.S., radiation shielding represented 27 % use of lead sheet in 2001 while it as 70 % use in japan.

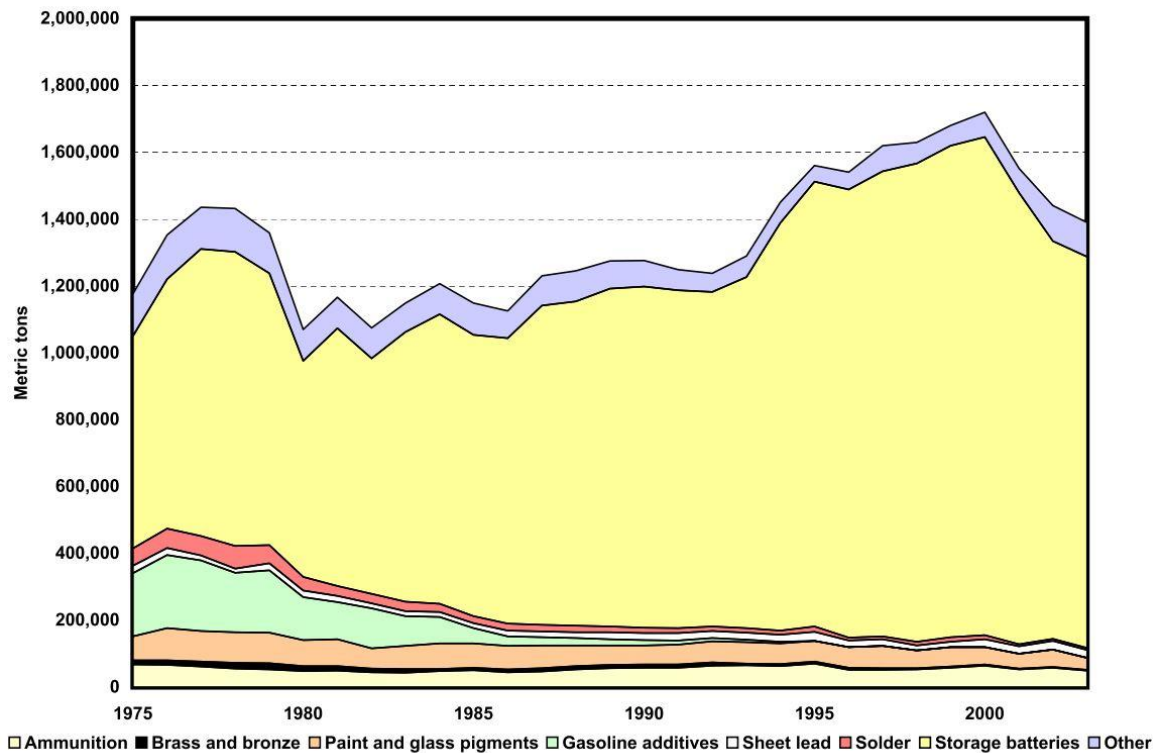
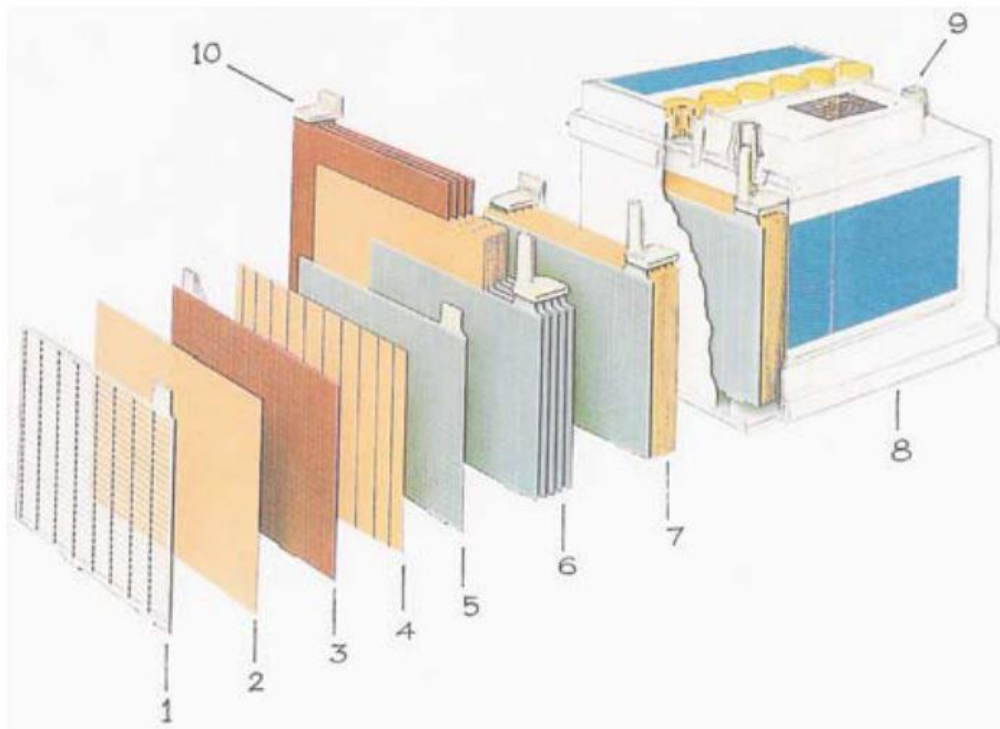


Figure 2.4 Lead end use recorded from 1975 to 2005 in the United States (Kelly et al., 2005)

Because of its corrosion resistance, lead was used in piping for water supplies; however, as knowledge of its toxicity grew, it was replaced by copper and PVC piping. It is still used in chemical industry especially in sulphuric acid plants. Lead is also used for sheathing of power cables; the alloying is designed for the specific application. Other applications of lead are shots and munitions. In Italy, 9 % of lead shot was used in alloying of steel. In the form of munitions, lead has the advantage of possessing a high destruction power, a long range, and a greater momentum due to its density. It also has the advantage of being cheap, easy to form, and causing minimal abrasion to the gun barrel.

High density and durability credit the use of lead as weights particularly in application that involve aqueous and marine environments. Weights are also used as wheel balance on motor cars, curtain weights, and yacht keels. Lead was also used as a gasoline additive; however, this application contributed to lead deportment in the environment, therefore its gradual decrease until the EPA issued a final rule prohibiting chemical additives in gasoline in 1996 (also reported by Sibley (Sibley, 2004)). Lead is also used in the form of lead oxide as an additive to glasses and glazes. The advantage here is the reduction in melting temperature, increase of refractive index which enhances its clarity, and suitability for optical glasses. Lead is also used as an alloying element in tin-lead solders; they are highly suitable for many applications because of their low melting point and flow characteristics, and they are also relative less expensive in comparison to their alternatives. Figure 2.4 showed the largest fraction of lead is used for storage batteries, and this trend is true also for lead consumption worldwide. Lead consumption in batteries has increased from 28 % in the 1960s to 74 % in 1999, and is projected to increase in the future.

Since batteries are lead's major consumer, it is important to understand how it is built and how lead is used therein; figure 2.5 shows the construction of a lead-acid battery. The battery consists of a grid made of lead alloy which is the negative terminal (spaces in the grid are filled with lead and lead oxide thus forming the positive terminal), an electrolyte for electrical conduction (sulphuric acid), separators made of insulating material, electrical connections (including the terminals), and a case which is normally made of heavy duty polypropylene box. The newly built battery is electrically charged, building up the lead oxide at the positive terminal.



- | | |
|--|---|
| 1. Lead alloy grid | 6. Negative electrode set for one cell |
| 2. Separator - porous insulating plate | 7. Full electrode and separator assembly for one cell |
| 3. Positive plate | 8. Battery case |
| 4. Separator | 9. Positive terminal |
| 5. Negative plate | 10. Positive electrode set for one cell |

Figure 2.5 Illustration of the construction of an automotive lead-acid battery (Sinclair, 2010)

Qualities of a good battery include durability, sustainability and ease of recycling. The grids used in the battery need to be corrosion resistant and possess a reasonably high strength; therefore, the use of soft lead was not suitable for that. Some alloying of lead is carried, and antimonial lead has been used for an extensive period of time. The antimony posed issues to the cell in the fact that over a period of time, it would corrode from the positive terminal during overcharging and collects in the electrolyte and is transported to the negative terminal where it is precipitated (Bagshaw, 1991). Consequently, the use of antimony in battery grids has gradually decreased over the years. Bagshaw also reported that while the decrease of antimony decreased antimony poisoning of the negative terminal, it also decreased the deep cycles that batteries could withstand.

Frost presented a paper in which he described the effect of alloying elements used on the grids on the battery performance (Frost, 1999). He mentioned that silver has the benefit of increasing the mechanical properties of lead especially at high temperatures and decreasing the rate of corrosion. Bismuth while reported to have negative effect on electrochemical properties, is reported here to have positive effect on the corrosion resistance in the 0.006 to 0.86 wt. % when added to a lead- 1.5 wt. % antimony alloys. It is reported that cadmium addition to low antimony alloys forms an intermetallic phase which in turn decreases the chances of antimony poisoning in the cell. When added in small amounts, arsenic is known to increase the strength of lead-antimony alloys by precipitation hardening, and to increase creep resistance. When tin is added to lead-calcium-tin alloys, it increases the stability, and corrosion resistance. Nickel is considered as extremely undesirable in any level in lead alloys for batteries. Some nickel contamination is still reported because nickel from nickel- tin batteries report to the lead battery recycling plant. Since it is rather challenging to remove nickel below 5 ppm, this becomes a

problem for the use of secondary lead in valve regulated lead-acid batteries; figure 2.6 show the specification of soft lead for use in VRLA batteries in as of 1997.

National soft-lead specifications as they currently stand (maximum ppm) ^a

Element	National standards			
	AS 1812-1975 9999	ASTM B29-92 Refined pure	BS 334-1982 Type A	DIN 1719-1986 Pb99,99
Ag	10	25	25	10
As	10	5	5	10
Bi	5	25	5	5
Cd	10	NS	5	NS
Co	^b	NS	NS	NS
Cu	10	10	30	10
Fe	10	10	30	10
Ni	^b	2	10	NS
S	10	NS	5	NS
Sb	10	5	20	10
Sn	10	5	10	10
Te	NS	1	NS	NS
Zn	10	5	20	10

^a NS = not specified.

^b Co + Ni < 10 ppm.

Figure 2.6 Specifications of soft lead for use in VRLA batteries (Rice and Manders, 1997)

2.4 Lead Recycling

USGS July commodity summary for lead revealed that 1.3 million tons of lead was produced from secondary production from lead scrap, and the majority of the scrap originated from recycling of lead-acid batteries (USGS, 2019). It is obvious then that recycling is important to the lead's US industry. Before diving into lead acid batteries recycling, this section will briefly mention recycling of other end uses of lead. Lead used as sheet and in piping are known to have a high recycling rate, and as a feed material they do not contain many of the impurities mentioned in previous sections. Thornton reported that their collection and reprocessing can be done in days. It is reported that lead from power cables can be recycled, but the recycling is not economical. Lead shots can be collected from indoor and outside shooting ranges, and its re-melting is fairly easy. Lead weights can easily be recycled. The frequency of recycling is

depended on the ease of collection. Lead recycling from glasses and glazes is not as easy as for other applications; these glasses are undesirable in the normal collection and recycling of glass because lead is considered a contaminant. Since there are only used in small amount, solder recycling is not possible; however, residues from the soldering plants are easily recycled. So far, one can see that recycling of lead is fairly easy.

In the recycling of lead-acid batteries, the acid is first drained before the battery is broken into pieces through a shredder, trommel, and roll circuit. The broken materials go through screening, classification, and gravity separation at the end of which they are separated into metallic, fines or pastes, and plastics. The metallic fraction and the pastes are used as feed material together with scrap for lead secondary production using methods described in sections 2.1 to 2.2. According to Frost, silver added to lead alloy reports in the recycling circuit in about 6 years; its recycling however is difficult because of the requirement for most sophisticated equipment which most secondary refineries do not possess. Those that possess the technology are faced with poor economics; it would require refinery of a substantial amount of silver from the melt for the value to offset the operating cost. Like silver, bismuth removal from lead is only economical if high concentration are present; it still need to be removed however because any increase in its concentration in soft lead would penalize secondary lead use.

Figure 2.5 shows that specifications for arsenic and antimony in soft lead for VRLA batteries is about 10 ppm. On this basis, the research aim is to study the possibility of removing arsenic and antimony down these levels. Though high antimony level 6-9 wt. % are found in other type of batteries, 10 ppm is still chosen as the goes because of the reported growing interest in VRLA batteries.

CHAPTER THREE

THERMODYNAMIC MODELS FOR THE CALCULATION

OF THE ACTIVITY COEFFICIENT

In the study of the removal of impurities from bullion, the activity coefficient of the impurities at the various temperatures is necessary. Many thermochemistry data available to researchers only contain information at 1 atm, and a fixed temperature. To obtain experimental data for multiple temperature of each binary, ternary, quaternary and so on would take a significant amount of time. Most studies have resorted to the use of statistical thermodynamics to develop models for calculating the activity coefficient. From literature, three such models have been used for distillation in metal systems, and they are described in subsequent subsections of chapter three. Section 3.1 will provide an overview of the thermodynamics of vaporization under reduced pressure, section 3.2 will present detailed information about thermodynamics models for the prediction of the activity coefficient that has been considered in this study. Section 3.3 will present results of the calculated parameters and VLE prediction for the Pb-As and Pb-Sb binary systems.

3.1 Thermodynamics of Vacuum Distillation

Metallurgical processes are successful based on their selectivity, feasibility and practicality. This is achieved when there exists a difference in physico-chemical properties between the entities one wants to separate that is large enough; one of these properties include volatility. The process whereby an impurity is vaporized from a solvent liquid phase is called

distillation, and it requires temperatures close to the boiling point (St Clair, 1958). Boiling point of metals at atmospheric pressures are relatively high, which means distillation processes would not be economical; however, conducted such a process under reduced pressures results in a decreased boiling point. Vacuum distillation is very important to the metallurgical field and has been used to remove volatile impurities from liquid metal such as iron (Pehlke, 1975). Vacuum distillation of metals has been studied quite extensively; in his doctoral thesis, Westerheide presented a very thorough and detailed history of distillation from liquid metals before his publication in 1963 (Westerheide, 1963). The research mentioned in his publication are shown in table 3.1.

Table 3.1 History of research on vacuum distillation of metals presented by Westerheide

Year	Ref. No	Investigator	Research
1912	1	Turner	Behavior of metals when heated under vacuum. Study conducted on brass and hard zinc
1922	2	Bronsted and Hevesy	Separation of isotopes of mercury. Research credited for being the first to apply the volatility as a function of atomic weight based on Raoult's law
1936	3	Pierce and Waring	Refining of zinc by re-distillation (fractional distillation)
1939	4	Fawcett	Effect of distillation pressure, temperature, and distance between evaporating and condensing surface on performance of molecular stills
		Burrows	Continuous and non-continuous molecular distillation equipment
		Burch and Van Dijck	Theory and development of high vacuum distillation
1944	5	Hickman	Survey on high vacuum short path distillation

Table 3.1 Continued

Year	Ref. No	Investigator	Research
1945	6	Kroll Price	Survey of factors involved in melting and evaporation of metals under reduced pressure Determination of the determination of alloy composition by loss of weight (Zn in Sn-Zn, Pb in Sn-Pb solders, P in P-Sn, Zn in brass, Pb in Cu-Pb and gun metals, and Cd in Cd-Cu)
1946	7	Erway and Simpson	Fractionation of fission products and heavy elements by volatilization methods
1947	8	Isbell	Commercial process for vacuum dezincing of lead
1948	9	Carman Kroll et al.	Theory of molecular distillation and separation Large scale laboratory process for the production of ductile zirconium
1949	10	Spendlove and St. Clair	Low pressure distillation of zinc from Al-Zn alloy
1950	11	Hudswell et al. Kaufman et al. Rogers and Vines	Separation of zirconium from hafnium Purification of Beryllium by distillation Refining of magnesium by vaporization at pressures lower than 10^{-5} mm Hg pressure
1951	12	Kroll Rogers and Vines Schlechten and Doelling Betcherman and Pidgeon Enderbrock	Survey on potential uses of vacuum methods in metallurgy Refining of lithium by vaporization at 10^{-5} mmHg Pilot plant scale vacuum treatment of Parkes process Distillation of calcium and magnesium Polonium distillation. Work published in 1957 due to its proprietary nature.
1952	13	Leuze Miller	Volatility process for uranium recovery Production of calcium, magnesium, tantalum, and zirconium by vacuum techniques

Table 3.1 Continued

Year	Ref. No	Investigator	Research
1953	14	Kotov	Theory of distillation of metals from thermodynamic standpoint. Predicted and experimental work on Zn-Cd system
		Vivian	Relative evaporation from liquid metal surface and diffusion to the surface in the liquid Volatilization of tracer plutonium from uranium melts
		Davey	Continuous pilot plant process for the vacuum dezincing of desilverized lead
		Endebrook and Engle	Review on separation of polonium separation from bismuth by distillation
1954	15	Cubicciotti	Followed on 1953 paper
		Spedding and Daane	Laboratory distillation column to separate rare earths
		Vivian	Principles of vacuum distillation of metal mixtures
		Burrows	Influence of mean free path on molecular distillation
1955	16	Spendlove	Coverage of Vacuum distillation of metals, work conducted by US Bureau of Mines. Theory of mechanism of evaporation and calculation of theoretical evaporation rates using Raoult's law
		Keys et al.	Development of molecular distillation pilot plant for lithium isotope separation
		A. J. Martin	Theoretical and practical considerations for the purification of beryllium by high vacuum distillation
		Milne and Young	Volatilization of fission products from molten and solid irradiated Th-U
		Bagnall and Roberston	Survey on evaporation of plutonium from a bismuth melt

Table 3.1 Continued

Year	Ref. No	Investigator	Research
1957	17	Burrows	Effect of attraction and repulsions molecules discussed in a simplified way to describe evaporation, diffusion, and absorption
		F. S. Martin and R. E. Brown	Examination of equation based on simple kinetic theory that represent evaporation at low pressures. He developed semi-empirical equations based on probability of molecular collisions Distillation of liquid metal reactor fuel (bismuth)
1958	18	Horsley	Vacuum distillation unit for purification of alkali metals
		St. Clair	Review of vacuum distillation der reduced pressure
1959	19	Devoe	Radiochemical separation of cadmium and application of distillation of metals to radiochemical separation
1960	20	Hooper and Keen	Process for purification of beryllium by distillation
		Ehn and Woelk	Construction of apparatus for the distillation of feed-solution of Berlin Experimental Reactor, BER
		Burrows	Molecular distillation (book)
1962	22	Davey	Mathematical treatment of molecular distillation
		Dushman, Bockris et al.,	Books on high vacuum and high temperature techniques
		Kubaschewski and Catterall	Books on thermodynamics of alloy system

The research team was not able to locate the publications mentioned in table 3.1 for cross reference at the exception of Kubaschewski et al.'s book cataloging thermochemistry data for

liquid metals. It is obvious that vacuum distillation has been extensively documented in literature in the 20th century. A series of vacuum refining work has also been conducted at McGill university with an emphasis on copper melts, and copper mattes, and a series of theses were produced (Ozberk, 1980; Danovitch, 1982; Allaire, 1986, 1991). All theses were conducted for inductively stirred liquid melts. These work were structured as followed: defining of the theory of vacuum refining, spending an extensive portion of the study in describing and developing the kinetic mechanism for the refining process being studied, and developing a design of analysis to study the effect of the parameters considered in the study.. With the same structure, Dimayuga's thesis focused on the refining of molten Aluminum (Dimayuga, 1986). Harris focused on the refining of inductively stirred steel melts (Harris, 1980). His thesis also included computational predictions of the kinetics of removal from which he obtained a patent (Harris and Davenport, 1984) and produced two highly cited publications (Harris and Davenport, 1982).

The first step to study vacuum distillation is the description of the thermodynamics associated with it. The vaporization reaction of the impurity is described by the reaction 1, and the reaction Gibb's energy is described by equation 3.1. When the vapor and the liquid are at equilibrium, the chemical potential of component i for all phases, in this case liquid and gas, are equal (see equation 3.2). The simplest approach to vapor liquid equilibrium has always been Raoult's and Henry's laws (Smith et al. 2005). In the case of distillation of dilutes solutes from dilute solution, the assumption is that the liquid phase behaves non-ideally. In the medium to high vacuum, the vapor phase is said to behave ideally. Consequently, the vapor-liquid equilibrium is expressed with the modified Raoult's law shown in equation 3.3.

$$i_l \rightarrow i_g \text{ [1]}$$

$$\frac{\Delta G_{rxn 1}}{RT} = \ln \frac{a_i^g}{a_i^l} \text{ (3.1)}$$

$$a_i^g = a_i^l \text{ (3.2)}$$

$$P_i = P_i^0 x_i \gamma_i \text{ (3.3)}$$

Where

a_i^g is the activity of component i in the gas phase;

a_i^l is the activity of component i in the liquid phase;

P_i is the partial pressure of component i;

P_i^0 is the vapor pressure of pure component i;

x_i is the mole fraction of component i in the liquid phase;

γ_i is the activity coefficient of component i in the liquid phase;

The ease of separation via distillation is expressed by the ratio between the partial pressure of the component being removed to that of the solvent (in this case, lead). The term relative volatility is defined as the molar ratio of the component to be separated to the solvent as shown in equation 3.4, and it is a measure of the easiness with which the distillation achieves the removal of impurities. Should alpha be both lower or higher than 1, the separation is possible, and this the present study, alpha values larger than 1 are sought after.

$$\alpha = \frac{\gamma_i P_i^0}{\gamma_{Pb} P_{Pb}^0} \quad (3.4) \text{ (Pehlke, 1978)}$$

Table 3.2 Vapor pressure coefficients for the calculation of saturated vapor pressure of pure metals (Kubachewski, 1979)

Elements	A	B	C	D
Lead (Pb)	-10130	-0.985	0	11.16
*Arsenic (As)	-6160	0	0	*9.32
Zinc (Zn)	-6620	-1.255	0	12.34
Antimony (Sb)	-6500	0	0	6.37
Bismuth (Bi)	-10400	-1.26	0	*12.35
Silver (Ag)	-14400	-0.85	0	11.7
Tin (Sn)	-15500	0	0	8.23
Copper (Cu)	-17520	-1.21	0	13.21

* Iida and Guthrie lists $D_{As} = 11.945$, $D_{Sb} = 8.495$, and $D_{Bi} = 14.47$ (Iida and Guthrie, 1988)

The saturated vapor pressure data are readily available, and have been calculated with high accuracy (see table 3.2). Figure 3.1 shows the saturated vapor pressure of pure metals that often occur as impurities in lead bullion; based on pure metals volatility, thermodynamics indicates that As, Zn, and Sb are more volatile than Pb, and thus they have better chances of being removed from the bullion. Ag, Sn, and Cu on the other hand are much less volatile than Pb; consequently, lead would have to be removed from the melt leaving them behind as residues. Bi volatility is much closer to that of Pb; consequently, its separation from lead in the form of metal vapor will be challenging. Although Sb is more volatile than Pb, their respective volatilities are not far from each other; therefore, its distillation might also be challenging when its activity is low in the melt.

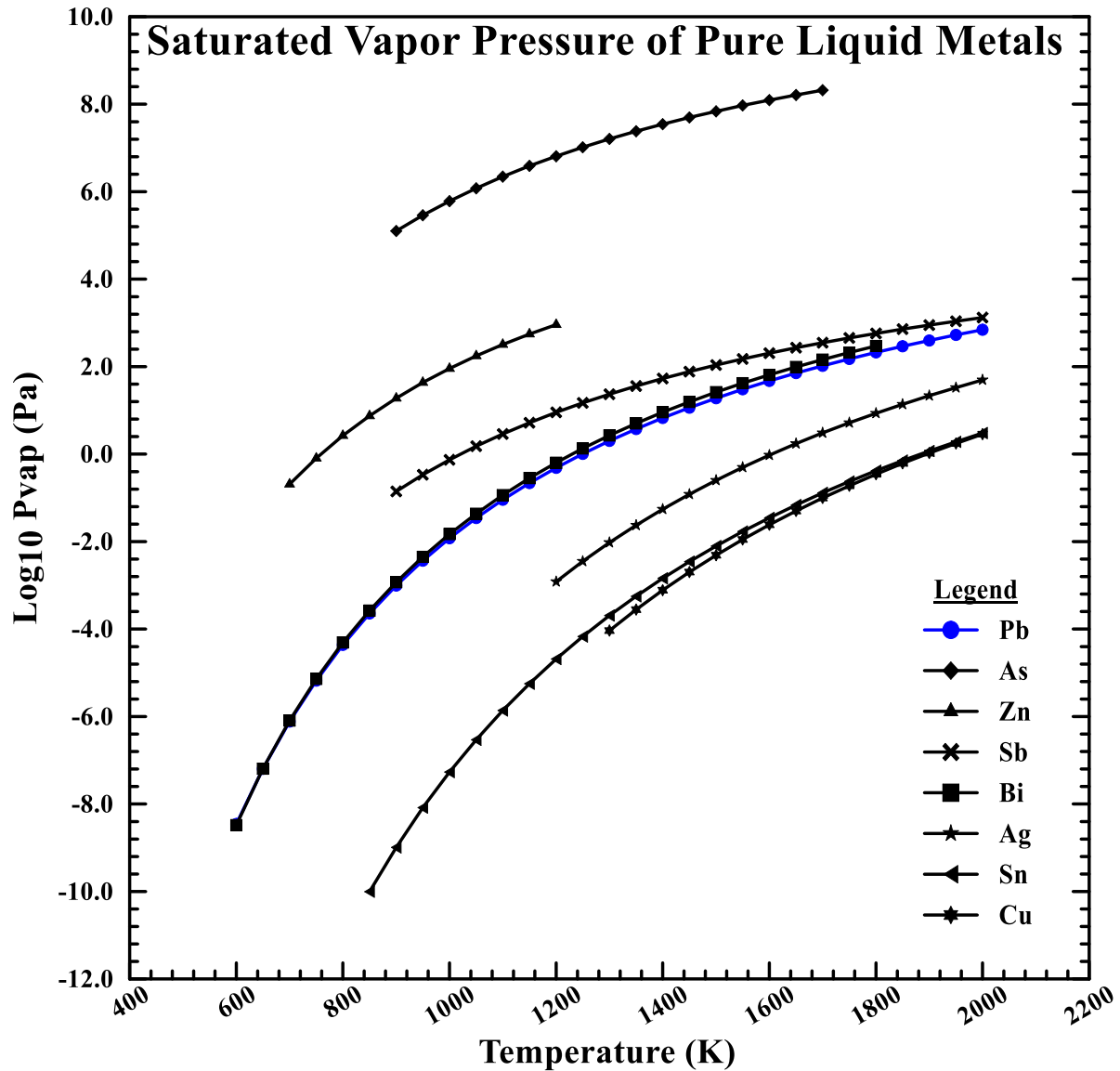


Figure 3.1 Saturation vapor pressure of pure metals

Information about the activity coefficient of the component to be separated is important to the distillation process. However, little thermodynamic data is available for binary and multicomponent systems at low pressure and different temperatures. As such, extensive research has been conducted to develop thermodynamic models for predicting the activity coefficients. Among such models are the molecular interaction volume model (MIVM), the Wilson equation,

and the Non-Random Two Liquid (NRTL) model; these models are based on the excess Gibbs free energy which is related to the activity coefficient. Other models are available, and are used in the field of chemical engineering; however, the 3 models mentioned above have been in the field of metallurgical research, hence they were chosen for the present study.

3.2 Thermodynamic Models for Prediction of the Activity Coefficient

3.2.1 The Molecular Interaction Volume Model (MIVM)

Dong Ping Tao developed the molecular interaction volume model (MIVM) based on local composition statistical thermodynamic model in the liquid state (Tao, 2000). The model was created on the claim that molecules in liquids do not move randomly like gas molecules, and not by vibration as in the case for molecule motion in solids. With that, he developed an equation for the Gibbs free energy which is shown in equation 3.5.

$$\frac{G_m^E}{RT} = \sum_{i=1} x_i \ln \frac{V_{mi}}{\sum_{j=1} x_j V_{mj} B_{ji}} - \frac{1}{2} \sum_{i=1} Z_i x_i \left(\frac{\sum_{j=1} x_j B_{ji} \ln B_{ji}}{\sum_{j=1} x_j B_{ji}} \right) \quad (3.5)$$

The activity coefficient of component i is the derivative of the excess Gibbs free energy with respect to temperature, pressure and component j ($j \neq i$) expressed $\left(\frac{\partial G_m^E}{\partial x_i} \right)_{T,P,x_{j \neq i}}$ and can be calculated as shown in equation 3.6.

$$\begin{aligned}
\ln \gamma_i &= 1 + \ln \frac{V_{mi}}{\sum_{j=1} x_j V_{mj} B_{ji}} \\
&- \sum_{j=1} \frac{x_j V_{mi} B_{ij}}{\sum_{k=1} x_k V_{mk} B_{kj}} - \frac{1}{2} \left(\frac{Z_i \sum_{j=1} x_j B_{ji} \ln B_{ji}}{\sum_{k=1} x_k B_{ki}} \right. \\
&\left. + \sum_{j=1} \frac{Z_j x_j B_{ij}}{\sum_{k=1} x_k B_{kj}} \left(\ln B_{ij} - \frac{\sum_{l=1} x_l B_{lj} \ln B_{lj}}{\sum_{k=1} x_k B_{kj}} \right) \right) \quad (3.6)
\end{aligned}$$

For a binary system, the activity coefficient is defined as shown in equations 3.7 and 3.8.

$$\begin{aligned}
\ln \gamma_i &= \ln \left(\frac{V_{mi}}{x_i V_{mi} + x_j V_{mj} B_{ji}} \right) + x_j \left(\frac{V_{mj} B_{ji}}{x_i V_{mi} + x_j V_{mj} B_{ji}} - \frac{V_{mi} B_{ij}}{x_j V_{mj} + x_i V_{mi} B_{ij}} \right) \\
&- \frac{x_j^2}{2} \left[\frac{Z_i B_{ji}^2 \ln B_{ji}}{(x_i + x_j B_{ji})^2} + \frac{Z_j B_{ij} \ln B_{ij}}{(x_j + x_i B_{ij})^2} \right] \quad (3.7)
\end{aligned}$$

$$\begin{aligned}
\ln \gamma_j &= \ln \left(\frac{V_{mj}}{x_j V_{mj} + x_i V_{mi} B_{ij}} \right) - x_i \left(\frac{V_{mj} B_{ji}}{x_i V_{mi} + x_j V_{mj} B_{ji}} - \frac{V_{mi} B_{ij}}{x_j V_{mj} + x_i V_{mi} B_{ij}} \right) \\
&- \frac{x_i^2}{2} \left[\frac{Z_j B_{ij}^2 \ln B_{ij}}{(x_j + x_i B_{ij})^2} + \frac{Z_i B_{ji} \ln B_{ji}}{(x_i + x_j B_{ji})^2} \right] \quad (3.8)
\end{aligned}$$

Where:

V_{mi} and V_{mj} are the molar volumes of component i and j;

B_{ij} and B_{ji} are the i-j and j-i pair potential energy interaction parameters ($B_{ij} \neq B_{ji}$);

x_i and x_j are the mole fractions of components i and j;

Z_i and Z_j are the first coordination numbers of components i and j;

The molar volume, the energy interaction parameters and the coordination number are temperature dependent as shown in equations 3.9 to 3.12. Equation 3.12 is a correction to the

original equation published in 2005 by Tao (Tao, 2005), and it has been used in subsequent publications in which MIVM was used to calculate the activity coefficient.

$$B_{ij} = \exp \left[- \left(\frac{\varepsilon_{ij} - \varepsilon_{jj}}{kT} \right) \right] \quad (3.9)$$

$$B_{ji} = \exp \left[- \left(\frac{\varepsilon_{ji} - \varepsilon_{ii}}{kT} \right) \right] \quad (3.10)$$

$$V_{mi} = V_{mel} [1 + \alpha_i (T - T_m)] \quad (3.11)$$

$$\alpha_i = \frac{\Lambda_i}{\rho_{mi}} \quad (3.12)$$

$$\rho_{mi} = \rho_{mel,i} + \Lambda_i (T - T_{mel,i}) \quad (3.13)$$

$$Z_i = \frac{4\sqrt{2\pi}}{3} \left(\frac{r_{mi}^3 - r_{0i}^3}{r_{mi} - r_{0i}} \right) \rho_i r_{mi} \exp \left(\frac{\Delta H_{mi} (T - T_{mi})}{Z_c R T T_{mi}} \right) \quad (3.14)$$

Where

r_{mi} and r_{0i} are the beginning and first peak of the radial distribution function;

Z_c is the close-packed coordination, $Z_c = 12$;

ρ_i is the molecular number density, and is given by the ratio of Avogadro's number to the molar volume of component i ;

α is the thermal coefficient of expansion;

V_{mel} is the molar volume of component i at the melting point;

T_{mi} is the melting temperature of component i ;

ΔH_{mi} is the change in enthalpy associated with the melting of component i ;

ε_{ii} , ε_{jj} , ε_{ij} , and ε_{ji} are energy parameters for the i - i , j - j , i - j , and j - i interactions ($\varepsilon_{ij} = \varepsilon_{ji}$, and $\varepsilon_{ii} \neq \varepsilon_{jj}$);

When x_i and x_j approaches zero, equations 3.7 and 3.8 are reduced to

$$\ln \gamma_i^\infty = 1 - \ln \left(\frac{V_{mj} B_{ji}}{V_{mi}} \right) - \frac{V_{mi} B_{ij}}{V_{mj}} - \frac{1}{2} (Z_i \ln B_{ji} + Z_j B_{ij} \ln B_{ij}) \quad (3.15)$$

$$\ln \gamma_j^\infty = 1 - \ln \left(\frac{V_{mi} B_{ij}}{V_{mj}} \right) - \frac{V_{mj} B_{ji}}{V_{mi}} - \frac{1}{2} (Z_j \ln B_{ij} + Z_i B_{ji} \ln B_{ji}) \quad (3.16)$$

Equations 3.15 and 3.16 are combined and expressed as a function of either B_{12} or B_{21} .

Next the parameters can be calculated by using the Newton-Raphson method of finding roots to equation 3.17 shown below.

$$f(B_{ij}) = \ln \gamma_j^\infty - 1 + \left(\frac{2 + Z_j}{2} \right) \ln B_{ij} - \ln \frac{V_{mi}}{V_{mj}} - \left(\frac{V_{mj}}{V_{mi}} + \frac{Z_i}{2} B \right) e^B \quad (3.17)$$

$$\frac{\partial f(B_{ij})}{\partial B_{ij}} = \frac{2 + Z_j}{2 B_{ij}} + \left[\frac{V_{mi}}{V_{mj}} + (1 + B) \frac{Z_i}{2} \right] B' e^B \quad (3.18)$$

$$B = \left(\frac{2}{2 + B_{ij}} \right) \left(1 - \ln \gamma_i^\infty - \ln \frac{V_{mj}}{V_{mi}} - \frac{V_{mj}}{V_{mi}} B_{ij} - \frac{B_{ij}}{2} Z_j \ln B_{ij} \right) \quad (3.19)$$

$$B' = \left(\frac{-2}{2 + Z_i} \right) \left(\frac{V_{mi}}{V_{mj}} + \frac{Z_j}{2} \ln B_{ij} + \frac{Z_2}{2} \right) \quad (3.20)$$

3.2.2 The Wilson Equation

Grant Wilson worked on the development and building of an apparatus to study vapor liquid equilibrium of mixtures; he based his study on the water-2Butoxy system (Wilson, 1958). He measured the total pressure and overall composition of the vapor phase for the system, and after determining the best fit, he obtained an analytical expression of the excess Gibbs free energy of mixing as a function of the mole fraction of water. On the basis of his thesis' results,

he developed a general expression for the excess Gibbs free energy that was applied to a majority of hydrocarbon systems, and the data were in agreement (Wilson, 1964). Wilson's equation was since then utilized in multiple research in chemical engineering, and metallurgy; the present research focused only on its application to vacuum distillation in of liquid metals as has been reported by various authors (Zhang *et al.*, 2015; Jiang *et al.*, 2016; Yang *et al.*, 2016; Zhao *et al.*, 2017).

The general expression for the Gibb's free energy and the activity coefficient using the Wilson equation are shown in equations 3.21 and 3.22.

$$\frac{G_m^E}{RT} = - \sum_{i=1}^m x_i \ln \left(1 - \sum_{j=1}^m x_j A_{ji} \right) \quad (3.21)$$

$$\ln \gamma_i = 1 - \ln \left(\sum_{j=1}^m x_j A_{ij} \right) - \sum_{j=1}^m \left(\frac{x_j A_{ji}}{\sum_{k=1}^m x_k A_{jk}} \right) \quad (3.22)$$

For a binary system, the activity coefficient of components i and j are given by equations 3.23 and 3.24, and the expression for the temperature dependency of the binary parameters are shown in equations 3.25 and 3.26.

$$\ln \gamma_i = - \ln(x_i + x_j A_{ij}) + x_j \left(\frac{A_{ij}}{x_i + x_j A_{ij}} - \frac{A_{ji}}{x_i A_{ji} + x_j} \right) \quad (3.23)$$

$$\ln \gamma_j = - \ln(x_j + x_i A_{ji}) - x_i \left(\frac{A_{ij}}{x_i + x_j A_{ij}} - \frac{A_{ji}}{x_i A_{ji} + x_j} \right) \quad (3.24)$$

$$A_{ij} = \frac{v_{mj}}{v_{mi}} \exp \left(- \frac{\lambda_{ij} - \lambda_{ii}}{RT} \right) \quad (3.25)$$

$$A_{ji} = \frac{V_{mi}}{V_{mj}} \exp\left(-\frac{\lambda_{ji}-\lambda_{jj}}{RT}\right) \quad (3.26)$$

λ_{ii} , λ_{jj} , λ_{ij} , and λ_{ji} have the same significance as ε_{ii} , ε_{jj} , ε_{ij} , and ε_{ji} in the MIVM equation; the same applies to the binary parameters A_{ij} and A_{ji} . One of the major drawback of the Wilson equation is its inability of accurately predicting the activity coefficient for systems with limited miscibility; however, its main advantage is its ability to project to multicomponent system without the introduction of a new parameter. When x_i and x_j approaches zero, equations 3.23 and 3.24 are reduced to:

$$\ln \gamma_i^\infty = 1 - A_{ji} - \ln A_{ij} \quad (3.27)$$

$$\ln \gamma_j^\infty = 1 - A_{ij} - \ln A_{ji} \quad (3.28)$$

Equations 3.25 and 3.26 are then combined to obtain equations 3.27 to 3.32, and the parameters can be obtained from the Newton-Raphson methodology.

$$f(A_{ij}) = 1 - \ln \gamma_i^\infty - \ln A_{ij} - e^B \quad (3.27)$$

$$\frac{\partial f(A_{ij})}{\partial A_{ij}} = \frac{A_{ij}A_{ji} - 1}{A_{ij}} \quad (3.28)$$

$$B = \ln A_{21} \quad (3.29)$$

$$B' = -1 \quad (3.30)$$

3.2.3 The Non-Random Two Liquid Model (NRTL)

To overcome the inability of the Wilson equation to accurately predict the activity coefficients of systems with immiscibility gaps, Renon expanded on Wilson's idea and came up with the Non-Random Two Liquid (NRTL) model (Renon and Prausnitz, 1968). The NRTL model is well applicable to the systems aforementioned. This equation involves three adjustable parameters with the introduction of the non-randomness parameter α . This is one instance in which the NRTL was applied to the study of distillation in lead bullion (Xu *et al.*, 2016). The excess Gibbs free energy and the activity coefficient using the NRTL model are mathematically expressed by equations 3.31 and 3.32.

$$\frac{G_m^E}{RT} = \sum_{i=1}^m x_i \frac{\sum_{j=1}^m \tau_{ji} G_{ji} x_j}{\sum_{l=1}^m x_l G_{li}} \quad (3.31)$$

$$\ln \gamma_i = \frac{\sum_{j=1}^m \tau_{ji} G_{ji} x_j}{\sum_{k=1}^m x_k G_{ki}} + \sum_{j=1}^m \frac{x_j G_{ij}}{\sum_{k=1}^m x_k G_{kj}} \left(\tau_{ij} - \frac{\sum_{l=1}^m x_l \tau_{lj} G_{lj}}{\sum_{k=1}^m x_k G_{kj}} \right) \quad (3.32)$$

For a binary system, the activity coefficient of components i and j are given by equations 3.33 and 3.34, and the expression for the temperature dependency of the binary parameters are shown in equations 3.35 to 3.38.

$$\ln \gamma_i = x_j^2 \left[\tau_{ji} \left(\frac{G_{ji}}{x_i + x_j G_{ji}} \right)^2 + \frac{\tau_{ij} G_{ij}}{(x_j + x_i G_{ij})^2} \right] \quad (3.33)$$

$$\ln \gamma_j = x_i^2 \left[\tau_{ij} \left(\frac{G_{ij}}{x_j + x_i G_{ij}} \right)^2 + \frac{\tau_{ji} G_{ji}}{(x_i + x_j G_{ji})^2} \right] \quad (3.34)$$

$$\tau_{ij} = \frac{g_{ij} - g_{jj}}{RT} \quad (3.35)$$

$$\tau_{ji} = \frac{g_{ji} - g_{ii}}{RT} \quad (3.36)$$

$$G_{ij} = \exp(-\alpha_{ij}\tau_{ij}) \quad (3.37)$$

$$G_{ji} = \exp(-\alpha_{ij}\tau_{ji}) \quad (3.38)$$

$$\alpha_{ij} = \alpha_{ji} \quad (3.39)$$

When x_i and x_j approaches zero, equations 3.33 and 3.34 are reduced to equations 3.40 and 3.41 which are then combined to yield equations 3.42 to 3.45.

$$\ln \gamma_i^\infty = \tau_{ji} - \tau_{ij} \exp(-\alpha_{ij}\tau_{ij}) \quad (3.40)$$

$$\ln \gamma_j^\infty = \tau_{ij} - \tau_{ji} \exp(-\alpha_{ji}\tau_{ji}) \quad (3.41)$$

$$f(\tau_{ij}) = \tau_{ij} - \ln \gamma_j^\infty + B e^{(-\alpha_{ji}B)} \quad (3.42)$$

$$\frac{\partial f(\tau_{ij})}{\partial \tau_{ij}} = 1 + B' e^{-\alpha_{ji}B} (1 - \alpha_{ji}B) \quad (3.43)$$

$$B = \tau_{ji} = \ln \gamma_i^\infty - \tau_{ij} \exp(-\alpha_{ij}\tau_{ij}) \quad (3.44)$$

$$B' = \exp(-\alpha_{ij}\tau_{ij})(\tau_{ij}\alpha_{ij} - 1) \quad (3.45)$$

Table 3.3. Illustration of binary parameters from the proposed activity coefficient models

Model	Pair potential interaction energies	i-i, j-j, i-j, and j-i pair potential interaction parameters	Non-randomness
MIVM	B_{ij} and B_{ji}	ϵ_{ii} , ϵ_{ij} , ϵ_{ij} , and ϵ_{ji}	None
Wilson	A_{ij} and A_{ji}	λ_{ii} , λ_{jj} , λ_{ij} , and λ_{ji}	None
NRTL	τ_{ij} , τ_{ji} , G_{ij} , G_{ji}	g_{ii} , g_{jj} , g_{ij} , and g_{ji}	α_{ij} , α_{ji}

The three equations shown bear similarities as shown in table 3.3; G_{ij} and G_{ji} are dependent upon two other parameters from the same model, and therefore does constitute additional parameters. In most cases α_{ij} is determined experimentally. When no experimental data is available for the system, it has been shown that its value varies between 0.1 and 0.39. For the majority of predictions in the liquid metal distillation, an arbitrary value of 0.2 is adopted.

It is evident from equations 3.15, 3.16, 3.27, 3.28, 3.40, and 3.41 that the knowledge of the activity coefficient at infinite dilution for both components i and j facilitates the prediction of the binary parameters. Also, equations 3.9, 3.10, 3.14, 3.25, 3.26, 3.35 and 3.36 show the temperature dependence of the binary parameters. The predictions of the binary parameters are carried out at the temperature for which experimental data is available; therefore, it is necessary to calculate new binary parameters when predicting the vapor liquid equilibrium at a different temperature. While the temperature dependence of these parameters were discussed at length by various authors, the pressure dependence was not explained, nor was there references to guide through a deep study of the dependence on pressure.

3.3 Calculated Binary Parameters for the Pb-As, Pb-Sb, and As-Sb Binary Systems

One of the challenges that the research team came across was the lack of most needed thermochemistry data for liquid arsenic which primarily is due to the fact that arsenic metal sublimates rather than melt at 1.013 bar (1 atm); therefore, a deeper literature survey needed to

be conducted to find liquid arsenic data, and it was fruitful. Based on HSC and EPSI metals (reference), the heat of melting of arsenic was determined to be 27743 J/mole. Li and coworkers conducted a study on liquid arsenic at 1150 K using the ab-initio molecular dynamic and the pair potential molecular dynamic method to determine its structure; they attributed their success by comparing the two methods with experimental data (reference). Using their results' graphical representation of the radial distribution, the beginning (r_0) and first (r_m) peaks were determined to 2.05E-08 and 2.22E-08 cm. Thermochemistry data for lead, arsenic, and antimony are summarized in table 3.2. Using the data from table 3.4, the coordination number necessary to calculate the activity coefficient using the MIVM was calculated, and the data is shown in table 3.5. The numbers in bold font denotes the Z_i and Z_j used for the specific binary system.

Table 3.4 Thermochemistry data for lead, arsenic and antimony

Element	Lead	Arsenic	Antimony
Symbol	Pb	As	Sb
Crystal system*	FCC	STR	STR
Molecular weight (g/mole)	207.2	74.9216	121.7
T_{melting} (K)	601	1090**	904
T_{melting} (°C)	327	817	631
T_{boiling} (K)	2023	889***	1913
T_{boiling} (°C)	1750	616	1640
Molar volume at T_{melting}, V_m (cm³/mole)	19.42	14.4	18.8
Molar density at T_{melting}, ρ_m (g/cm³)	10.67	5.22	6.48
$\Lambda \equiv (\partial\rho/\partial T)_P$ (g/cm³-K)	1.32E-03	5.40E-04	8.20E-04
Coefficient of thermal expansion, α (K⁻¹)	1.24E-04	1.03E-04	1.27 E-04
r₀ (cm)	2.76E-08	2.05E-08*****	2.22E-08
r_m or σ (cm)	3.26E-08	2.22E-08*****	19874
Heat of melting, ΔH_m (J/mole)	4810	27743	19874
Entropy of melting, ΔS_m (J/mole-K)	8.02	25.45*****	25.97

* FCC: face centered cubic, STR; simple trigonal

** determined at 36 atm pressure (Iida, 1988; Gokcen, 1990)

*** Sublimation point at 1 atm

**** Calculated using 1090 K as T_{melting}

***** Reference: Lu et al., 1990

Table 3.5 Coordination numbers for the Pb-As, Pb-Sb, and As-Sb systems

T (K)	Coordination Number Z		
	Pb	As	Sb
913	9.3149	4.3803	8.9583
905	9.3097	4.3886	8.9665
1373	9.7273	4.1493	8.8421

Two of the most common statistical metrics used to measure the accuracy of model predictions are the Mean Average Deviation (MAD) and the Root Mean Square Deviation (RMSD). Both metrics report the error in the units of the variable of interest; however, the RMSD has the advantage of penalizing large errors due to its quadratic nature (JJ, 2016). A lot of debate takes place in the scientific community on the capability of one metric over the other. Cha and Draxter presented a paper in which they attempted to define both metric measures and the circumstances in which one is more advantageous than the other (Chai and Draxler, 2014). In the prediction of the binary parameters, it is imperative the deviation from calculated to experimental values be minimized. They show that RMSD is best suited for situation in which errors follow a uniform distribution; they also showed that the RMSD's advantage over the MAE is the fact that it avoids absolute values which is undesirable in many mathematical calculations. The research team decided then that the performance of the prediction models would be done through the minimization of the RMSD on the activities of both components i and j; the expression for the RMSD is shown in equation 3.46. The RMSD for convergence was set at 1.0E-5 to 0.02.

$$RMSD = \pm \left[\frac{1}{n} \sum_{i=1}^n (a_{i,exp} - a_{i,pred})^2 \right]^{\frac{1}{2}} \quad (3.46)$$

Experimental activity data for the Pb-Sb systems was extracted from Hultgren and coworkers (Hultgren et al., 1977); those for the Pb-As were calculated using the freezing point excess Gibbs free energy equation provided by Gokcen in his assessment of the As-Pb diagram. (Gokcen, 1990). Activity data for the As-Sb was obtained from the Landolt-Börnstein - Group IV Physical Chemistry-Volume 12A 2006 (SGTE, 2006). Results on the prediction of binary parameters are shown in table 3.6. All models were adequate in calculating the binary parameters for the Pb-Sb system. The binary parameters determined using with the MIVM a comparable to those determined by Tao(Tao, 2002); he reported B_{Sb-Pb} as 1.0176 and B_{Pb-Sb} as 1.0269. Difference with his results can be attributed to the use of slightly different values for the activity coefficient at infinite dilution as well as the first peak of the radius distribution for antimony. Binary parameters determined using the NRTL model was an exact match with results reported by Xu and coworkers (Xu *et al.*, 2016); they reported RMSD values of 0.0009 and 0.0007 for the activity of lead and antimony respectively which is comparable to the 0.0007 and 0.0006 RMSD reported in the present research. For the Pb-As and the As-Sb systems, the author obtained the combination of parameters that yielded the minimum error both each activity.

Table 3.6 Calculated binary parameters for Pb-As, Pb-Sb, and As-Sb binary systems

MIVM								
Temp (K)	i	j	B _{ij}	B _{ji}	RMSD a _i	RMSD a _j		
913	Pb	As	1.1754	0.9248	0.0114	0.0210		
905	Pb	Sb	1.0224	1.0223	0.0004	0.0004		
1373	As	Sb	0.7971	1.4150	0.0217	0.0255		

Table 3.6 Continued

Wilson								
Temp (K)	i	j	A_{ij}	A_{ji}	RMSD_{ai}	RMSD_{aj}		
913	Pb	As	3.9968	0.0199	0.0124	0.0339		
905	Pb	Sb	1.1287	1.1287	0.0003	0.0003		
1373	As	Sb	0.3881	2.0806	0.0456	0.0257		
NTRL $\alpha_{ij} = 0.2; \alpha_{ji} = \alpha_{ij}$								
Temp (K)	i	j	Tau_{ij}	Tau_{ji}	G_{ij}	G_{ji}	RMSD_{ai}	RMSD_{aj}
913	Pb	As	4.0669	-2.3885	0.4434	1.6124	0.0249	0.0163
905	Pb	Sb	1.7258	-1.4718	0.7081	1.3423	0.0007	0.0006
1373	As	Sb	-2.2890	3.9908	1.5806	0.4502	0.0103	0.0142

CHAPTER FOUR

PROCESS DEVELOPMENT AND EXPERIMENTATION

Chapter four presents details pertaining to the methodology which was undertaken to study the distillation process. Section 4.1 goes over the considerations that were implemented in the design of the reactor tube as well as showing the resulting apparatus. Section 4.2 details the development and setup of the alloy preparation and alloy casting stations. Section 4.3 briefly talks about the sample preparation of solid and liquid representative samples as well as the analytical techniques that were used to analyze them.

4.1 Vacuum Distillation Reactor Design and Setup

Available to the research team was an MHI horizontal furnace rated for 1700°C. The furnace was designed for a reactor tube with an outside diameter (OD) of 2.75 inches and an inside diameter (ID) of 2.5 inches; consequently, the vacuum distillation reactor had to be built with these dimensions in mind. The furnace operates molydisilicide (MoSi_2) heating elements, and is equipped with a type B thermocouple which is calibrated for accurate temperature measurements between 600 and 1700 °C.

4.1.1 Design Considerations

In building the vacuum distillation apparatus, the research team aimed to be able to measure the temperature inside the furnace and slightly above the melt surface, to accurately measure the vacuum pressure, to condense the metal vapors as a solid, and to capture all of the vapors before the residual gas is pulled through the vacuum pump. To maximize the vacuum pulling, and to eliminate chances of oxidation during experiment, it is imperative that the reactor be well sealed. For that purpose, the use of a gasket is recommended; if the gasket used is made

of rubber, it is beneficial to cool the ends of the reactor so as not to fuse the flanges, gasket and covers together. Based on these criteria and bearing in mind the available space of 2.5 inches, the following key parts were identified:

1. The furnace thermocouple: A type K thermocouple which is inserted into a mullite sheathe that is closed on one end. Its length was chosen such that its tip rests at the center of the heated zone.
2. The sample thermocouple: A type K thermocouple which is inserted in a mullite sheathe opened on both ends. Its length is selected such that its bear tip rests slightly above the melt surface for better temperature control during experiments
3. The condensation unit: A cold finger was the condensation unit of choice mainly due to the available space on the flange. Because the metal vapors condense rather rapidly, the cold finger's length was chosen such that its tip was located one inch away from the end of the heated zone.
4. Inlet and outlet ports for gas flow: Because of the need to minimize oxidation during experimentation, oxygen had to be displaced from the reactor to provide a neutral atmosphere, hence the need for an inlet and outlet for argon.
5. The vacuum port: This port was chosen such that during vacuum pulling the metal vapors would flow past the cold finger to promote their condensation. Consequently, it was located on the side of the tube that housed the condensation unit.
6. The sample boat: the sample boat was to be designed such that it curved coincidentally with the bottom of the reactor tube.

4.1.2 SolidWorks Design Considerations

Figure 4.1 shows the detailed view of the furnace assembly. As shown in the figure, the vacuum distillation reactor was designed with a 2 tubes configuration such that the smaller tube fit the 2.75 inches OD while the larger tube was 3.00 inches OD; the inside diameter was kept at 2.5 inches throughout the total lengths of the combined tubes. The small tube cover was designed to house the gas inlet port, the furnace thermocouple, and the sample thermocouple. The sample boat was designed such that the sample thermocouple mullite sheathe could pass through it; while the left cover was sealed, the sample boat could be positioned at the center of the heated zone from the large tube side by pulling it on the sheathe. The larger tube housed the gas outlet, the cold finger as well as the vacuum port.

Figure 4.2 shows a detailed view of the condensation unit that is the cold finger. It consists of a one-inch OD outer tube which inner surface is cooled by flowing cold water; the water flows in through an inner tube. Cold water flowing from the inner would displace the warm water at the tip of the cold finger hence keeping the outer tube constantly cold during experiment; the warm water would then exit the cold finger through a running tee compression fitting. The cold finger's vertical position was chosen such that it was in the direct path of the vapor while the vacuum is pulled. The reactor tubes, flanges, covers, and condensation unit tubes were machined and built locally by J&B Machine shop.

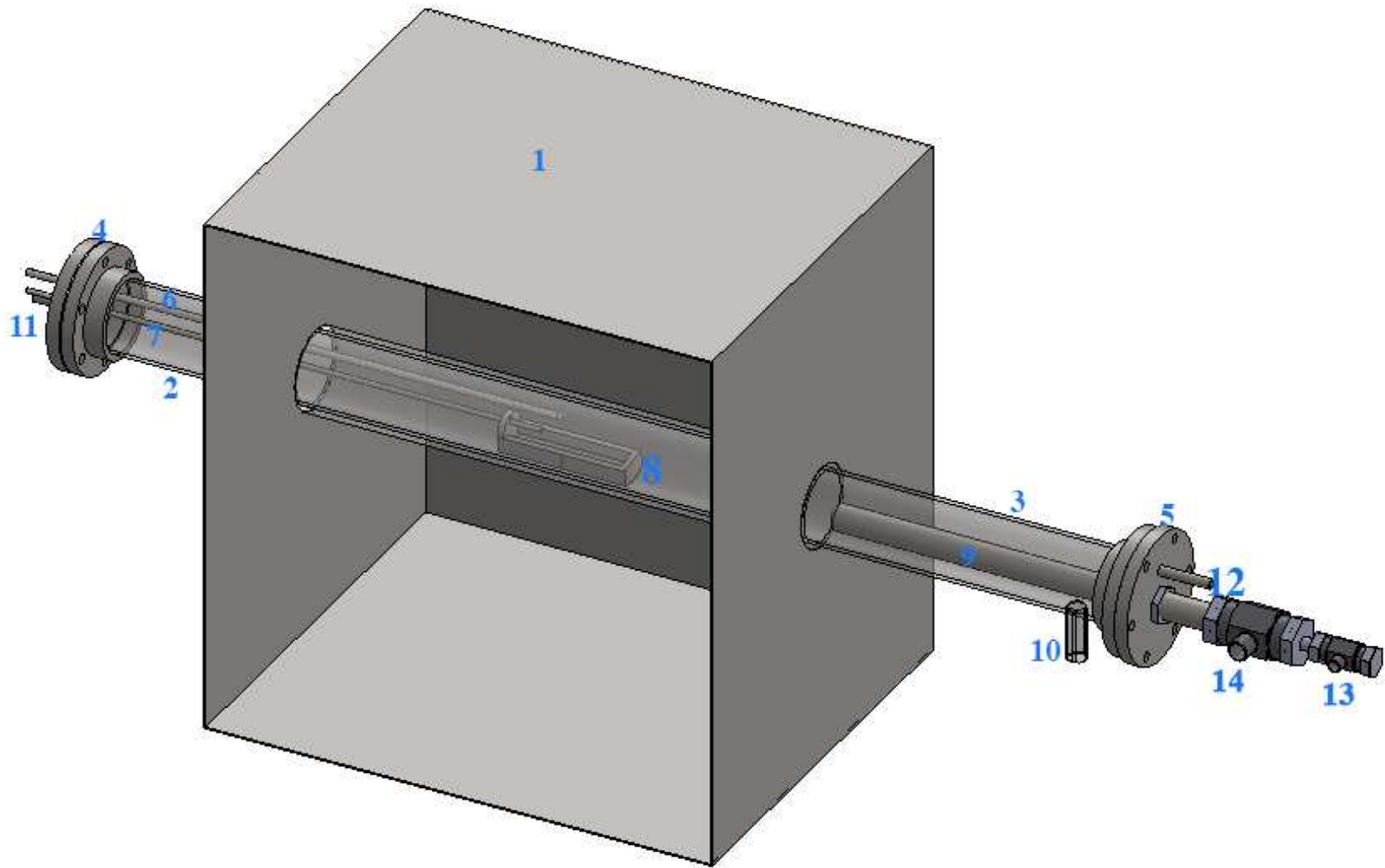


Figure 4.1 Schematic of the designed vacuum distillation reactor. 1) furnace cover, 2) 2.75" OD SS304 tube, 3) 3.00" OD SS 304 tube, 4) left cover, 5) right cover, 6) furnace thermocouple, 7) sample thermocouple, 8), sample boat, 9) cold finger, 10) vacuum port, 11) gas inlet port, 12) gas outlet port, 13) Cold finger water inlet port, 14) cold finger water outlet port.

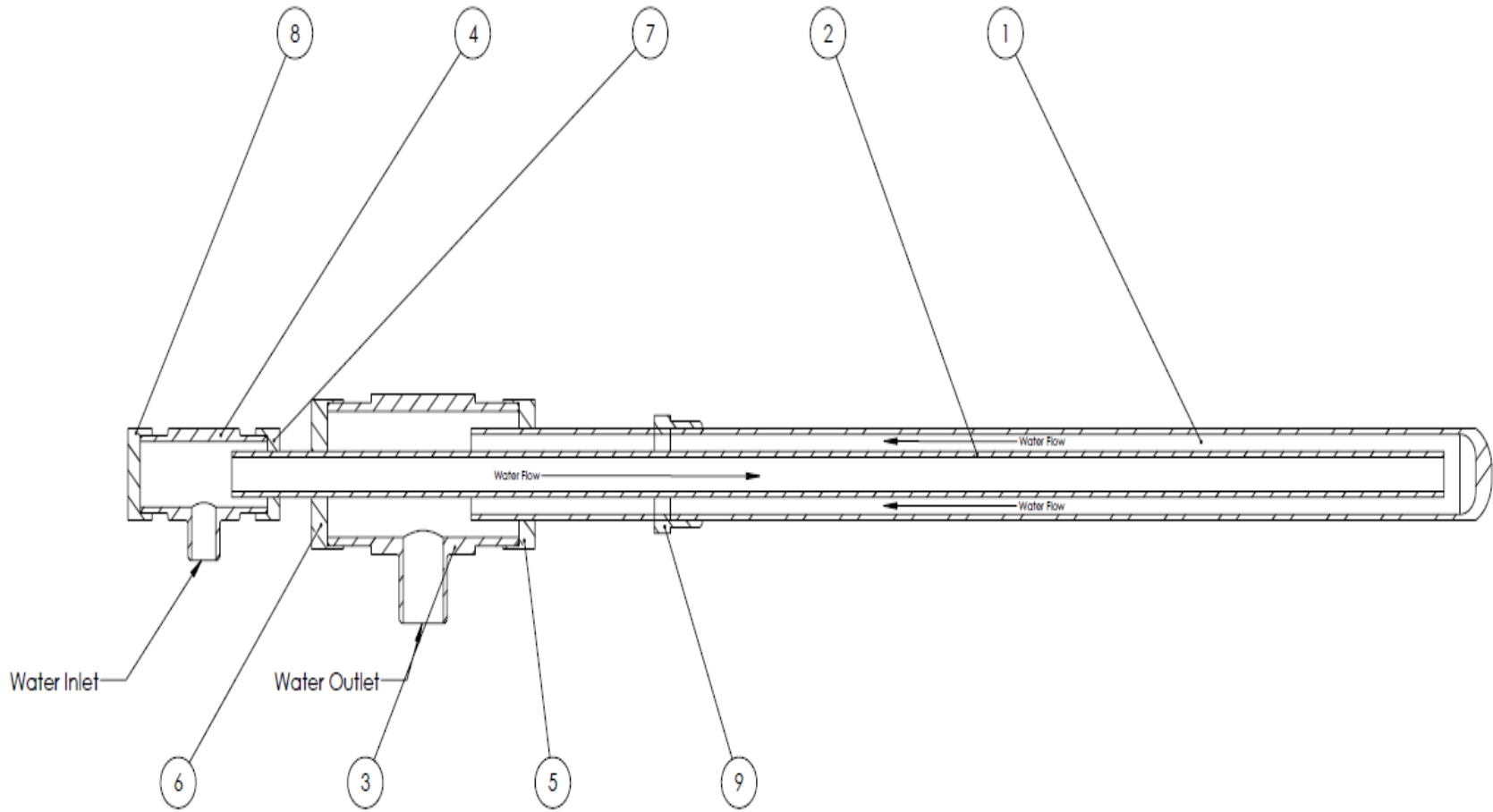


Figure 4.2 Section view of the condensation unit. (1) outer tube, (2) inner tube, (3) large compression fitting, (4)small compression fitting, (5) and (6) nuts for the large fitting, (7) & (8) nuts for the small fitting, (9) compression fitting to fit on the right cover

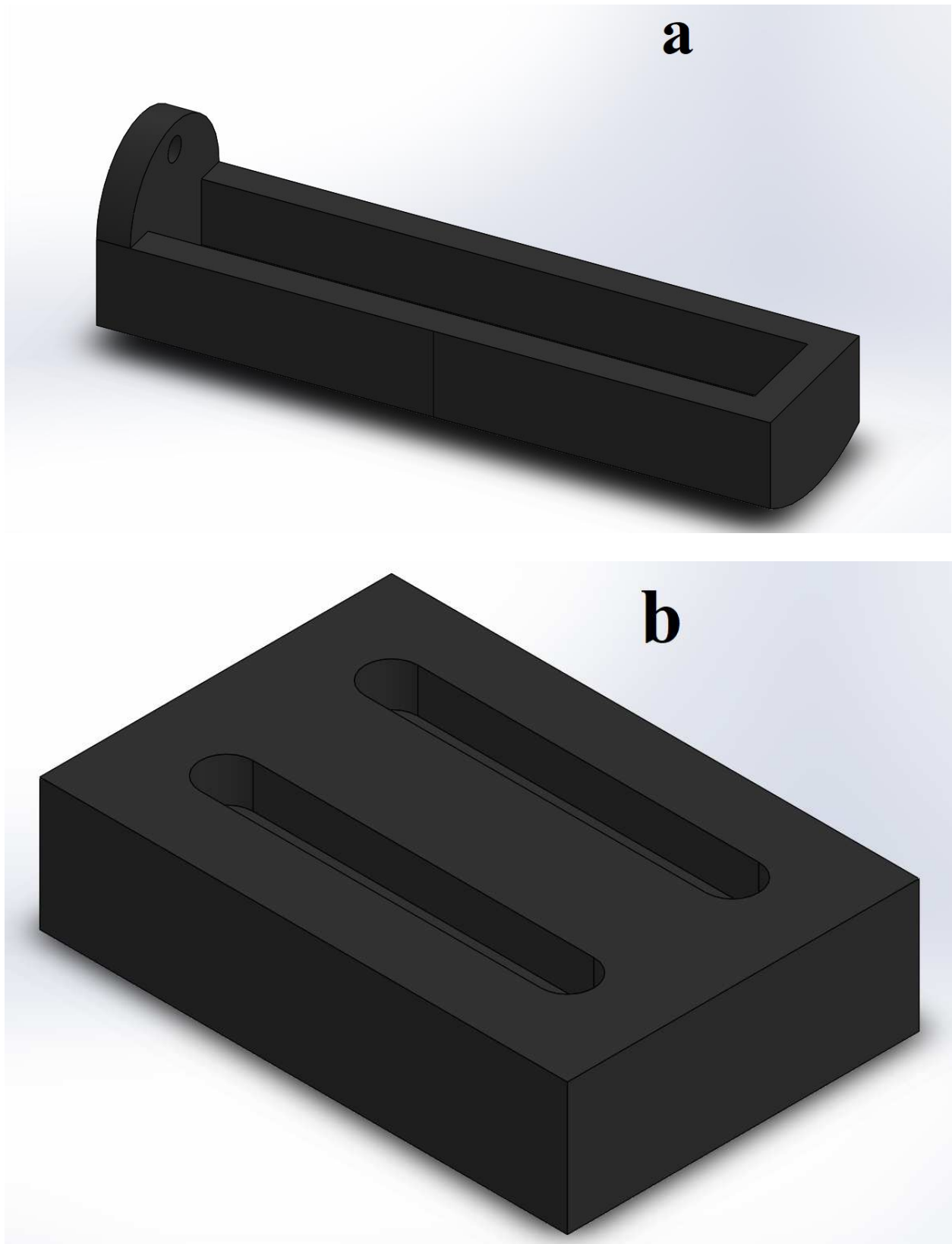


Figure 4.3 Illustration of the sample boat (a) and the casting mold (b)

Figure 4.3a and 4.3b show the sample boat and the sample casting mold respectively. Since lead is the major component in the alloy projected to undergo distillation, its density is used to calculate the bulk melt volume of a 200 grams sample (see appendix A). The research team opted for a sample boat that was a quarter inch in wall thickness such that the available volume is 30.382 mL. With a density of 11.3 g/cm³ at its melting point, 200 grams of lead alloy sample would fill about 18 mL of the available space; therefore, eliminating chances of splashing during experiment. The available length in the sample boat is 4.5 inches; consequently, the sample casting mold was designed such that the cast sample lengths is 4.48 inches. Both the sample boat and the casting molds were machined from graphite acquired from Graphite Product Corp where the sample boats were machined as well. A total of 18 molding blocks were machined locally at the Colorado School of Mines Physics Department machine shop.

4.1.3 Experimental Setup Assembly

Figure 4.4 shows the assembled vacuum furnace reactor which was machined from grade 304 stainless steel which has a melting point in the range of 1330 and 1400 °C. The small tube was inserted in the furnace first; silver goop was then applied on the threads on both tubes prior to joining then. 3 inches wrenches were utilized to thread the tubes together (the task required at least two individuals to be completed). After the two tubes were successfully joined, the extra silver good was carefully applied at the joint along the circumference to ensure that the reactor was well sealed. The curing period for the anti-seize is 24 hours at room temperature, and 3 hours when conducted at 360 °C. Since the whole assembly would take more than 24 hours, the research team opted for the curing at room temperature.



Figure 4.4 Illustration of the assembled vacuum distillation reactor. 1) 2.75" OD tube, 2) 3.00" OD tube, 3) copper cooling coil found on both sides of the reactor, 4) type k temperature reader, 6) cold trap, 7) needle valve used for pressure control, 8) vacuum gauge, 9) ball valve, 10) recirculating oil filter, 11) vacuum pump.

As per the SOLIDWORKS design shown in figure 4.1, the left cover was machined to house ports for the furnace and the sample thermocouple, and the gas inlet port. Half inch National Pipe Tapered (NPT) threads compression fitting were used for the thermocouple slots. The furnace thermocouple tube connection was one quarter inches bored through while that of the sample thermocouple was three sixteenths of an inch bored through as well. As such, the mullite sheathes dimensions were chosen respective of the application. The gas inlet tube was connected to an SS304 elbow compression fitting which was in turn connected to a quarter turn plug valve. The valve was connected to the argon tank via a one-half inch fiber reinforced PVC tube. Ungrounded type K thermocouples were obtained from Omega engineering; the dimensions were one eighth of an inch and one sixteenth of an inch for the furnace and sample thermocouple respectively. The right cover was machined to house a gas outlet tube, and the cold finger. The gas outlet tube was also connected to an SS304 elbow fitting that was connected to a quarter turn valve. From the valve, a clear polypropylene tube was connected and went to the water scrubber. The cold finger outer and inner tubes' dimensions were one inch and half an inch respectively

Vacuum distillation experiments were run according to the following procedure:

1. Open the cooling water circuit for both the condenser (cold finger), and the tube cooling; start by slightly opening the outlet valve, then open the inlet valve. A satisfactory flow is obtained when the valve level makes a 30 degrees approximate angle with horizontal. Allow the flow to stabilize for about 10 minutes.
2. Meanwhile, accurately weight the sample to be used in the experiment and record the weight. Place the sample in the sample boat.

3. Load the sample boat in the furnace. The sample boat was designed such that it implemented a hole that has the inside diameter equal to the outside diameter of the SAMPLE thermocouple protective mullite tube. Insert then the mullite tube into the whole in the sample tube and use it as a guide for positioning the sample boat further inside the tube; make sure to support the weight of the boat on the thermocouple with your hand until the boat sits on the bottom of the tube, then slide it in.
4. Going over to the opposite end of the tube, use a light source to inspect the position of the boat, and check if it slid back allowing the sample thermocouple sheath to go beyond 0.5 inches. If yes (which will be the answer most of the times), then use the hooked aluminum bar to slightly pull the boat towards you until approximately 0.5 inches of the SAMPLE thermocouple extend out inside the boat.
5. One way to know if the boat is sitting correctly on the bottom of the tube is by observing the plane of the thermocouple connectors. If the plane is parallel to the bench's surface, then you have positioned the lid well. Close the left side and fasten the bolts.
6. Insert the cold finger in the furnace. A good position of the lid can be inspected by looking at the Argon exit valve. If perpendicular with the vacuum port on the tube, then you have positioned the lid well. Close the lid and fasten the bolts. At this point the vessel should be sealed.
7. The tube may have rotated during fastening of the bolts. Check that the thermocouple connections' planes are parallel with the bench, and that the vacuum port is normal to the bench. Make the necessary adjustment before proceeding further.

8. Open both the inlet valve and the outlet argon valve; turn the argon flow to 1.0 L/min. If the vessel was correctly sealed, you should see bubbling in the water scrubber. Purge the system for 3 minutes after which you will close the outlet valve.
9. Pressurize the system to a pressure such that ΔP is approximately $0.30E4$ Pa. Next, stop the Argon flow and close the inlet valve.
10. Turn on the vacuum pump and let it draw vacuum until you see a stable reading (usually between 1.4 and 2.45 Pa; record the duration of this process.
11. Using the needle valve located vacuum system line, adjust the pressure (counterclockwise turn to increase the pressure in the range of 5.25 to 5.65 Pa.
12. Switch the circuit breaker ON and turn ON the furnace
13. The furnace will not heat up when the over temperature control (OTC) alarm is not disarmed. To disarm the alarm, press the program button to scroll the menu until "All" appears. Then press the button until "ctl" appears, then press the same button again. Until the "all" light turns off. Once the alarm is off, turn the furnace ON by pressing the green button
14. On the controller, press the program button until you see "Prog List," then hit the button until you see "tgt" and set the target temperature to the experiment temperature. Type B and type K have a temperature difference of approximately 20-30 °C, to set the target temperature higher to compensate for that.

15. Hit the “run/hold” toggle button and check that the “run” light is on. Time the heating process and record the type B and type K sample every 10 minutes.
16. Once the temperature reading reaches the target temperature, hit the “run/hold” button such that the “hold” signal is lighted up. Wait for the type K temperature reading to stabilize.
17. If the type K temperature stagnate at $T_{\text{tgt}} < T_{\text{B}}$, increase the type B temperature by 5 to 10°C and run until the type B reaches the target temperature. This pint marks the $t = 0$ -time stamp. Record T_{B} , T_{sample} and P_{sys}
18. Record the sample temperature and the system pressure at 3 minutes interval for the duration of the experiment.
19. At the end of the experiment, turn the furnace OFF by pressing the red button. Leave the pump running until the type B reading gets to approximately 350°C at which point, turn off the pump, and the cooling water circuit. Turn off the circuit breaker.
20. Once the furnace cools off to room temperature, proceed to collect the distillate and residue fraction using proper PPE.

4.2 Alloy Preparation and Casting

For convenience and simplicity of the study, vacuum distillation experiments were to be carried out using samples prepared in the laboratory. In order to evaporate a substantial amount of distillate fraction to generate accurate results during chemical analysis, the sample size was set at 150 grams. Oxidation of the impurities of interest and lead is spontaneous, hence the need of

an inert atmosphere during the preparation process. Nitrogen and argon are two most common inert gases used.



Figure 4.5 Alloy preparation and casting setup. 1) crucible furnace, 2) lead melting pot, 3) type K thermocouple reader, 4) argon distribution point, 5) funnel for argon blanketing, 6) scrubber, 7) HEPA filter dust and fume collector.

Across the many fields in which inert atmosphere is needed, there are many reasons that governs the choice of nitrogen over argon and vice versa and it can be concluded that the choice is mainly depended on 1) the application and 2) the budget. First, both nitrogen and argon can create an inert atmosphere, hence they are both good candidates for displacing air. Second, nitrogen is cheaper to acquire compared to argon; consequently, it is favored most of the time, especially when the application is displacement of air or oxygen only. Third, argon is denser than nitrogen, which means that reaction blanketing is more effective when using argon. Finally, nitrogen reacts with many alloys to form nitride while argon is completely inert. On these

grounds, ultra-high purity (UHP 5.0) argon gas was selected as the gas for the creation and/or maintenance of an inert atmosphere.

4.2.1 Alloy Preparation

A Lindberg crucible furnace with the rated at 1100°C and equipped with a type K thermocouple for temperature measurement was used for the preparation of alloys (fig. 4.5). The sample needed to be homogenous so that analysis of the solid sample on either top or bottom faces would be within acceptable error; therefore, the melt should be well mixed. Collection of the batch sample would be done only after the furnace has cooled down to room temperature. Adding mixing capability would have resulted in the sample being stuck on the stirrer; therefore, the melting the sample for casting would be a challenge. Consequently, no stirring was applied; however, a higher temperature of preparation was selected in order to enhance the diffusion of the solute (the impurity) in the solvent (lead metal). Graphite crucibles were used for the preparation of the various alloys, a new crucible being used per alloying element to avoid cross-contamination. The crucible had an outside diameter (OD) of four inches and a height of four inches.

Individual metals powders and/ or granules were obtained in order to prepare the synthetic samples. A maximum of 2700 to 2800 grams of lead could be filled inside the graphite crucible in its granular form; consequently, a single batch of alloy could yield 18 samples after casting with the targeted sample size. Because the impurities of interest were obtained in a fine powder form, they would have been susceptible to be entrained and blown out of the reactor chamber by argon. To remediate to the issue, a sandwich layering configuration was adopted as

shown in figure 4.2. The accurately weighed lead metal was divided into three portions; one third of which was thoroughly mixed with the accurately weighed fraction of the impurity.

Table 4.2 Pure metals used for the preparation of synthetic alloy samples

Element	Manufacturer	Form	Purity (wt. %)
Pb	Alfa Aesar	+ 30 mesh granules	99.99
As	Beantown Chemical	- 20 mesh powder	99
Sb	Sigma Aldrich	- 100 mesh powder	99.5

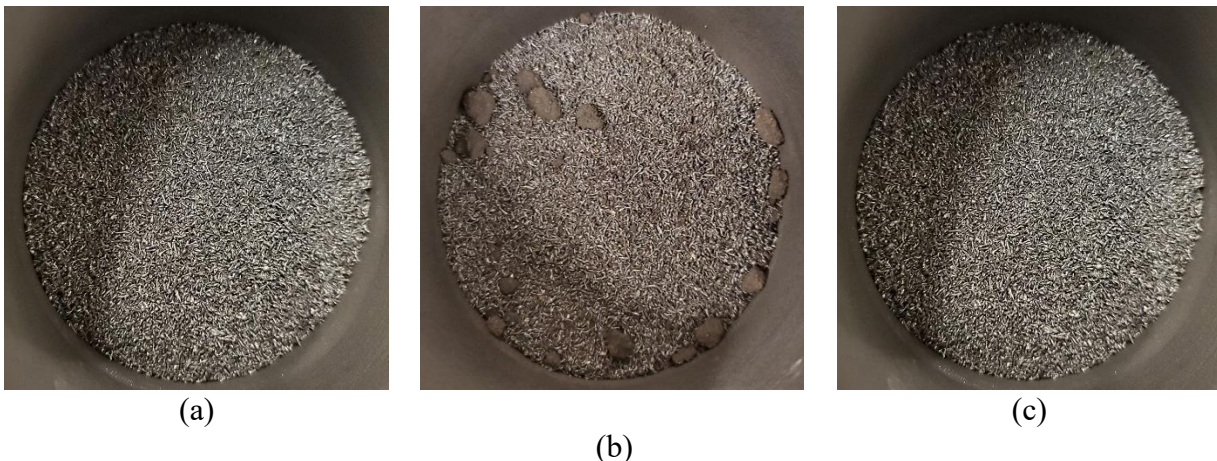


Figure 4.6 Sandwich configuration of the batch alloy. a) bottom layer comprised of lead metal, b) middle layer comprised of a mixture of lead and the impurity, c) top layer comprised of lead metal

The procedure for alloy preparation is as followed:

1. Accurately weight the target masses for lead and the impurity of interest. Split the lead mass in three different fractions
2. First layer the first fraction of the lead mass in the flat bottom crucible.
3. To the second fraction of lead, add the mass of the impurity of interest, and thoroughly mix the two. Add the mixtures to the crucible.
4. Finally, add the last fraction of lead to the crucible.

5. Place the crucible in the reactor chamber and seal it not forgetting to use the graphite gasket.
6. Place the reactor chamber inside the furnace, and turn on argon flow to 0.2 L/min. If the reactor is well sealed, bubbling will take place in the scrubber cylinder. Allow the argon to displace oxygen for 3 minutes.
7. Turn on the furnace and adopt a step size heating cycle. First heat until 650 °C, then 850 °C, and finally to 1000°C. The average duration of heating in the first segment is two hours. It takes another hour and a half to reach T2. Finally, let the sample sit for another hour and a half with T3 as the target temperature.
8. After 5 hours total running time, turn off the furnace and allow it to cool down.
9. Remove the reactor chamber from the furnace, open it and remove the crucible.
10. Accurately weight the resulting alloy and collect a representative sample from it prior to the casting process.

4.2.2 Alloy Casting

A Lyman 25 lead melting pot was utilized to cast samples. To accommodate the molding block dimensions for ease of casting, the storing shelves were removed as shown in figure 4.7. The argon blanket was established above the melt with a flow of 0.5 L/min. the melting point of lead being 327°C (621 °F), the melting pot was set at 750°C. The casting process requires two individuals to be completed for safety reasons (wear the appropriate PPE for the process).



Figure 4.7 Remodeling of the lead melting pot for the casting process

The procedure for the casting process is as followed:

1. 5 hours prior to the casting process, turn on the Deltech furnace with the molds inside.
Start the heating cycle. The heating rate is set at 2 °C/ minute, so it will take 4 hours and 30 minutes for the molds to reach a temperature of 500 °C.
2. Turn on the HEPA filter fume extractor and place the suction duct by the top of the melting pot.
3. 15 minutes before the molds reach their temperature, set the argon flow to 0.5 L/min and commence the melting process
4. Accurately weigh the alloy batch and place it in the lead melting pot. Turn on the pot and set the temperature to 750 °F. Waiting until the alloy is fully melted, then use a glass stirring rod to thoroughly mix it.
5. Once everything is ready, Operator 1 will open the door to the furnace while Operator 2 will grab the hot molding block, travel with it and position it at the melting pot opening port.

6. After closing the furnace door, Operator 1 will make his/her way to the casting station and open the pouring port; pouring can then take place. Since the process is not automated, visual inspection of the fill line is the only criteria for Operator 2 to call the opening and closing of the port.
7. The molding block has two slots for casting. Once the first slot has been filled, operator 2 calls the closing of the pouring port to operator 1, then places the block on the refractory block, rotates the block and grabs it again to pour into the second slot.
8. Once both slots have been filled, operator 2 shall place the block onto the refractory block to allow the sample to slightly solidify before putting it on the concrete floor where it will air cool.
9. Repeat steps 5 to 8 until the entirety melt has been cast.

4.3 Chemical Analysis

A combination of analytical techniques were employed for the analysis of feed, residue, and distillate samples; the rule of thumb was that solid samples were to be analyzed via arc spark OES while powder or shard samples were to be analyzed via atomic absorption spectroscopy (AAS) or Inductively-Coupled Plasma- Mass Spectrometry (ICP-MS). The following subsections detail principles for each analytical technique.

4.3.1 Sample Preparation and dilution

Common digestion methods for powder (or more accurately phrased, soil) samples include nitric acid (HNO_3), aqua regia ($\text{HNO}_3 + \text{HCl}$) cold or hot, borate fusion ($\text{LiBO} + \text{LiBO} + \text{KBr}$), and total dissolution ($\text{HNO}_3 + \text{HCl} + \text{HF}$). In the present study, the alloy samples do not contain silicates or complex oxides that would require the use of HF. Additionally, most salts of

lead (lead being the predominant element in the alloy samples) are insoluble in water; consequently, a nitric acid digestion was employed. For the distillate fraction that was larger than 1.000 gram, a representative sample was obtained by quartering after a thorough mixing. For fraction less than 0.500 gram, the whole sample was digested for analysis. Shards of samples were obtained from all surfaces of the feed and residue samples; the pile was well mixed, then quartered to obtain a representative sample. The sample preparation procedure used in the present research is as followed:

1. Accurately weigh roughly 0.5000 grams of representative sample whenever possible and transfer the content in a 150 ml beaker with a magnetic stirrer.
2. Add approximately 50 ml of 30 wt. /vol % nitric acid (HNO_3) to the beaker and cover it with a watch glass. Place the beaker on a hot plate at 110 °C, and 500 rpm mixing speed.
3. Once you observed complete dissolution of the sample, remove the baker from the hot plate and let it cool down to 50 degrees, or when the amber color disappears.
4. Obtain a 100 ml graduated cylinder, a glass funnel, and a grade 54 filter paper (folded for filtering)
5. Pour the leachate in the funnel until the magnetic stirrer is exposed to air. At this point, use a magnetic bar to extract the stirrer; rinse the stirrer inside the beaker. Pour the remaining solution into the funnel and rinse the beaker into the funnel.
6. After the leachate has filtered, spray the filter paper some more to insure complete collection of the sample. Let the rinse filter as well. Remove the funnel from the cylinder, read and record the solution volume.
7. Clean the beaker, stirrer, and funnel and repeat steps 1 to 6 for the next sample.

4.3.2 Arc Spark Optical Spectroscopy (Arc Spark OES)

Spectroscopy is the study of absorption and emission of energy by atoms, molecules, protons, ions, electrons relative to their interactions with light. Based on the Bohr's atomic model, atoms have specific energy levels for its electrons. As such, interaction of interaction between mater and light is either through absorption or emission (Thompsen, 1996). When energy is supplied to an atom, one of its electrons will transitions to a higher energy level with an excitation energy matching that of the energy supplied. The excitation state being extremely short, the electron will return to ground state by forgoing the excitation energy in the form of an emitted light. The quantification of the emitted energy and its relation to the element being analyzed can be done using optics, which is the case of the present study. Another factor of importance is the source of excitation, which in this case is sparking.

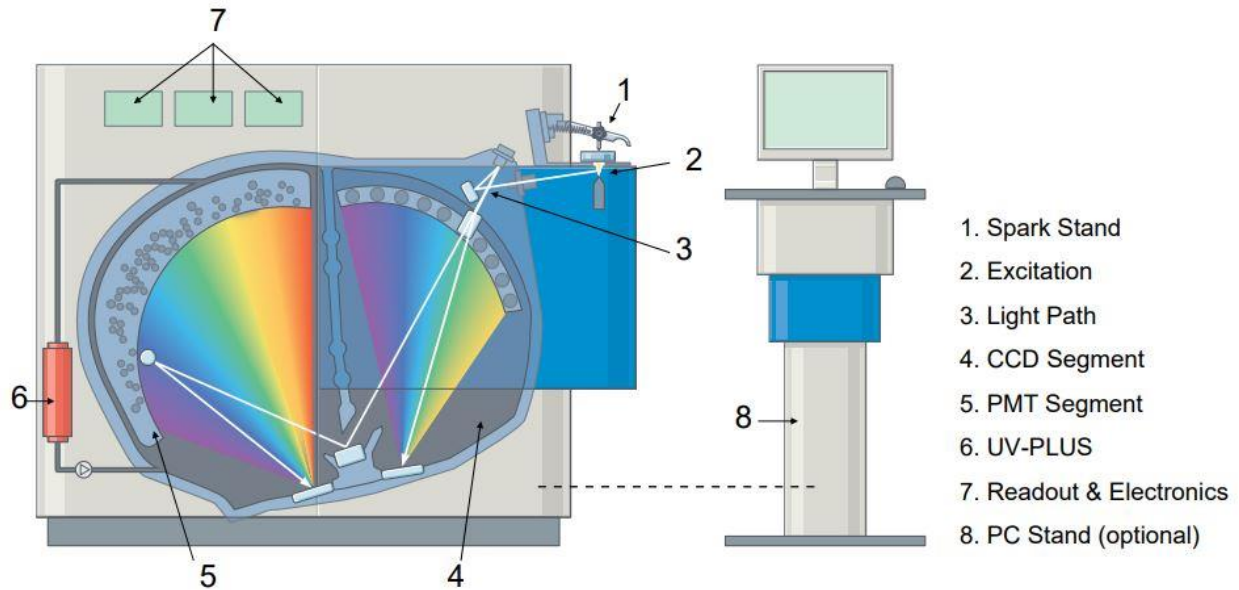


Figure 4.8 Schematic of a hybrid optics arc/spark OES (Spectrolab, 2016)

For the purpose of this research, an Arc/Spark Optical Spectroscopy (spark OES) from SPECTROLAB was used. Arc/Spark OES is known as a non-destructive method of analysis (Mogorosi, 2013). A typical OES analyzer consists of an excitation source, an optical system, and a computer read out system (Thompsen, 1996, Vizcarra, 2018). Figure 4.8 shows a schematic of an arc/spark OES. An electric discharge is created between the sample and the tungsten electrode. A minute fraction of the sample surface is obliterated, thus producing atoms in an excited state. Upon their return to ground state, the different atoms in the sample emit light at different wavelengths which then pass through the double slit entrance. One light path is directed in the CCD segment; the light is directed onto a grating (diffraction mirror) through which it is dispersed into its different spectral lines (different wavelengths) which are extracted and analyzed against reference spectral lines in the software. Another light path is directed to a reflective mirror which directs the light into the photo-multiplier tubes (PMT) segment; the reflected light is in turn reflected on the opposite side of the optic onto another grating which disperses it into different wavelengths. Detectors such as the photomultiplier tube are electronic devices (vacuum tubes) that measure the absence or presence of the incoming light spectrum (Shimadzu, 2019). It converts the light intensity from the extracted spectrum into an electric signal which is collected by the read-out system, and eventually used in the quantification of each element in the sample.

For accurate analysis the sample surfaces are milled, and the freshly prepared surface should not be touched until the analysis is complete. The procedure for an analysis on Spark OES is as follows:

1. Inspect and ensure that the water in the filter system is at the right level, and that the filter cartridge is still serviceable (replace if need be). Also check and ensure that the spark stand, and the electrode are clean prior to analysis.
2. If the instrument has been dormant for more than a week, turn the plasma on 24 hours prior to the analysis so that the instrument acclimates itself. In other case, warm up the instrument for about 2 hours prior to analysis.
3. Open the OES software and log into the “Operator” tab. Once logged in, an initialization step will automatically occur. A pop-up window might appear signaling the need to purge the system with argon for a fixed amount of time. Click yes, and let the purging occur simultaneously with the warmup.
4. While the instrument is warming up, make sure that the control samples and the global standardization samples are prepared as well as the unknown samples. Conduct the appropriate milling procedure if need be.
5. Select the method for which the control samples have been entered and analyzed.
6. In the analysis tab, select the control sample test icon. A pop-up window will appear with the control standard samples set for the chosen method. Select the first sample to initiate analysis. Place the Control sample onto the spark stand and lower the clamp onto the sample to make establish an electrical contact with the sample. If the electrical contact is not well defined, or if one worries about wearing off the surface containing the sample label, a metallic razor or a coin can be used between the sample and the clamp. As long as the sensor does not recognize the electrical contact, the software will not allow the analysis to go through.

7. Click on “analyze single” or press F2 to initiate the first burn. Each burn takes about 30 seconds, and a minimum of three *good* burns are required for the analysis. After three burns, toggle between the statistics and initial burns concentrations using F4 and F6. To remove a *bad* burn from the statistical analysis, hit the “delete” button on the keyboard. To reinsert it back, hit Shift+Insert on the keyboard.
8. Once you obtain the good burns and achieve a reasonable RSD level for each element, accept the analysis. The pop-up window will reappear for the selection of the next control standard.
9. Repeat Steps 6 to 8 until all control samples are run
10. At the conclusion of the control sample tests, a message will appear notifying the operator whether the instrument has passed the test or not. If the control sample test is passed, proceed to analyze the unknown samples.
11. If the instrument does not pass the control sample test, a global standardization must be performed. After that, rerun the control sample test. If the global standardization was carried out expertly, the control sample test will be passed, and the unknown samples can be analyzed.
12. The OES will give the concentration of traces in the base alloy, and the major component’s concentration is report as the balance.

4.3.3 Flame Atomic Absorption Spectroscopy (FAAS)

Flame atomic absorption Spectroscopy (FAAS) is an analytical technique commonly used to determine metals down the ppm levels. The liquid sample is introduced in the instrument through a nebulizer. The nebulizer sprays the sample solution thus forming droplets. The droplets are heated up to drive off the solvent leaving behind the analyte in the form of a dry

aerosol which enter the flame. A Hollow cathode lamp (HCL) or an electron discharge lamp (EDL) are used as the light source. The lamp provides an energy wave corresponding to a specific wavelength. Every element has a specific energy spectrum; therefore, only the element with one of the light source energies will absorb that energy provided by the lamp. The absorbance of the sample is then correlated to the metal concentration in the solution sample.

4.3.4 Inductively Coupled Plasma Mass Spectrometry (ICP-MS)

Inductively coupled plasma mass spectrometry (ICP-MS) is the method most commonly used for trace analysis due to its lower detection limits that ranges from parts per trillions (ppt) to lower parts per billions (ppb). For the purpose of this research an iCAP-Q ICP-MS from Thermo Fisher Scientific was utilized. To enhance the sensitivity of the analysis, Kinetic Energy Discrimination (KED) was used as the collision cell. The use of KED mode was particularly important for precise and accurate analysis of arsenic. Lead analysis using ICP-MS has been shown to produce numbers that are biased down when only a single isotope is measured for. According to a report on lead determination by Eastern Research Group (Eastern Research Group, 2010), lead is reported as isotope 208; however, isotopes 206, 207 and 208 should be measured account for the variabilities of lead isotopes in nature. An interference correction is then applied to isotope 208 as shown in equation 4.1.

$$(1.000) (^{206}\text{Pb}) + (1.000) (^{207}\text{Pb}) + (1.000) (^{208}\text{Pb}) \quad (4.1)$$

CHAPTER FIVE

VAPOR LIQUID EQUILIBRIUM PREDICITONS

As mentioned in chapter 3, the determination of the binary parameters required knowledge of the experimental activity and activity coefficients of each component, especially the activity coefficient at infinite dilution for ease of calculation. For the MIVM, certain physico-chemical properties are required. Chapter 5 will present results of the predictions on VLE. Section 5.1 will present results for the Pb-As system while section 5.2 will show those for the Pb-Sb system. Each section will show the temperature vs. composition diagram, the vapor composition vs. liquid composition diagram at fixed pressures, and the kinetics of removal of the impurity.

5.1 The Pb- As Binary system

5.1.1 VLE Temperature - Composition Diagram

For arsenic, the concentration range of interest is 0.1 to 3.1 wt. % which translates to a mole fraction range of 0.0028 to 0.0183. Using the coefficient of the Clausius-Clapeyron equation (table 3.2), the normal boiling point as well as the calculated boiling points at 5, 10, 15, and 20 Pa were calculated for both lead and arsenic; the results are shown in table 5.1. As shown in the table, the boiling point of lead at 5 and 20 Pa is 780 and 854 °C respectively; that of arsenic is 274 and 615°C. If pure lead metal were to be heated up at 20 and 5 Pa, the first vapor particle should form at 854 and 780 °C respectively. Similarly, pure arsenic metal heated under

the same pressure conditions should start forming the first vapor particle at 305 and 274 °C respectively. A well written algorithm should yield these numbers at $x_{As} = 0$ and 1.0.

Table 5.1 Boiling point of lead and arsenic as a function of pressure

Pressure (Pa)	Pb boiling Point, Tb		As boiling Point, Tb	
	(K)	(°C)	(K)	(°C)
103325	2016	1743	888	615
20	1127	854	578	305
15	1111	838	571	298
10	1089	816	562	289
5	1053	780	547	274

The calculations of the T-x-y diagram were performed with a composition increment of 1.0×10^{-6} , and algorithm converged after sixteen iterations. Figure 5.1 shows the T-x-y diagram for the Pb-As system using the MIVM; the red rectangle illustrates the concentration range of interest. The diagram is deemed well calculated within error of γ_{As} and γ_{Pb} because one can observed the predicted boiling points of the pure metal which were shown in table 5.1.

According the diagram, the required distillation temperature decreases with decreasing distillation pressure for the same liquid mole fraction. Thermodynamic suggests that the required distillation temperature for the concentration range of interest is between 340 and 440 °C (513 and 613 K) across the 5–20 Pa pressure range.

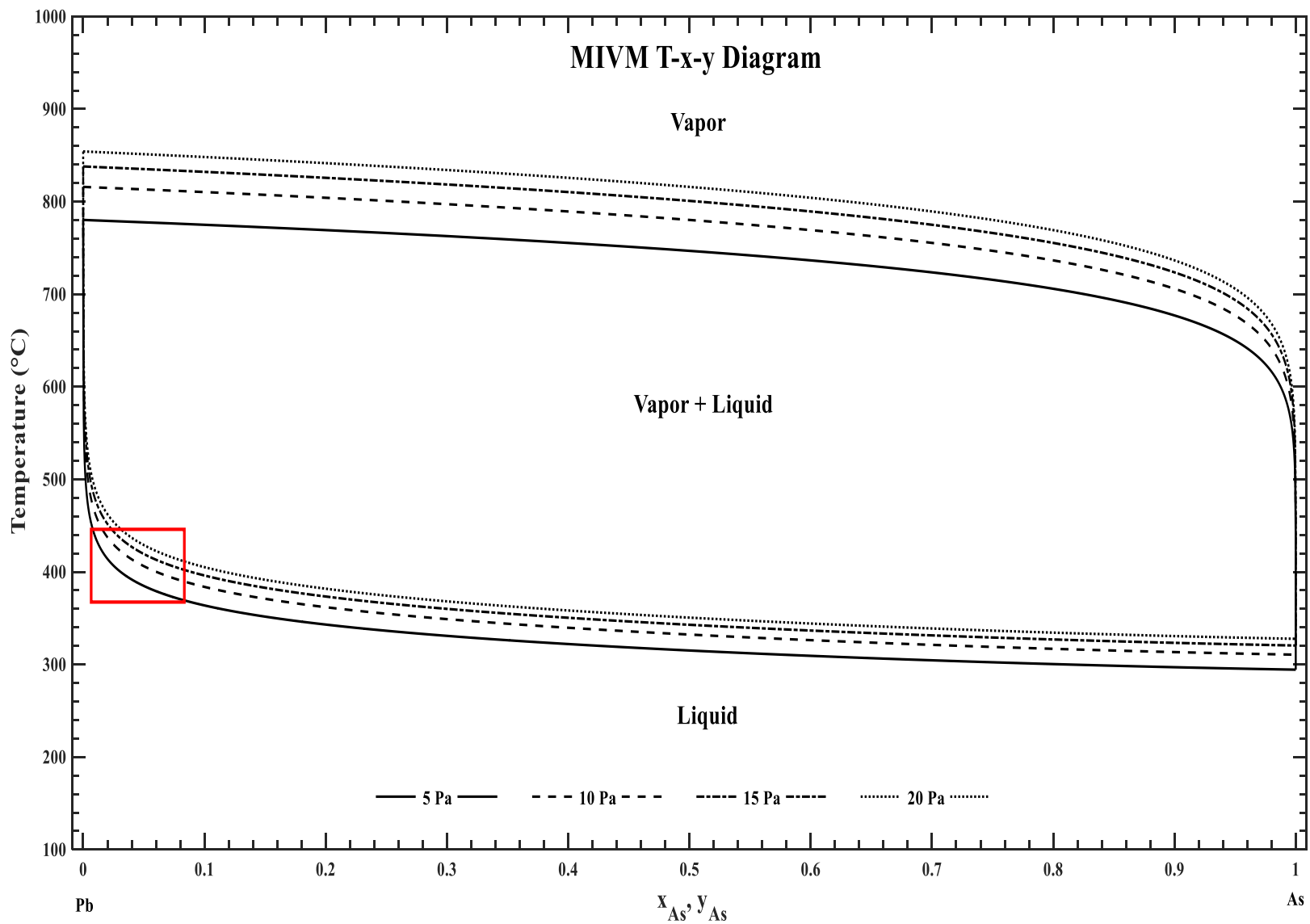


Figure 5.1 T-x-y diagram for the Pb-As system using MIVM between 5 and 20 Pa

A comparison between the three models was undertaken. Results for the Wilson and NRTL models are shown in figures 5.2, and 5.3 respectively. For these two models the algorithm converged after eight and eleven iterations respectively. Results obtained from the three models agreed with each other regarding the prediction of the temperature vs. composition diagram of the Pb-As binary system. Because most of the literature findings were conducted using the MIVM, subsequent predictions in the present research was also conducted using the same model to better corroborate with other researchers results. Unfortunately, to the author's knowledge, no studies have been conducted exclusively on the Pb-As system to allow comparison with results in the present research. More research needs to be conducted to compare with the research team's findings.

5.1.2 VLE Composition Diagram for Arsenic

Figure 5.4 shows the correlation of the equilibrium arsenic content in the vapor phase to its composition in the liquid phase. In the 340 to 440°C range, arsenic content in the vapor phase is greater than the 5N grade. Figure 3.1 shows that the volatility of pure arsenic is much higher than that of lead; consequently, there is a higher thermodynamic drive for the vaporization of arsenic despite its low activity in the melt. As such, the vapor phase obtained from the distillation process will almost entirely be comprised of arsenic. Also shown in the figure is the fact that the arsenic content on the vapor phase decreases with increasing temperature for the same liquid phase content. An increase in temperature increases the likelihood of lead vaporization as well, thus it can be concluded that running a distillation test at higher temperatures would result in an increase in lead content in the vapor phase. The kinetic study will shine light on this claim.

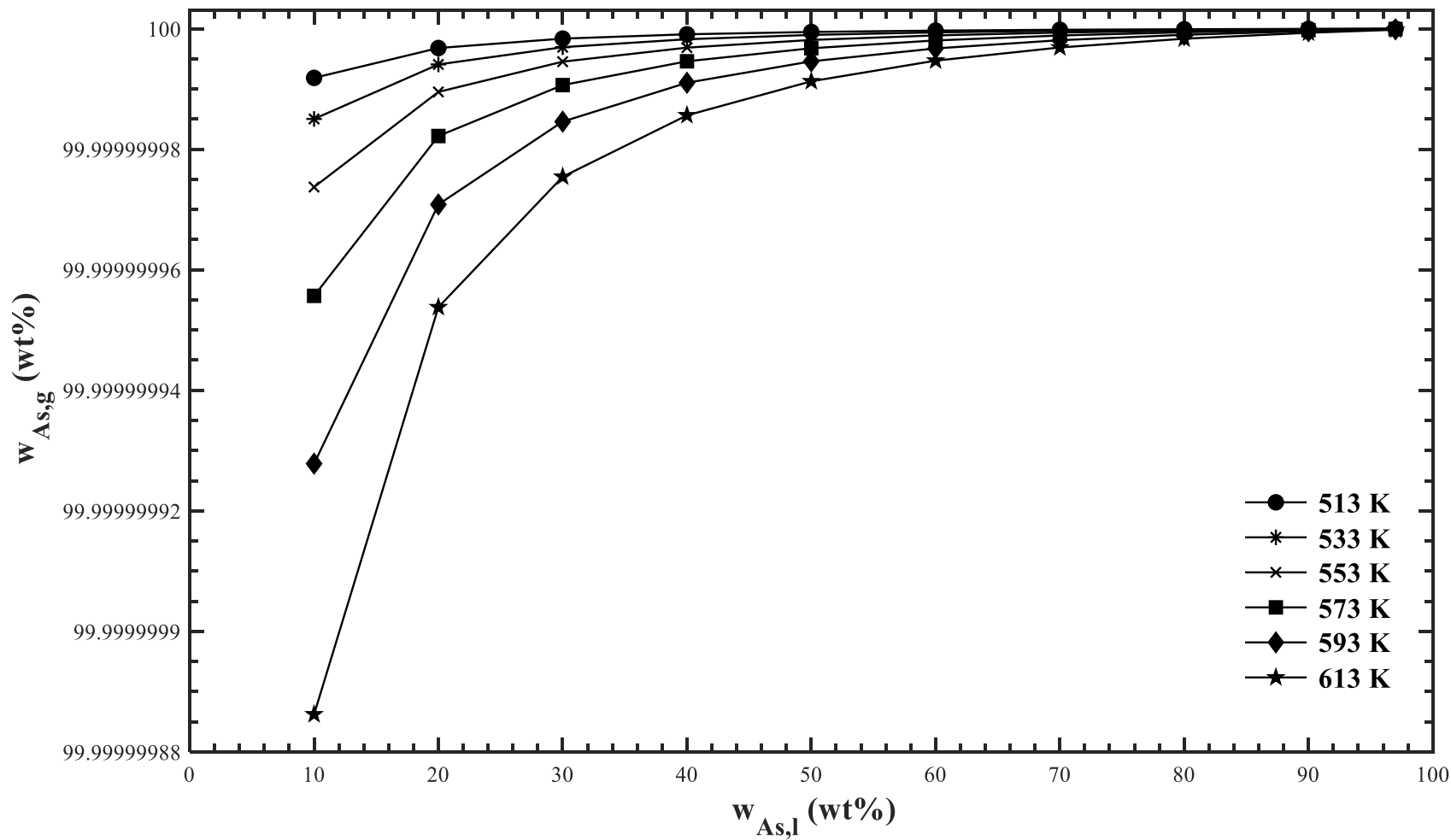


Figure 5.4 VLE composition for the Pb-As binary system at 5 Pa in the temperature range of 340 and 440 °C

5.2 The Pb-Sb Binary System

5.2.1 VLE Temperature – Composition Diagram

For antimony, the concentration range of interest is 0.8 to 5.2 wt. % which translates to a mole fraction range of 0.014 to 0.09. Like for the Pb-As binary system, the mole fraction increment was set at 1.0×10^{-6} , and the algorithm for the MIVM converged after 10 iterations. Figure 5.5 shows the T-x-y diagram for the Pb-Sb using the MIVM. As expected, the required distillation temperature decreases with decreasing distillation pressure. Thermodynamics suggests that in the pressure range of 5 to 20 Pa, and for the concentration range of interest, the required distillation temperature varies between 460 and 600 °C; the VLE composition was predicted in the temperature range of 400 to 600 °C.

The Wilson and NRTL models' algorithms converged after 10 and 11 iterations respectively for the prediction of the T-x-y diagram (figure 5.6 and 5.7 respectively). Once again, the results agreed with each other, and the MIVM was chosen to conduct further predictions for ease of comparison with existing experimental findings. One aspect worthy of notion between the Pb-As and the Pb-Sb binary systems is the temperature required for the first vapor particle to form. For example, a binary alloy with 0.1 mole fraction arsenic needs only be heated to 320 °C for the first vapor particle to form at 5 Pa. Should the same conditions be applied to a binary Pb-Sb alloy, the first vapor particle will form at 460 °C. This fact can be used as for inference on the selectivity of the distillation process pertaining to arsenic and antimony removal should these impurities be present together in the bullion.

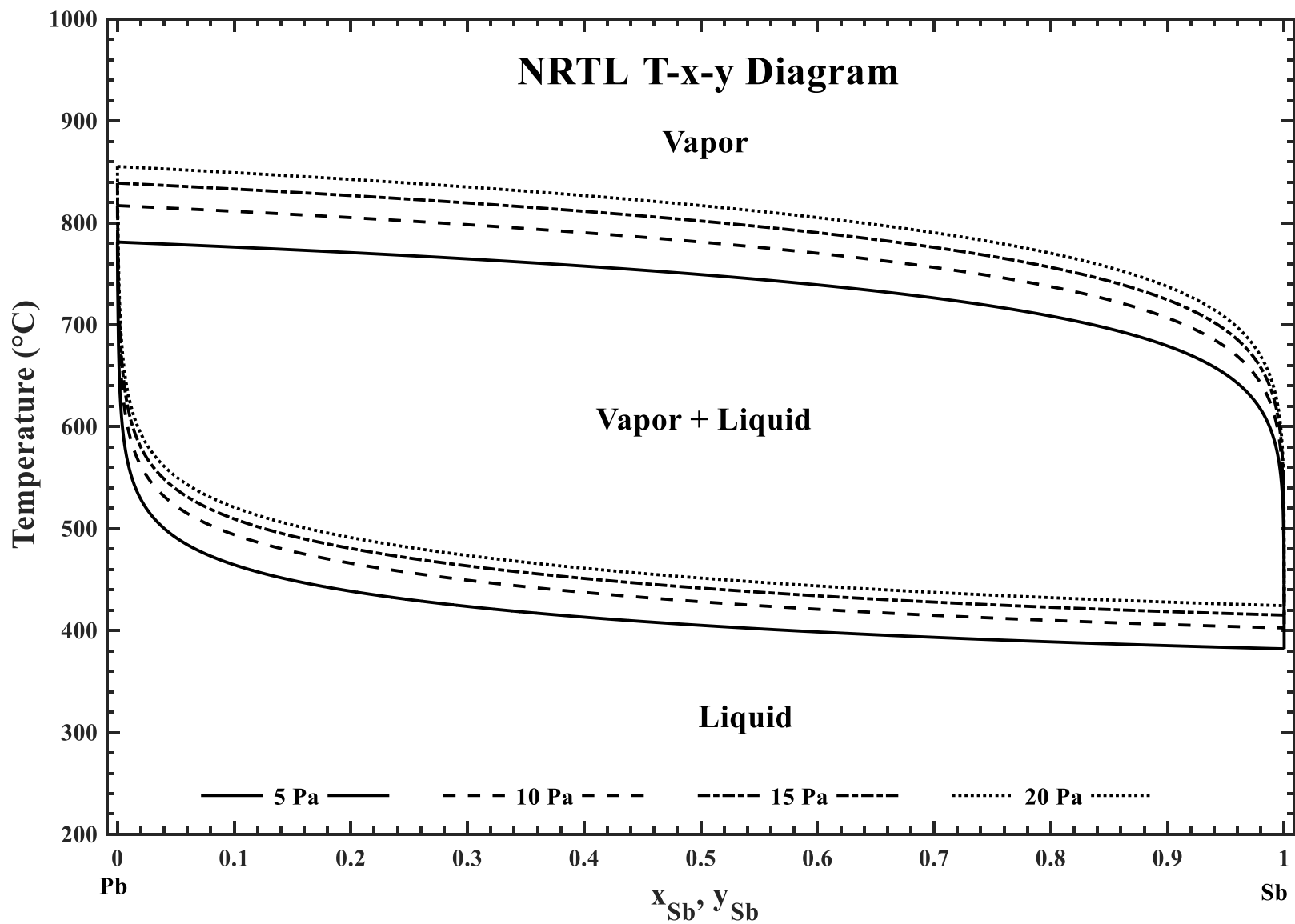


Figure 5.7 T-x-y diagram for the Pb-Sb system using NRTL model between 5 and 20 Pa

5.2.2 VLE Composition Diagram for Antimony

Figure 5.8 Shows the vapor composition vs. liquid composition for the Pb-Sb binary system at 5 Pa in the temperature range of 400 to 600 °C. According to this figure, the vapor phase obtained through distillation under the conditions mentioned above, will contain more than 99.0 wt. % antimony. The figure also shows that the antimony content in the vapor phase decreases with increasing temperature. The inscribed diagram shows data for the composition within the concentration range of interest. For example, an alloy with 2.0 wt. % antimony in the liquid phase will be in equilibrium with a vapor phase at 99.98 wt. % antimony at 400 °C while it would in equilibrium with a vapor phase containing 99.76 wt. % antimony at 600 °C.

CHAPTER SIX

RESULTS AND DISCUSSION

Chapter six presents the results of the distillation experiments that were conducted.

Section 6.1 shows results for the Pb-As binary system, and section 6.2 shows those of the Pb-Sb system. In the case of the Pb-As system, considerations for the adjustment of binary parameters using experimental results is presented in section 6.1.6. The use of a stainless-steel brush was important to collect the vapor phase (distillate) because a large fraction of it condensed on the walls of the reactor; consequently, it is expected that some material from the brush and the tube would transfer to the distillate. The mass balance was then set such that the composition of the feed and product fractions were used to calculate that of the distillate fraction.

6.1 The Pb-As Binary System

6.1.1 Lead-Arsenic Binary Alloys

For the first trial of Pb-As alloy preparation, 2800 grams of sample at 3.1 wt. % arsenic target was accurately weighted and placed in a gallon polypropylene bottle. The bottle was thoroughly shaken for 5 minutes to achieve homogeneity in the powder to be melted then it was transferred in the melting pot. A six inches funnel was used to create an argon blanket above the melting pot as shown in figure 6.1a, and the flow rate of argon was set at three liters per minute. The fume extractor was set slightly above the melting pot to protect the operator from breathing

in potentials fumes.



Figure 6.1 First alloy preparation trial; a) melting pot setup, b) trial 1 product

Observations made during the first alloy preparation trial are as followed:

1. Using the pure metals in fine powder form presented a higher health risk due to inhalation of the dust during the transfer of the well mixed powder to the melting pot. The use of shots became highly beneficial.
2. While the melting pot was set to 650 °F, half of the content therein melted while the other half floated to top still in the powder form (see figure 6.1b). The use of a spatula only resulted in the melted alloy temporarily covering the powder before it trickled back down to the bottom of the pot or formed a pool of top of the un-melted powder. No additional melting was achieved, and an increase in temperature up to 800 °F only increased the oxidation rate of the liquid pool that migrated to the top during mixing.

3. A thin layer of white deposited on the funnel which we inferred was arsenic trioxide before of its color, and the high volatility of arsenic and arsenic oxide, thus the arsenic loss was significant.
4. A cast iron ladle was used to cast the molten alloy. The solidification in the ladle was instant which resulted in the loss of alloy in the opening of the ladle. It was concluded then that pouring would have to be done directly in the casting mold. Hence the melting underwent modifications to the final state showed in figure 4.7.

Based on the observations made during the first alloy preparation trial, Changes were made to the setup to include a graphite crucial furnace to prepare the alloy in a better controlled atmosphere as shown in figure 4.4. From that point on, three Pb-As alloys were prepared, and the details are shown in table 6.1. A chemical analysis was conducted for each alloy prior to the casting process.

Put together the three alloys weighed 2729.45 grams prior to being melted. After being thoroughly mixed, the sample were cast following the procedure mentioned in section 4.2.2. Eighteen samples were cast from this batch and the total weight amounted to 2676.70 grams, which means that a 1.93 wt. % loss was incurred. Because visual aspect was the only criteria of sample filling in the mold for the research team, the samples weights somewhat significantly across the entire batch. The first batch's chemical analysis was conducted using Arc/Spark OES and is shown in table 6.2.

Table 6.2 Chemical composition of Pb-As alloys batch 1 by CSM

Sample ID	Analyte Concentration (wt. %)						
	Sn	Sb	Bi	Ca	Cu	P	Fe
Sample 2	0.0003	0.0055	0.0022	0.0018	0.0063	0.0086	0.0009
Sample 3	0.0004	0.0053	0.0022	0.0018	0.0059	0.0085	0.0007
Sample 4	0.0005	0.0044	0.0019	0.0019	0.0052	0.0062	0.0008
Sample 5	0.0003	0.0052	0.0021	0.0019	0.0054	0.0089	0.0007
Sample 6	0.0005	0.0052	0.0021	0.0020	0.0063	0.0071	0.0007
Sample 7	0.0005	0.0048	0.0019	0.0020	0.0056	0.0065	0.0007
Sample 8	0.0004	0.0051	0.0021	0.0020	0.0061	0.0059	0.0008
Sample 9	0.0004	0.0056	0.0022	0.0019	0.0067	0.0068	0.0011
Sample 10	0.0004	0.0053	0.0022	0.0018	0.0066	0.0069	0.0007
Sample 11	0.0004	0.0053	0.0021	0.0019	0.0063	0.0070	0.0007
Sample 12	0.0004	0.0057	0.0022	0.0020	0.0075	0.0072	0.0011
Sample 13	0.0004	0.0050	0.0020	0.0019	0.0057	0.0068	0.0011
Sample 14	0.0003	0.0058	0.0023	0.0018	0.0073	0.0081	0.0012
Sample 15	0.0004	0.0053	0.0021	0.0020	0.0063	0.0072	0.0007
Sample 16	0.0003	0.0055	0.0022	0.0018	0.0063	0.0086	0.0009
Sample 17	0.0003	0.0047	0.0020	0.0018	0.0058	0.0065	0.0009
Sample 18	0.0004	0.0057	0.0022	0.0020	0.0065	0.0073	0.0013

Table 6.2 (Continued)

Sample ID	Analyte Concentration (wt. %)						
	S	Zn	Ag	Ni	In	As	Pb
Sample 2	0.0008	0.0002	0.0003	0.0001	0.0001	2.57	97.40
Sample 3	0.0009	0.0004	0.0002	0.0001	0.0001	2.62	97.35
Sample 4	0.0010	0.0005	0.0001	0.0001	0.0001	2.85	97.12
Sample 5	0.0008	0.0003	0.0002	0.0001	0.0001	2.65	97.33
Sample 6	0.0011	0.0004	0.0002	0.0001	0.0001	2.73	97.24
Sample 7	0.0008	0.0004	0.0001	0.0001	0.0001	2.76	97.22
Sample 8	0.0009	0.0005	0.0002	0.0001	0.0001	2.63	97.35
Sample 9	0.0011	0.0003	0.0002	0.0001	0.0001	2.95	97.02
Sample 10	0.0009	0.0004	0.0002	0.0001	0.0001	2.60	97.38
Sample 11	0.0008	0.0004	0.0002	0.0001	0.0001	2.61	97.36
Sample 12	0.0010	0.0004	0.0003	0.0001	0.0001	2.64	97.33
Sample 13	0.0008	0.0004	0.0002	0.0001	0.0001	2.67	97.31
Sample 14	0.0008	0.0004	0.0003	0.0001	0.0001	2.65	97.33
Sample 15	0.0010	0.0004	0.0002	0.0001	0.0001	2.63	97.34
Sample 16	0.0008	0.0002	0.0003	0.0001	0.0001	2.57	97.40
Sample 17	0.0009	0.0003	0.0002	0.0001	0.0001	2.65	97.32
Sample 18	0.0009	0.0004	0.0002	0.0001	0.0001	2.62	97.35

Table 6.3 Chemical composition of Pb-As alloys batch 1 by Sponsor

Sample ID	Analyte Concentration (wt. %)						
	Sn	Sb	Bi	Ca	Cu	P	Fe
Sample 3	0.0004	0.0053	0.0022	0.0018	0.0059	0.0085	0.0007
Sample 5	0.0003	0.0052	0.0021	0.0019	0.0054	0.0089	0.0007
Sample 7	0.0005	0.0048	0.0019	0.0020	0.0056	0.0065	0.0007
Sample 9	0.0004	0.0056	0.0022	0.0019	0.0067	0.0068	0.0011
Sample 11	0.0004	0.0053	0.0021	0.0019	0.0063	0.0070	0.0007
Sample 13	0.0004	0.0050	0.0020	0.0019	0.0057	0.0068	0.0011
Sample 15	0.0004	0.0053	0.0021	0.0020	0.0063	0.0072	0.0007
Sample 17	0.0003	0.0047	0.0020	0.0018	0.0058	0.0065	0.0009

Table 6.3 (Continued)

Sample ID	Analyte Concentration (wt. %)						
	S	Zn	Ag	Ni	In	As	Pb
Sample 3	0.0009	0.0004	0.0002	0.0001	0.0001	2.62	97.35
Sample 5	0.0008	0.0003	0.0002	0.0001	0.0001	2.65	97.33
Sample 7	0.0008	0.0004	0.0001	0.0001	0.0001	2.76	97.22
Sample 9	0.0011	0.0003	0.0002	0.0001	0.0001	2.95	97.02
Sample 11	0.0008	0.0004	0.0002	0.0001	0.0001	2.61	97.36
Sample 13	0.0008	0.0004	0.0002	0.0001	0.0001	2.67	97.31
Sample 15	0.0010	0.0004	0.0002	0.0001	0.0001	2.63	97.34
Sample 17	0.0009	0.0003	0.0002	0.0001	0.0001	2.65	97.32

Table 6.4 Pb-As alloy preparation weights from trial 2 to trial 4

	Trial 2	Trial 3	Trial 4
As weight (g)	20.50	51.55	60.10
Pb weight (g)	484.55	1453.5	950.45
Expected total weight (g)	505.05	1505.50	1010.55
Actual total weight (g)	494.90	1492.50	990.90
Weight loss (wt. %)	2.1	0.083	1.94
Total weight prior to final cast (g)	440.6	1385.80	903.05
Measured Concentration (wt. %)			
As	3.79	3.68	3.42
Pb	96.19	96.31	96.57

Samples 3, 5, 7, 9, 11, 13, 15, and 17 were sent out to one of the sponsors for analysis using a similar analytical technique and the results are shown in table 6.3. The difference between the two data sets was assessed using the mean average deviation (MAD), and the results for each element is shown in table 6.4. The MAD for arsenic, lead, and all other element measured was well below 0.2 wt. % which shows that the analytical techniques used by the research team was adequate.

Table 6.4 Comparison between analysis from CSM and sponsor

Mean Average Deviation (MAD)	Sn	0.0002
	Sb	0.0005
	Bi	0.0003
	Ca	0.0008
	Cu	0.0019
	P	0.0035
	Fe	0.0012
	S	0.0002
	Zn	0.0002
	Ag	0.0002
	Ni	0.0000
	In	0.0000
	As	0.1846
	Pb	0.1878

Seven samples from this batch were used in trial tests to address any issues that might have arisen pertaining to oxidation during experimenting, poor pressure control, and / or poor temperature control. A second batch was prepared to complete the number of experiments projected. 1505.15 grams pure metals with a target of 2.75 wt. % target. The collected alloy weighed 1496.80 grams (0.55 wt. % loss). Prior to casting the alloy's weight was 1496.65 grams; 10 samples were cast from the second batch with a total weight of 1437.05 g. A chemical analysis of batch 2 was conducted using ICP-MS and is shown in table 6.5. The third batch consisted of 5 samples prepared individually with a target of 0.1, 0.5, 1.0, 2.0, and 3.5 wt. %; batch 3 chemical analysis was also conducted using ICP-MS and is shown in table 6.6

Table 6.5 Chemical analysis of Pb-As alloys batch 2

Sample ID	Analyte Concentration (wt. %)				
	Ni	Cu	Bi	As	Pb
Sample 1	0.0005	0.0049	0.0413	2.57	97.39
Sample 2	0.0001	0.0315	0.0085	2.61	97.35
Sample 3	0.0005	0.0193	0.0017	2.04	97.94
Sample 4	0.0021	0.0045	0.0025	2.51	97.49
Sample 5	0.0005	0.3820	0.0029	2.46	97.15
Sample 6	0.0001	0.0108	0.0009	2.56	97.43
Sample 7	0.0000	0.0126	0.0007	2.52	97.47
Sample 8	0.0005	0.0292	0.0006	2.47	97.50
Sample 9	0.0004	0.0097	0.0005	2.46	97.53

Table 6.6 Chemical analysis of Pb-As alloys batch 3

Sample ID	Analyte Concentration (wt. %)				
	Ni	Cu	Bi	As	Pb
Sample 1	0.0011	0.0222	0.0482	0.11	99.82
Sample 2	0.0006	0.0224	0.0135	0.53	99.43
Sample 3	0.0006	0.0227	0.0094	0.78	99.19
Sample 4	0.0013	0.0243	0.0079	1.52	98.44
Sample 5	0.0012	0.0213	0.0065	3.07	96.90

A series of distillation experiments were conducted by varying the distillation pressure, distillation temperature and the initial arsenic content in the feed sample; the experimental matrix is shown in table 6.6. Based on industry advice, the study was conducted in the pressure range of 5 to 20 Pa. The distillation time was studied between 30 and 90 minutes, while the temperature was varied from 450 to 650 °C. In order to cover concentrations within and beyond the range of interest, 5 experiments were conducted at initial arsenic concentration varying from 0.2 to 3.0 wt. %.

Table 6.7 Experimental matrix for the Pb-As binary system

Test No	Pressure (Pa)	Temperature (°C)	Time (minutes)
1	20	550	45
2	15	550	45
3	10	550	45
4	5	550	45
5	5	550	30
6	5	550	60
7	5	550	90
8	5	450	45
9	5	500	45
10	5	600	45
11	5	650	45
12	5	550	45
13	5	550	45
14	5	550	45
15	5	550	45
16	5	550	45

6.1.2 Effect of Time

Table 6.8 shows the results of the effect of time. Sample loss in this batch of experiment varied between 0.45 and 1.33 wt. %. The arsenic content in the feed samples were 2.67, 2.63, 2.62, and 2.57 wt. % for tests 5, 4, 6, and 7 respectively. The calculated distillate weight is shown

in the last column; the weight of distillation with an increase in time, did not significantly increase the amount of material volatilized.

Table 6.8 Effect of distillation time on the removal of arsenic

Test No	Time (min)	Feed weight (g)	Distillate Weight (g)	Product weight (g)	Weight loss (wt. %)	Calculated Distillate Weight (g)
5	30	170.11	2.048	166.44	0.95	3.66
4	45	148.67	2.716	145.28	0.45	3.39
6	60	154.09	1.793	150.42	1.21	3.66
7	90	160.78	1.778	156.86	1.33	3.92

Figure 6.2 shows the effect of time on the arsenic content in the distillation fraction for experiments conducted at 550 °C and 5 Pa. The arsenic content significantly decreased when the distillation time was increased from 30 to 45 minutes; the concentration decreased from 85.8 to 80.2 wt. %. A further increase in distillation time from 45 to 60 and 90 minutes resulted in a gradual decrease in the arsenic content (80.2 to 79.2 and 78.9 wt. % respectively). As would be expected, the longer the alloy undergoes distillation, the more lead is allowed to evaporate and report to the distillate fraction. As time increases, and in the absence of mixing, arsenic depletes at the liquid/vapor interface faster than it can be replenished from the bulk liquid phase. Ultimately, lead's activity at the interface increases, thus favoring its vaporization reaction; its content in the distillate fraction increased from 13.9 to 19.5 wt. % in the interval of 30 to 45 minutes, then to 20.7 wt. % from 45 to 90 minutes (see figure B-1 in appendix B).

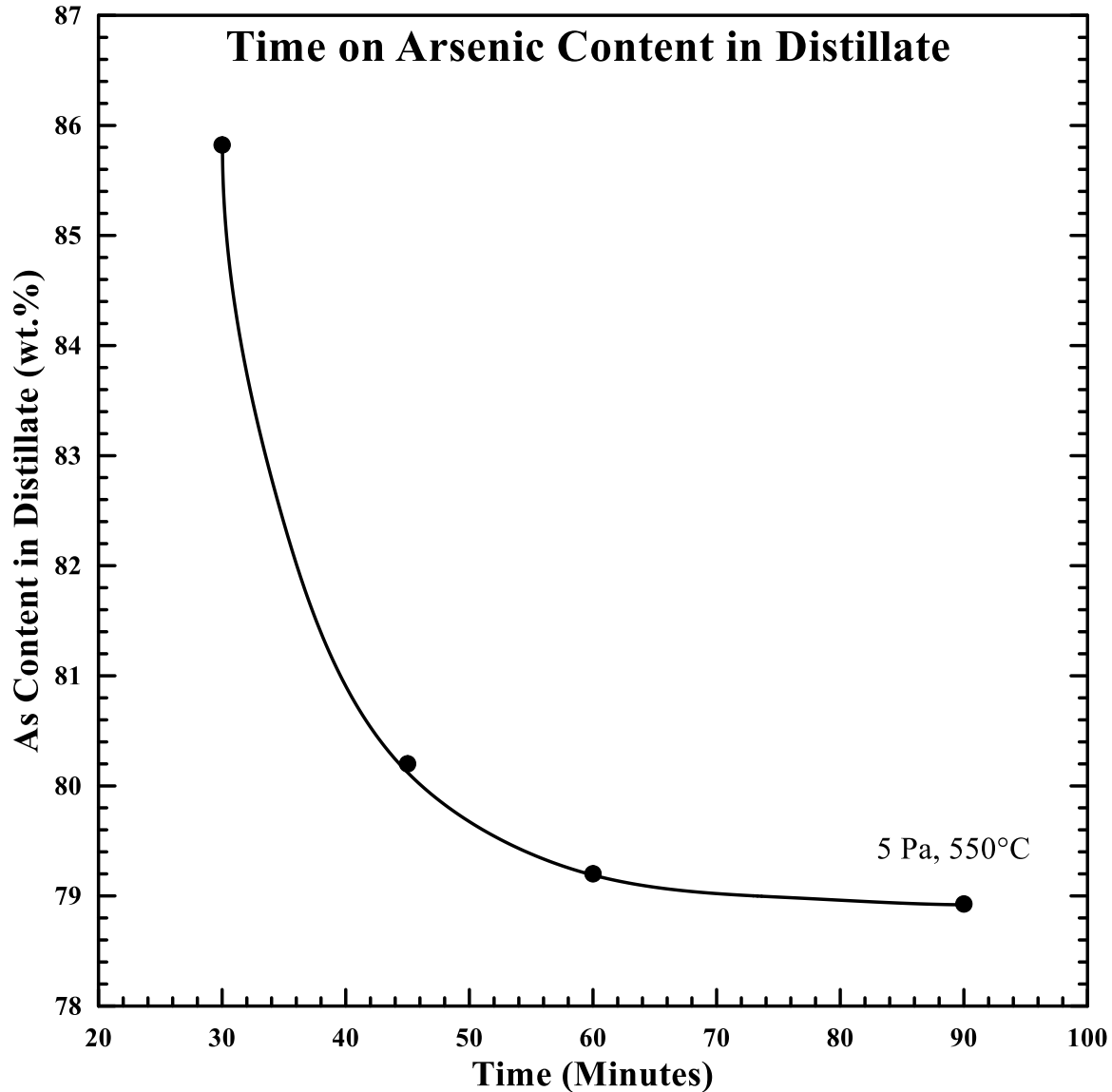


Figure 6.2 Effect of distillation time on the arsenic content in the distillate fraction; experiments conducted at 5 Pa and 550 °C

Figure 6.3 shows the effect of distillation time on the arsenic removal extent; as shown in the figure, the removal of arsenic from the alloy increases with an increase in distillation time. While there were no significant changes of removal when time is increases from 30 to 45 minutes (69.3 to 69.5 wt. %), the removal sharply increased from 69.5 to 74.8 wt. % when the time was increased further to 90 minutes. This phenomenon is obvious in the sense that the longer the alloy is heated under reduced pressures, the more material that volatilizes until its

concentration at the interface decreases significantly to a point where no marginal increase in volatilization is observed.

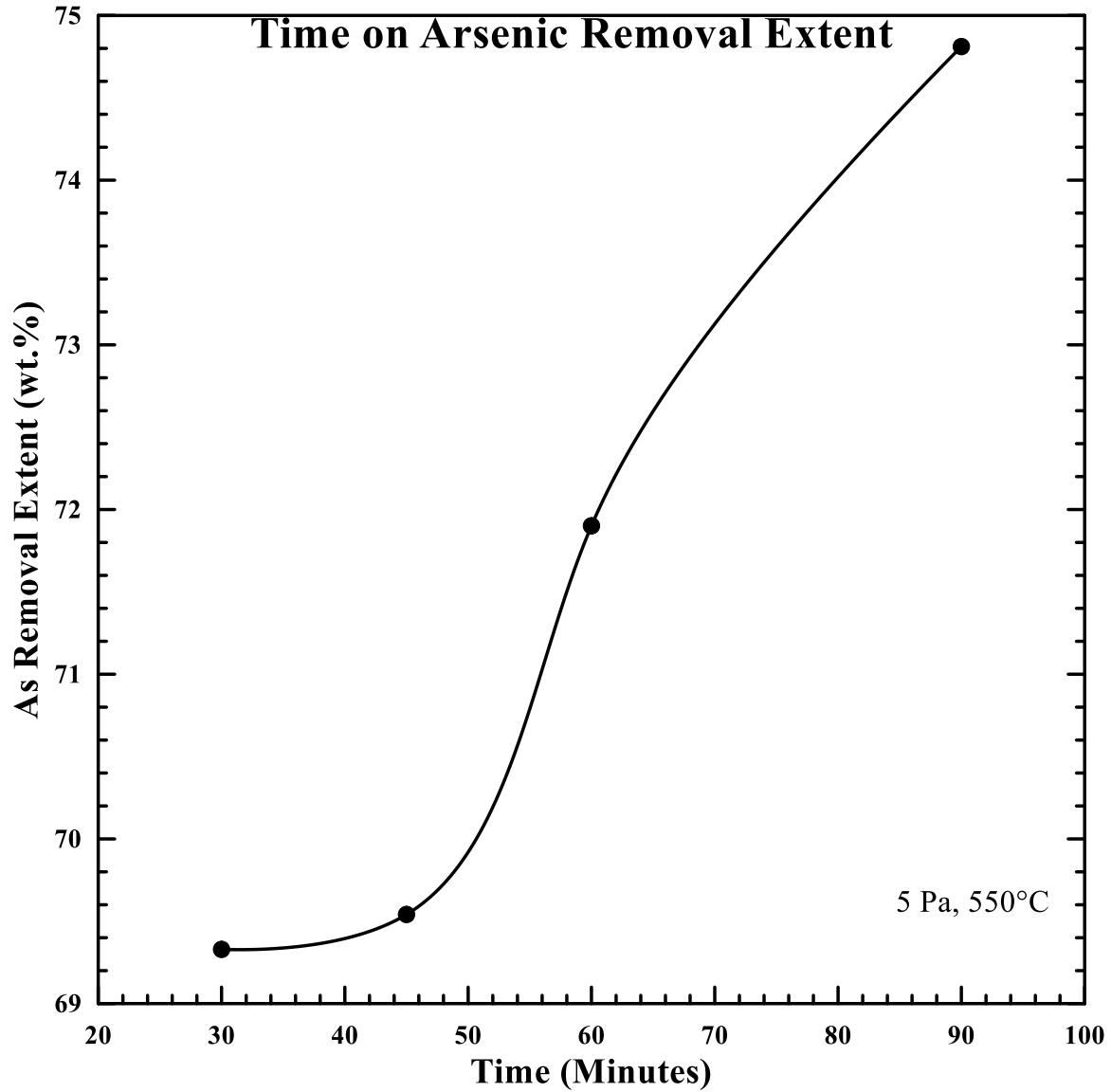


Figure 6.3 Effect of distillation time on the arsenic removal extent; experiments conducted at 5 Pa, and 550 °C.

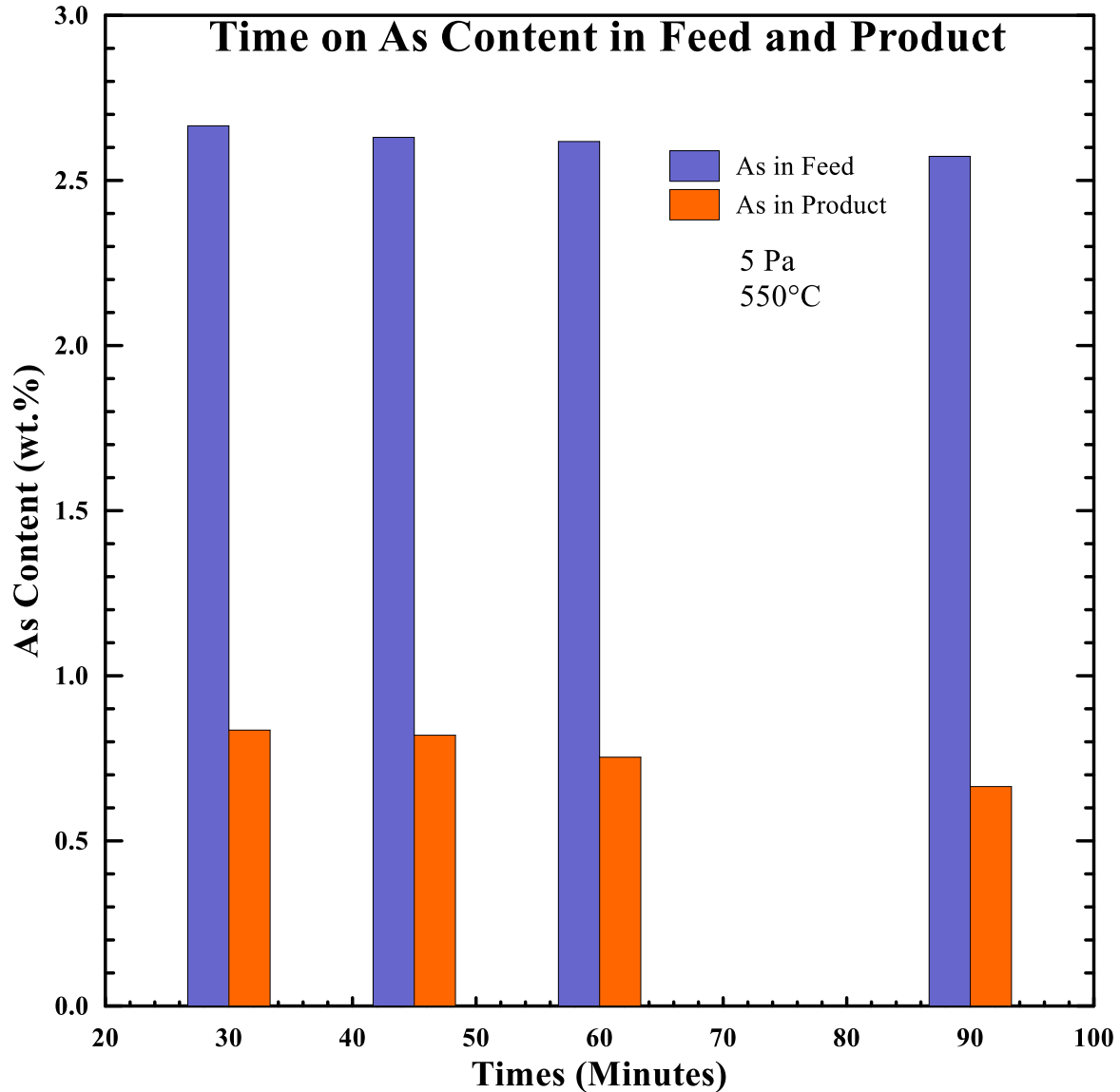


Figure 6.4 Effect of distillation time on the arsenic content in the feed sample as well as the product sample; experiments conducted at 5 Pa and 550 °C

Increasing the time increases the removal extent while decreasing the arsenic content in the distillate. How does this translate in terms of the end point of arsenic, thus the refining of lead, in the alloy is another important question, and figures 6.4 and 6.5 will address that. As shown in figure 6.4, the arsenic content decreased from an average of 2.7 wt. % in the feed samples to less than 0.9 wt. % in the product sample, all of which was attained in the absence of mixing. It should be noted however that the increase in distillation time from 30 to 90 minutes

did not results in significant decrease of arsenic content in the product bullion. Across the entire time range that was studied, lead refining is obvious as results in figure 6.5 shows. Lead was refined from roughly 97.5 to greater than 99 wt. %.

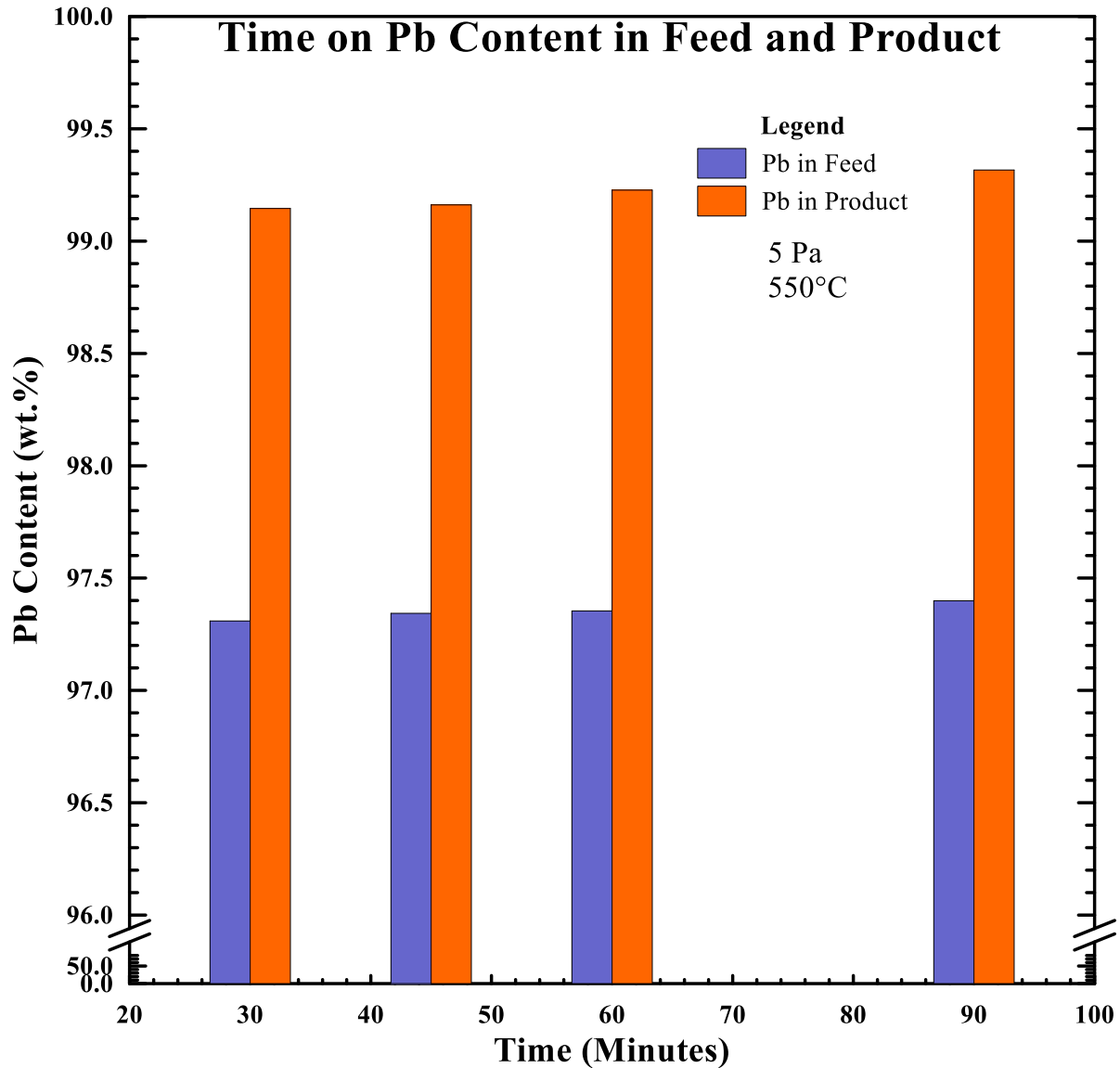


Figure 6.5 Effect of distillation time on the content of lead in the feed samples as well as the product sample; experiments conducted at 5 Pa and 550 °C

6.1.3 Effect of Pressure

Table 6.9 shows results of the effect of distillation pressure for experiments that were conducted at 550 °C for 45 minutes, and the arsenic content in the feed samples were 2.57, 2.85, 2.65, and 2.63 wt.% for tests 1, 2, 3, and 4 respectively. The distillate weight generally increased with a decrease in the distillation pressure, especially when the pressure was decreased down to 5 Pa. Based on the calculated distillate weight however, there is not much difference in the assumed weight of the distillate fraction.

Table 6.9 Effect of distillation pressure on the removal of arsenic

Test No	Pressure (Pa)	Feed weight (g)	Distillate Weight (g)	Product weight (g)	Weight loss (wt. %)	Calculated Distillate Weight (g)
1	20	167.78	1.700	164.75	0.79	3.03
2	15	170.45	1.840	167.24	0.80	3.21
3	10	164.20	1.530	160.75	1.17	3.45
4	5	148.67	2.716	145.28	0.45	3.39

Figure 6.6 shows the effect of distillate pressure on the arsenic content in the distillate fraction. According to the results shown in the figure, the arsenic content decreased with a decrease in pressure. No significant decrease was observed in the pressure range of 20 to 15 Pa (92.4 to 91.8 wt. %); however, a sharp decrease is observed in the 15 to 5 Pa range (91.8 to 80.2 wt. %). Since arsenic is much more volatile than lead, its equilibrium partial pressure above the melt is always much larger than that of lead. As the pressure of the system is decreased, the boiling point of both elements is also decreased; this means that at lower system pressure, lead generates a large enough partial pressure and is collected in the distillate fraction (see figure B-2 in appendix B), thus the arsenic content would decrease.

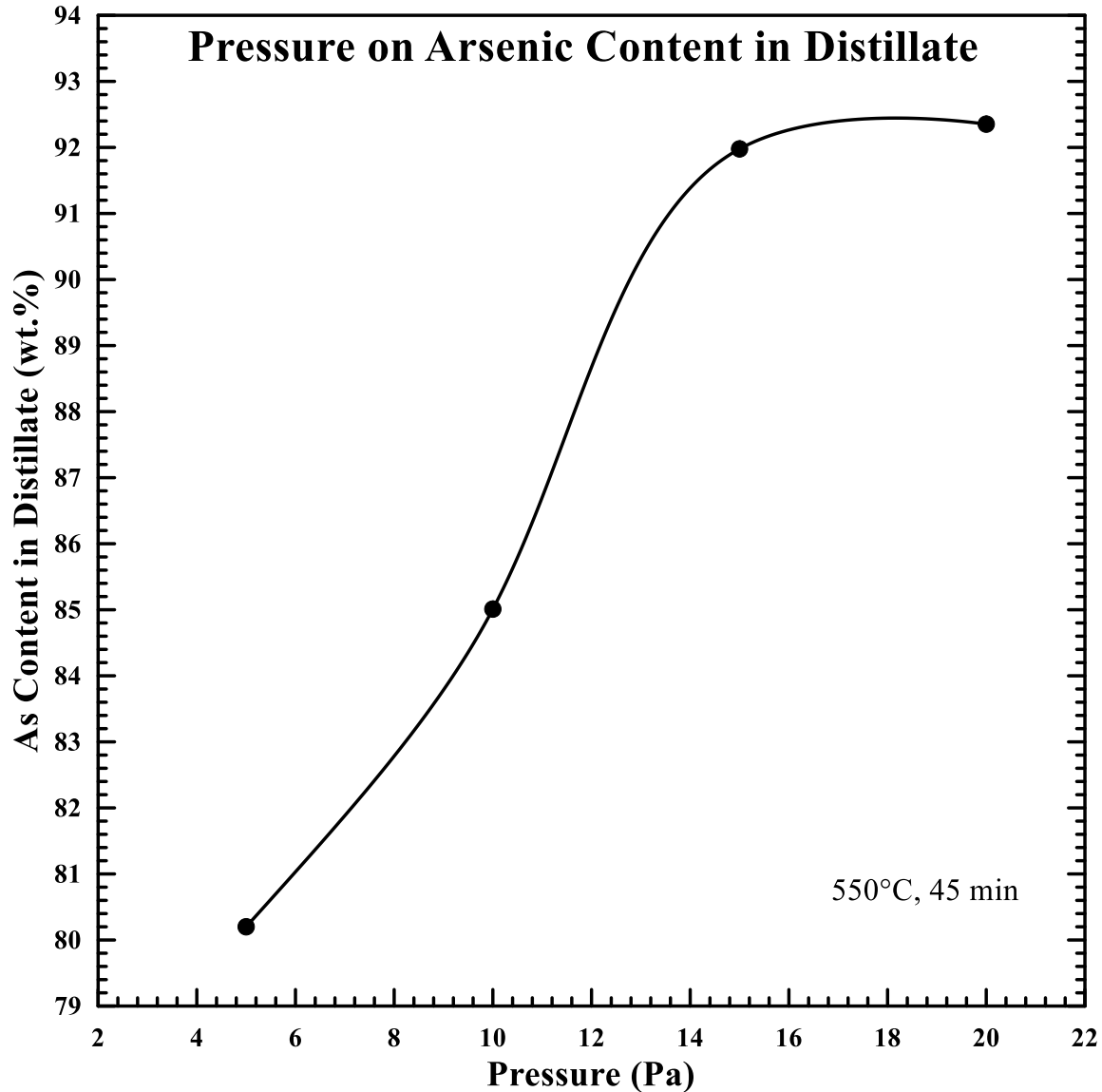


Figure 6.6 Effect of distillation pressure on arsenic content in the distillate fraction; experiments conducted at 550°C and 45 minutes

Figure 6.7 shows the effect of distillation pressure on arsenic removal extent; according to the results shown therein, the removal extent increased with a decrease in pressure. In the range of 15 to 10 Pa, the increase was significant (60.7 to 67.4 wt. %) while it was only gradual in the 10 to 5 Pa pressure range (67.4 to 69.4 wt. %). The increase of removal extent from 15 to 20 Pa bear no physical meaning to the effect of the distillation pressure and is considered to originate either from experimental error during analysis.

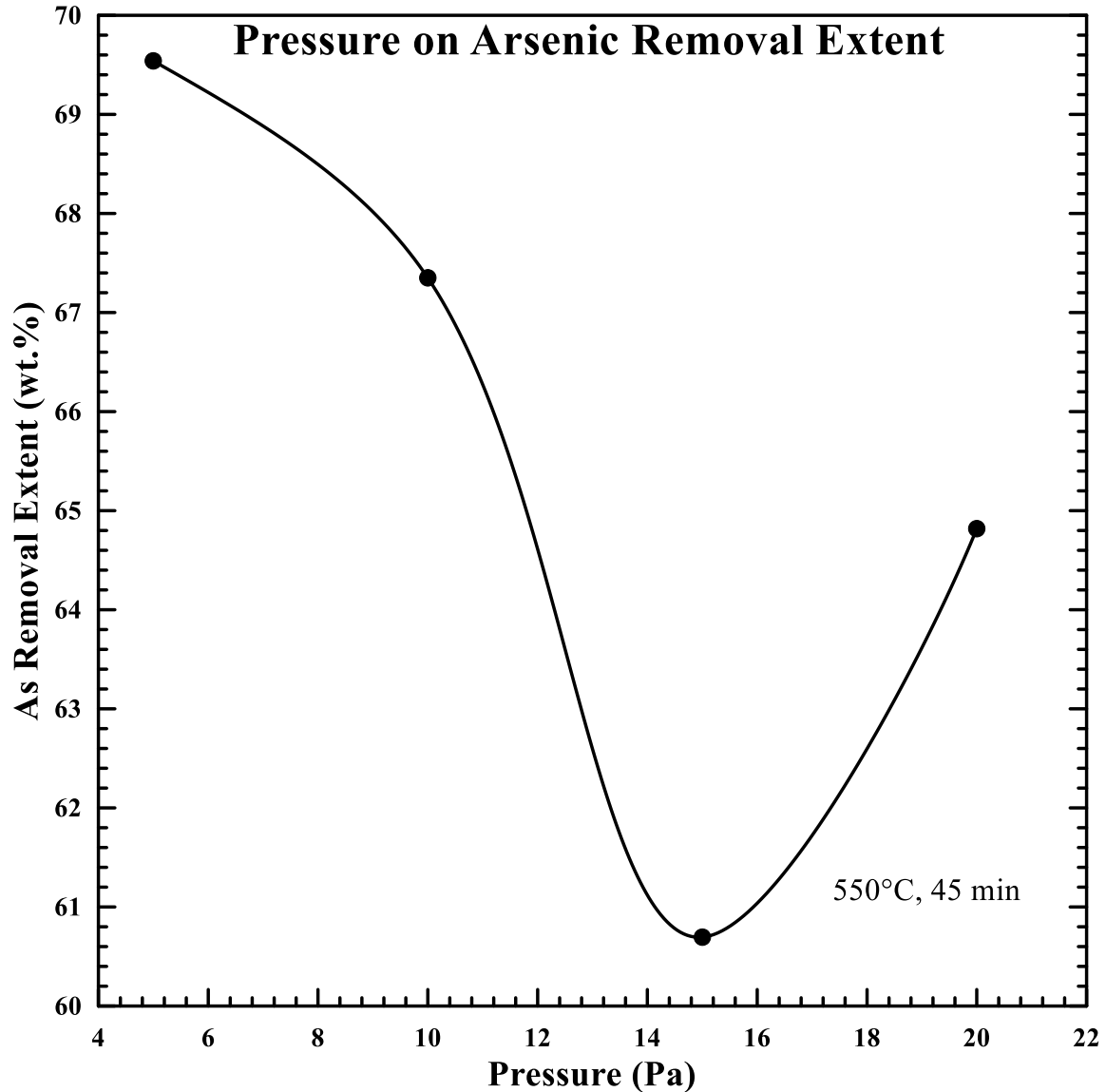


Figure 6.7 Effect of distillation pressure on arsenic removal extent; experiments conducted at 550°C and 45 minutes

Figure 6.8 shows the effect of distillation pressure on the arsenic content in both the feed and the product sample. When the arsenic content in the feed samples was ranging from 2.57 to 2.85 wt. %, it was decreased to a range of 0.82 to 1.14 wt. %. A noteworthy point in this case is that arsenic removal is of as strong a function of distillation pressure as it is of distillation time. Shown in figure 6.9 is the lead content in the feed and product samples. As in the case of

distillation time, lead was refined from about 97.5 wt. % in the feed sample to greater than 99 wt. % in the product sample.

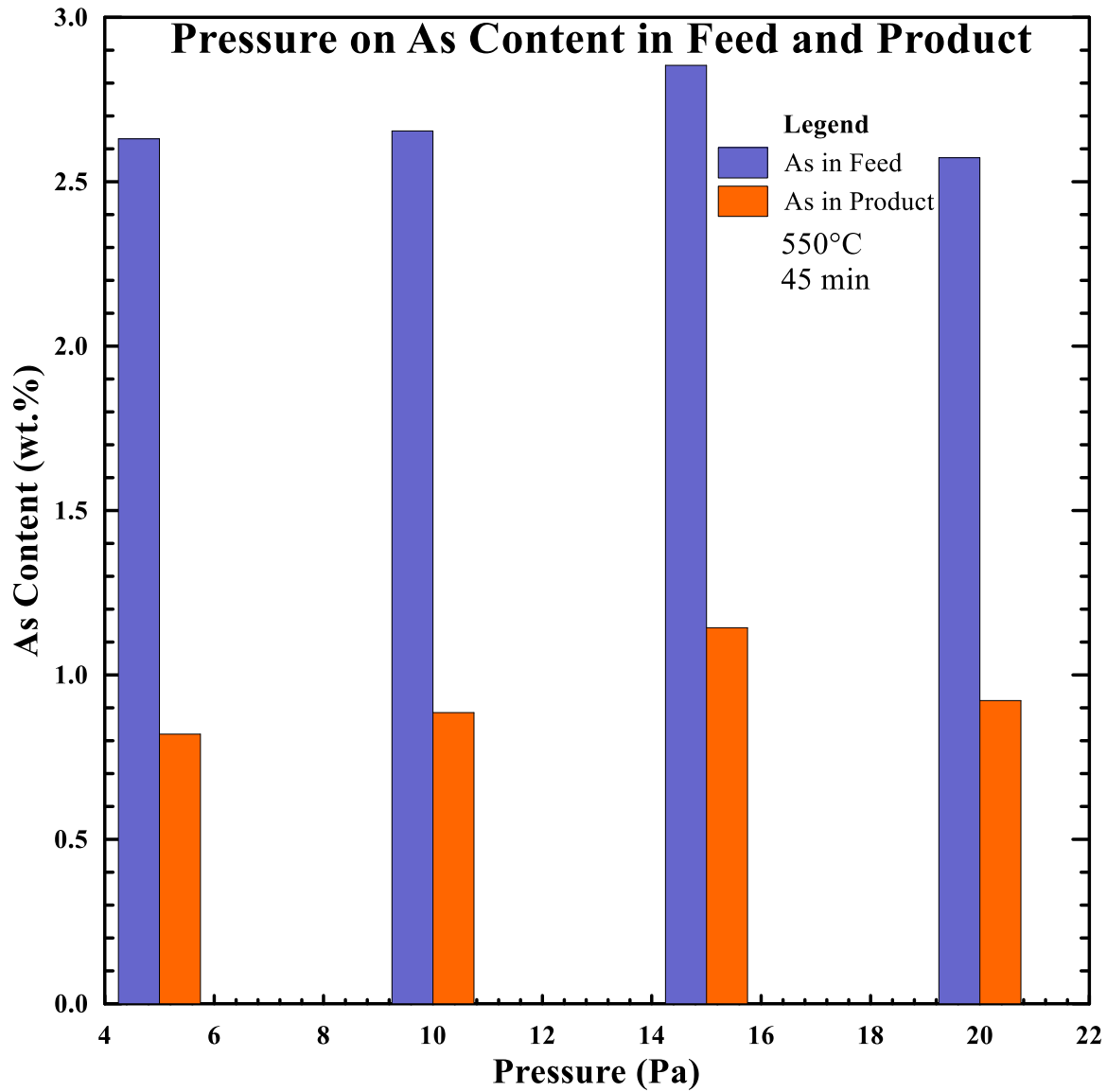


Figure 6.8 Effect of distillation pressure on the arsenic content in both the feed and product samples; experiments conducted at 550°C and 45 minutes

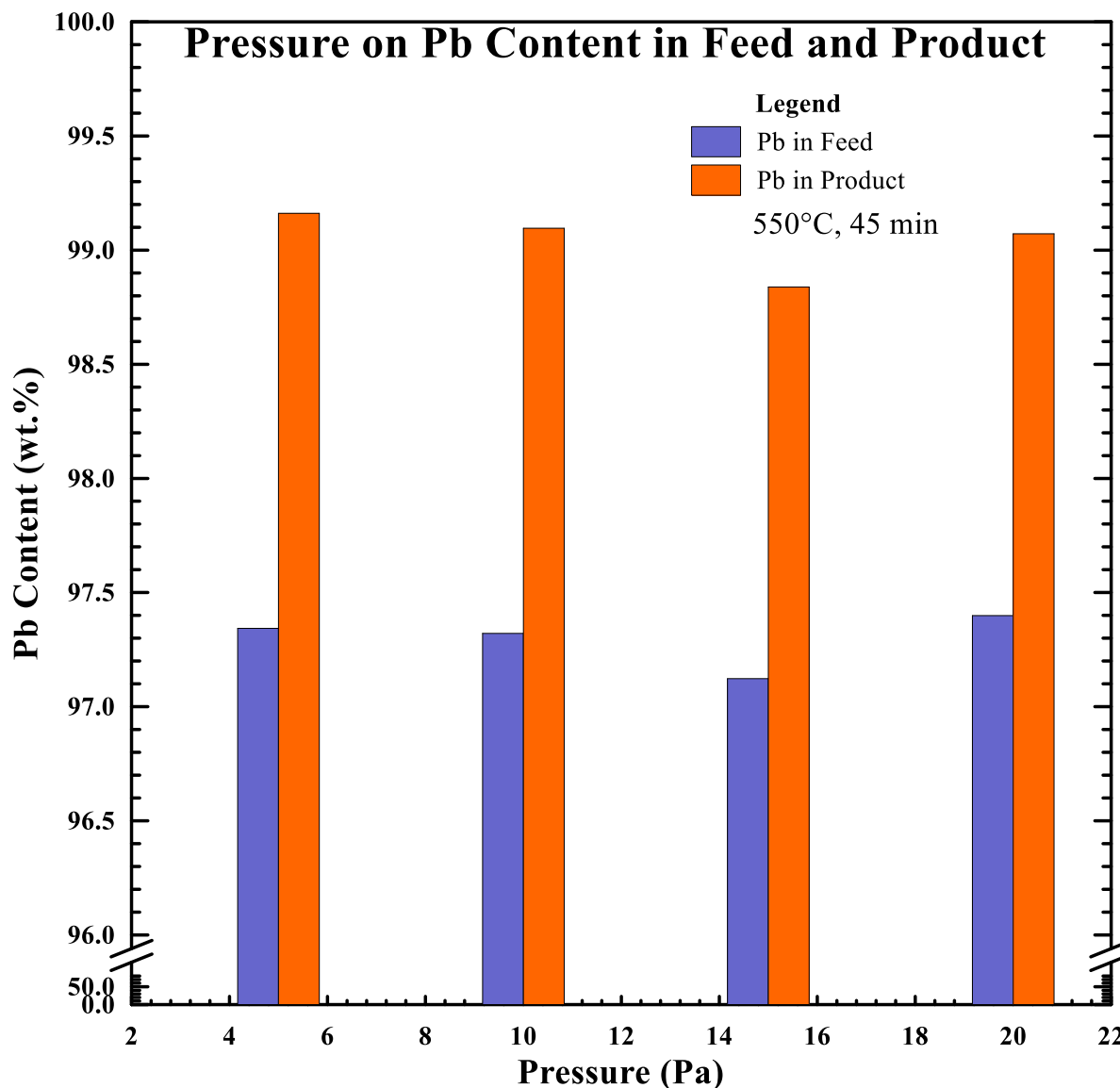


Figure 6.9 Effect of distillation pressure on the lead content in both the feed and product samples; experiments conducted at 550°C and 45 minutes

6.1.4 Effect of Temperature

Table 6.10 shows the results of the effect of distillation temperature for experiments conducted at 5 Pa and 45 minutes, and the arsenic content in the feed samples were 2.51, 2.30, 2.63, 2.04, and 2.46 wt. % for tests 8, 9, 4, 10, and 11 respectively. Increasing the distillation temperature increased the weight of the distillate fraction, the increment being high when the temperature was increased from 500 to 550 °C.

Table 6.10 Effect of distillation temperature on the removal of arsenic

Test No	Temperature (°C)	Feed weight (g)	Distillate Weight (g)	Product weight (g)	Weight loss (wt. %)	Calculated Distillate Weight (g)
8	450	153.42	1.500	150.81	0.72	2.61
9	500	169.53	2.240	166.97	0.19	2.56
4	550	148.67	2.716	145.28	0.45	3.39
10	600	147.38	1.509	144.12	1.19	3.26
11	650	148.84	1.708	145.00	1.43	3.84

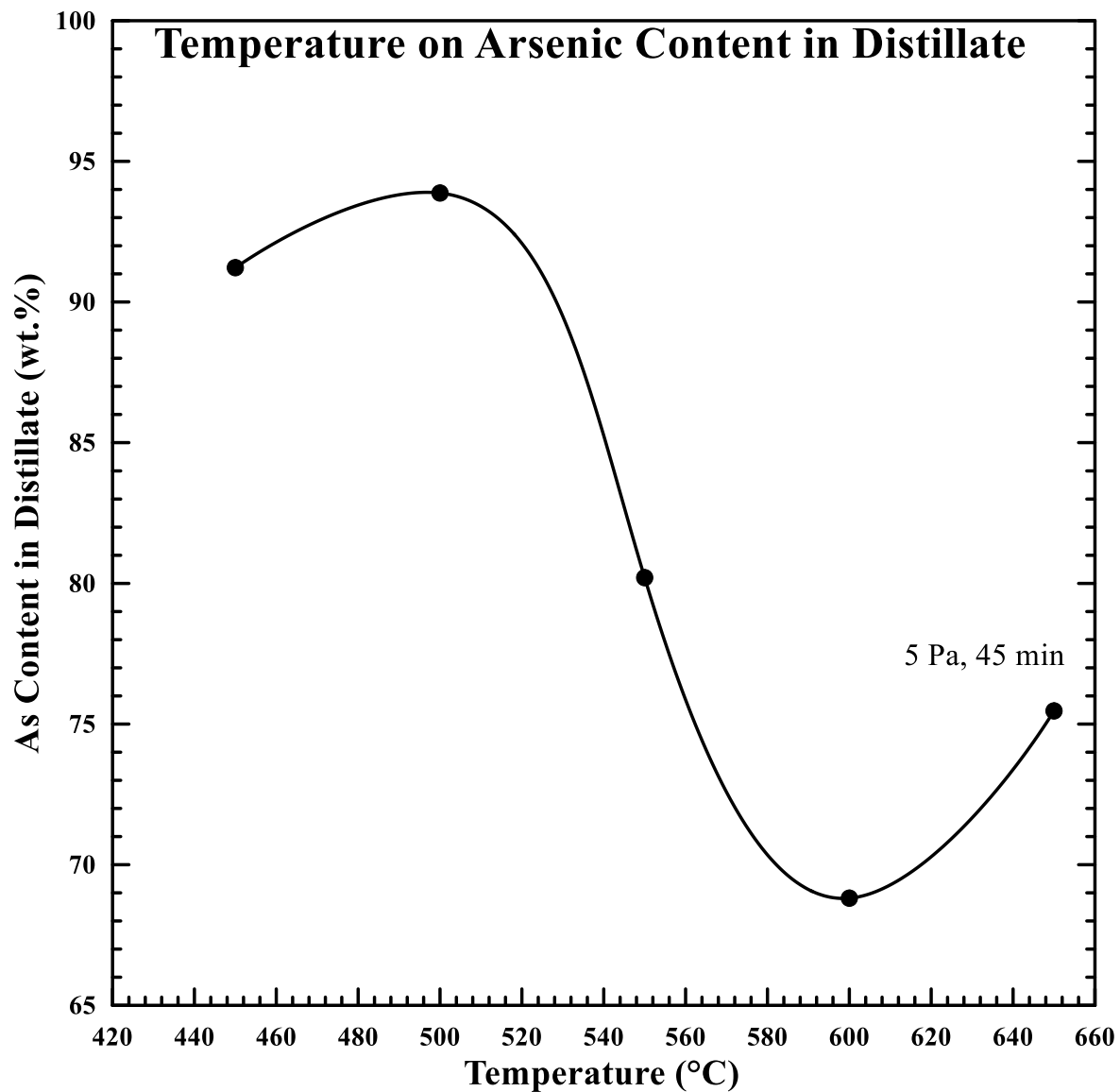


Figure 6.10 Effect of distillation temperature on arsenic content in distillate; experiments conducted at 5 Pa, and 45 minutes

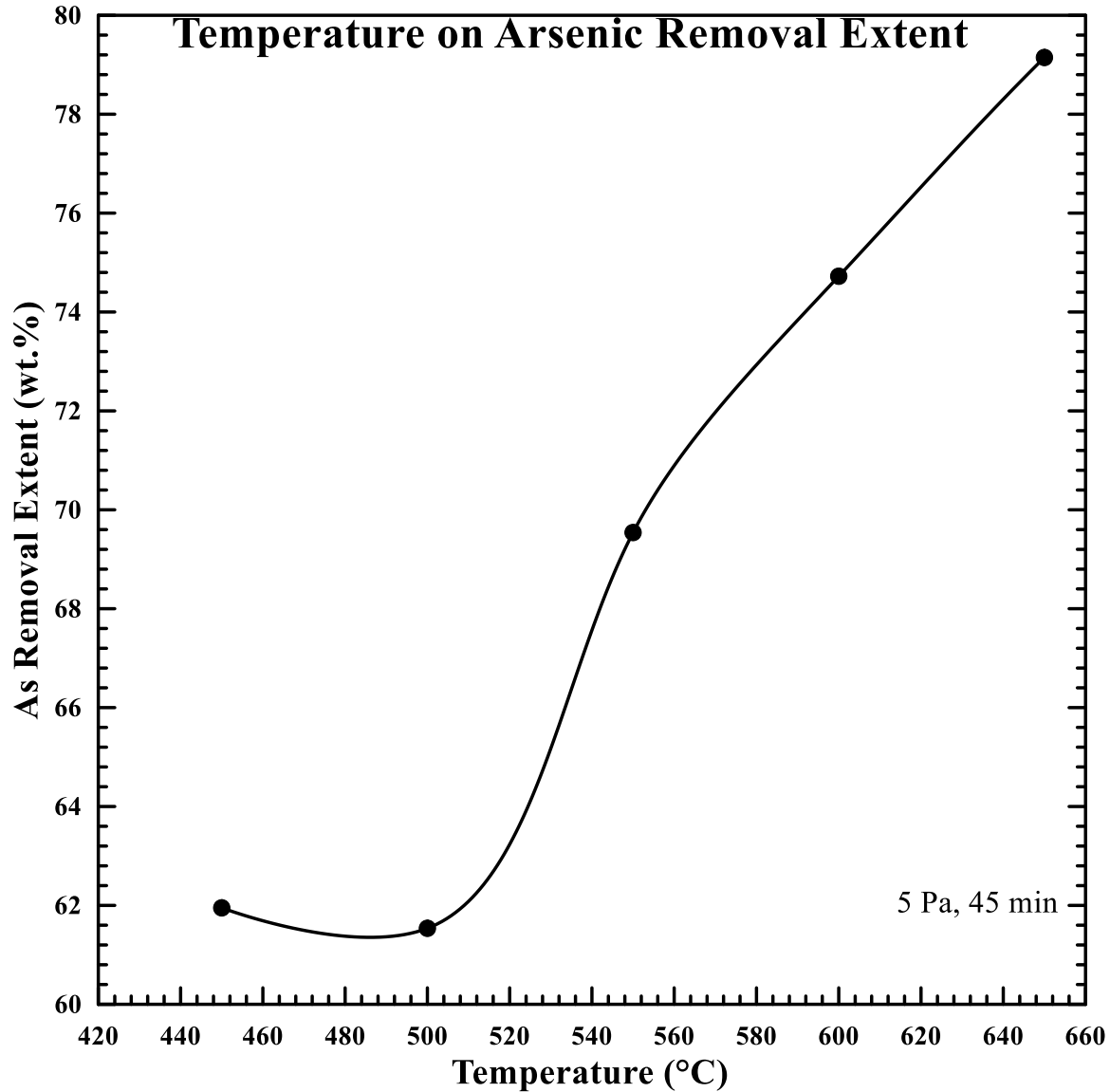


Figure 6.11 Effect of distillation temperature on arsenic removal extent; experiments conducted at 5 Pa, and 45 minutes

Figure 6.10 shows the effect of distillation temperature on the arsenic content in the distillate fraction. The arsenic content slightly sharply decreased from 91.3 to 68.8 wt. % when the temperature was increased from 500 to 650 °C. Results observed from 450 to 500°C and from 600 to 650°C are considered experimental error. Both the saturated vapor pressure and the activity coefficient of arsenic are dependent on temperature. Also, higher temperatures increased

the mobility of arsenic ions in the melt to the liquid/vapor interface. Consequently, more material is vaporized in a shorter amount of time. On the other hand, it also means that a higher amount of lead will report in the distillate fraction; its content increased from 8.4 to 30.4 wt. % when temperature was increased from 450 to 600 °C (see figure B-3 in appendix B). This translates in a higher removal extent of arsenic as is shown in figure 6.11; the removal extent increased from 61.5 to 79.2 wt. % when temperature was increased from 500 to 650 °C.

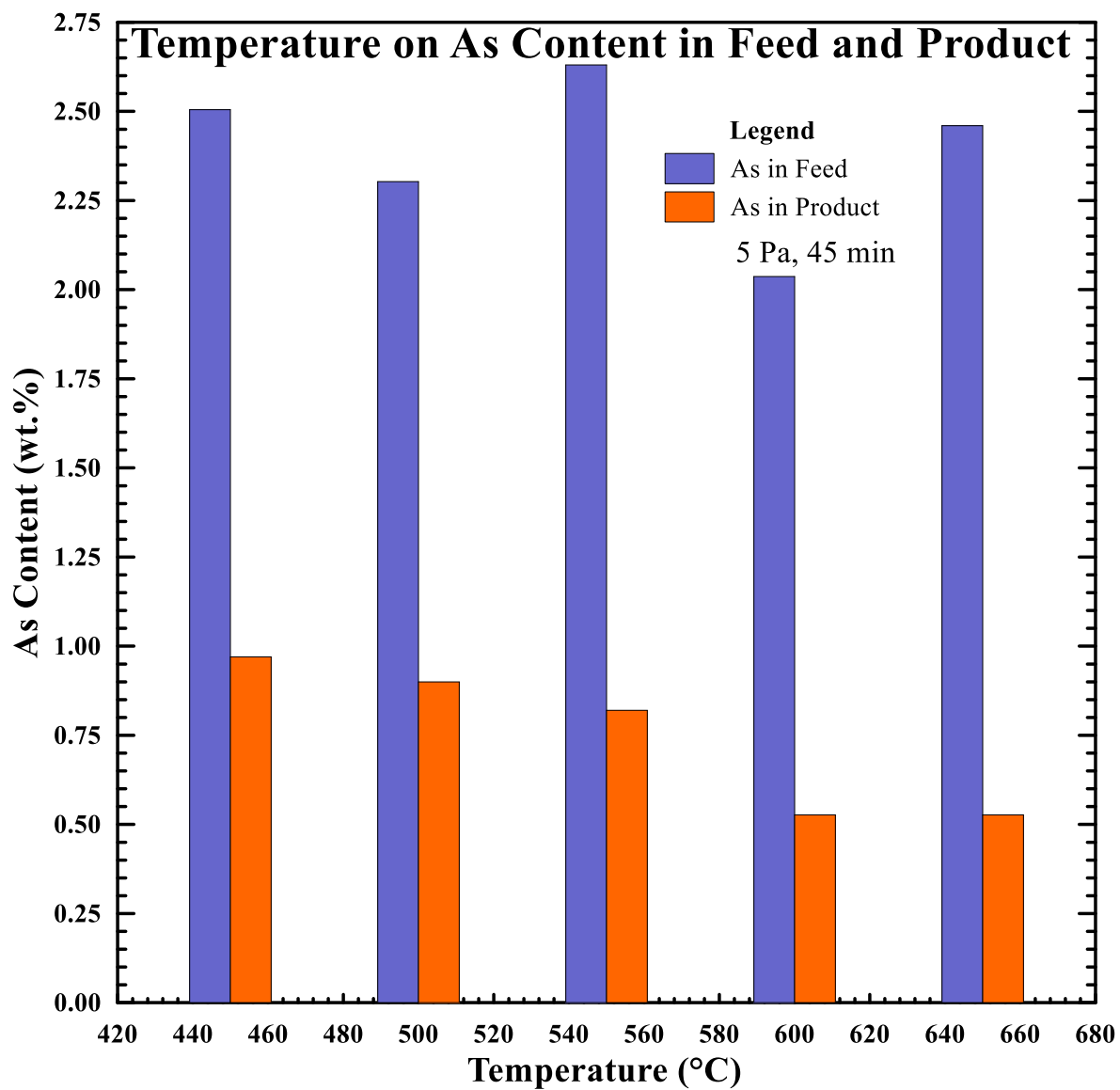


Figure 6.12 Effect of distillation temperature on arsenic content in both the feed and the product samples; experiments conducted at 5 Pa and for 45 minutes

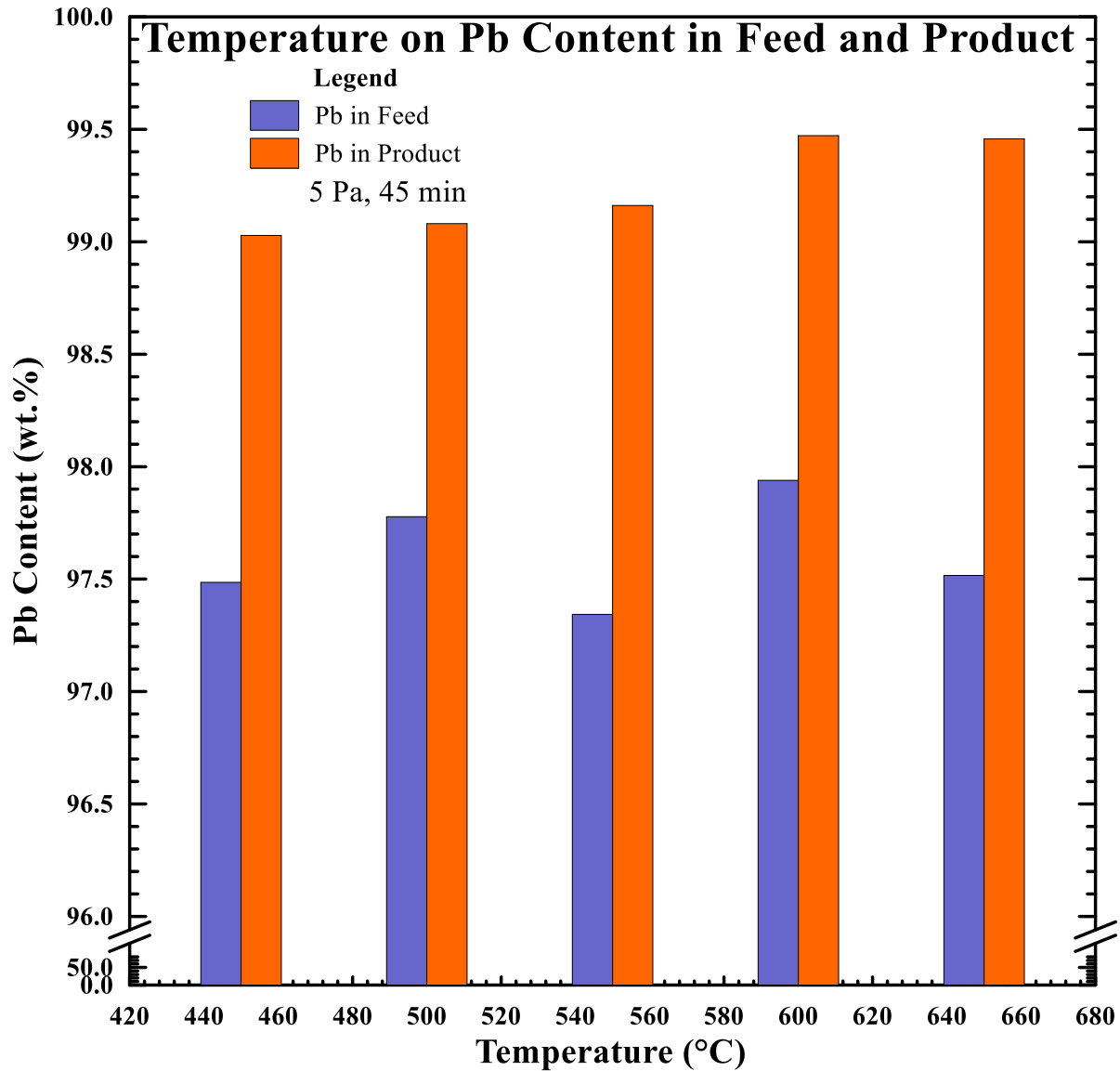


Figure 6.13 Effect of distillation temperature on lead content in both the feed and the product samples; experiments conducted at 5 Pa and for 45 minutes

Figure 6.12 shows the effect of distillation temperature on the arsenic content in both the feed and product fractions. Starting from a concentration in the range of 2.04 to 2.63 wt. % in the feed sample, the arsenic content was decreased to approximately 0.53 wt. % which is the lowest content achieved across the entire experimental matrix. It should be notice also that distillation at 650°C brings the arsenic content closer to the 10 ppm specification of soft lead for VRLA which

is shown in figure 2.5, although subsequently refining still needs to occur.. As shown in figure 6.13, lead refining was increased much more as temperature was increased; from about 97.5 wt. % in the feed sample, the lead content was increased to about 99.5 wt. % in the product. While an increase in time and a decrease in distillation pressure achieved arsenic removal and lead refining to greater than 99 wt. %, it is clearly obvious that arsenic removal is a stronger function of temperature. Should the aim of the process be solely the maximum refining of lead, 650 °C or higher, and 45 minutes or longer, and 5 Pa would be optimum.

6.1.5 Effect of Initial Arsenic Content in the Feed

Table 6.11 shows the results of the effect of arsenic initial composition for experiments conducted at 5 Pa, 550 °C, and for 45 minutes, and the arsenic content in the feed samples are listed in table 6.6. As the arsenic content in the feed sample increased, obviously, the amount of material vaporized also increased; the weight removed gets closer to its starting point as the content in the feed gets larger.

Table 6.11 Effect of arsenic initial composition on the removal of arsenic

Test No	Initial Arsenic Content (wt. %)	Feed weight (g)	Distillate Weight (g)	Product weight (g)	Weight loss (wt. %)	Available As Weight (g)	Calculated Distillate Weight (g)
12	0.11	190.37	0.055	190.28	0.02	0.209	0.09
13	0.53	193.23	0.059	193.08	0.05	1.024	0.15
14	0.78	196.10	0.393	195.68	0.01	1.530	0.42
15	1.52	193.48	0.826	191.62	0.53	2.941	1.86
4	2.63	148.67	2.716	145.28	0.45	3.910	3.39
16	3.07	192.39	2.186	187.74	1.28	5.906	4.65

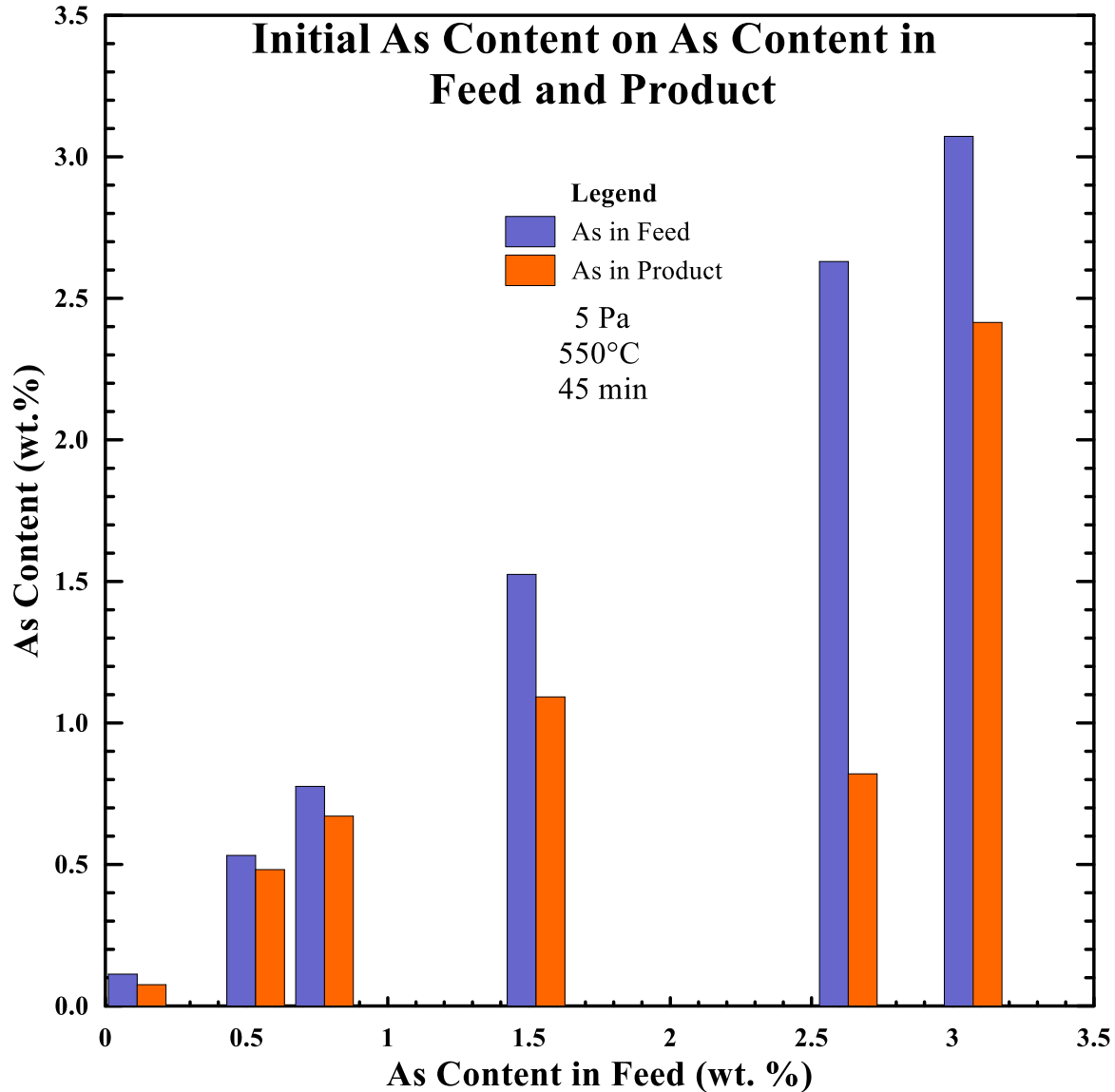


Figure 6.14 Effect of initial arsenic content on the arsenic content in both the feed and the product samples; experiments conducted at 5 Pa, 550 °C, and for 45 minutes

Figure 6.14 shows the effect of initial arsenic content on arsenic content in the feed as well as the product samples. The partial pressure of arsenic above the melt is dependent on its activity, hence activity coefficient; as the arsenic concentration in the feed sample gets smaller, its activity in the melt is reduced even more. This means that lead activity is larger and more of it reports to the distillate fraction; figure B-4 in appendix B shows that the lead content in the

distillate fraction is greater than 40 wt. %. Figure 6.15 shows the effect of initial arsenic content in the feed and product samples. The important information relayed by results shown in the figure is that the refining is more difficult as the content of arsenic in the feed sample is decreased.

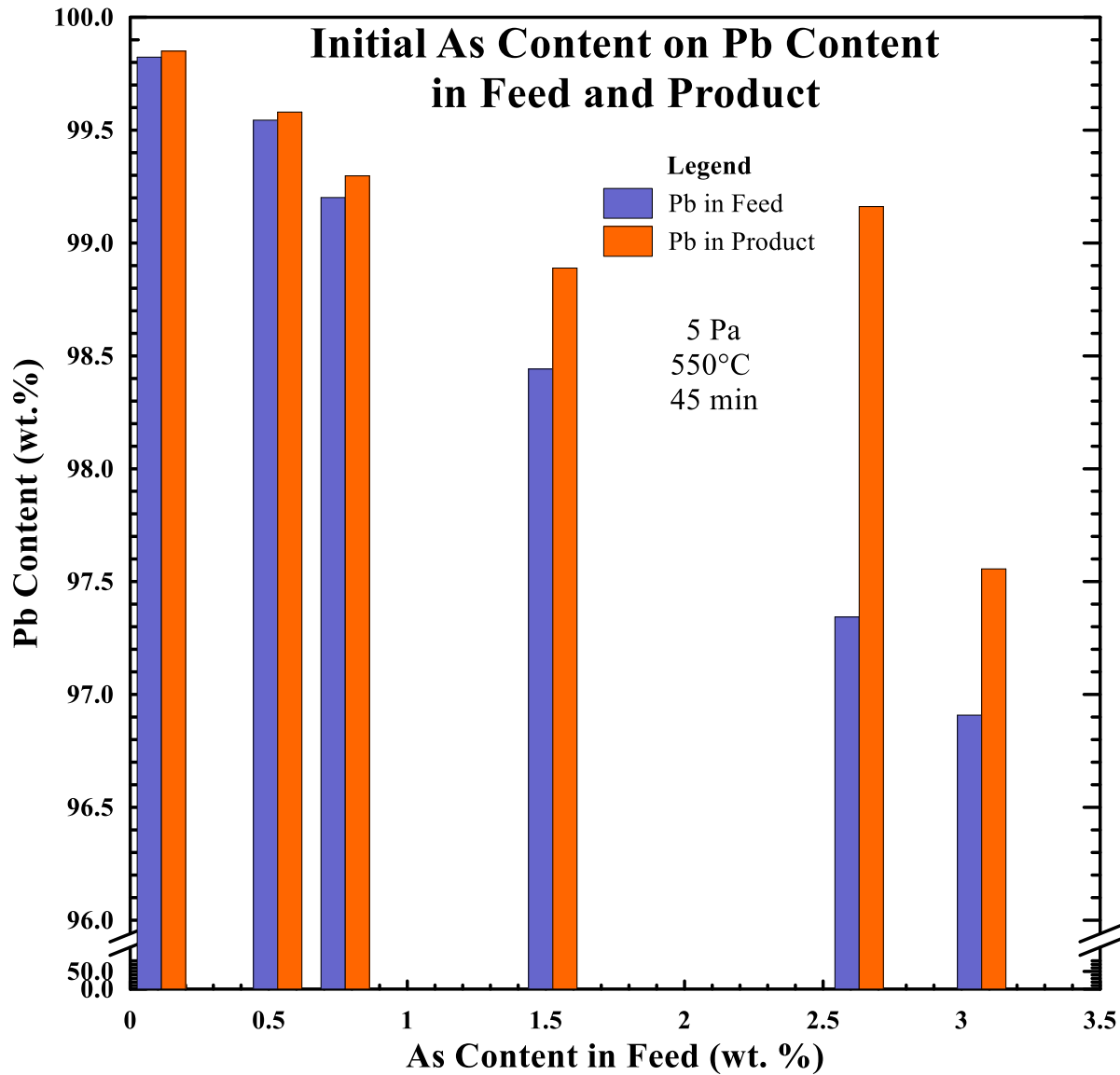


Figure 6.15 Effect of initial arsenic content on the lead content in both the feed and the product samples; experiments conducted at 5 Pa, 550 °C, and for 45 minutes

6.1.6 Considerations for the Adjustment of the Binary Parameters for the Pb-As System

From sections 6.1.1 to 6.1.5, the research team has demonstrated that the removal of arsenic from binary lead alloys is indeed possible. As mentioned in section 3.3, the melting point of thermochemistry data that were utilized in the prediction of the binary parameters were harvested from literature in which it was not clear at which pressure the measurement were conducted. The melting point that was used was reported as measured at 36 atm. and has been used by when describing the As-Pb system; this constitutes one place where experimental error comes into play. One way of verifying predictions shown in table 3.6 is to use results from experiments that showed adequate temperature and pressure control.

Knowing the composition of the distillate and the production fraction, the equilibrium mole fractions are calculated; rearranging equation 3.3 one can calculate the activity coefficient for the experimental conditions. In this case, equations 3.15, 3.16, 3.27, 3.28, 3.40, and 3.41 cannot be used for simplicity. It is necessary to use the actual equation for the activity coefficient. Given sufficient time and will, one can derive the analytical expressions for the derivatives equations 3.7, 3.8, 3.23, 3.24, 3.33, and 3.34 to use the Newton-Raphson methodology of finding root. The research team has opted however to utilize the modified secant method as the approach to find the roots. The modified secant method is known to produce results that are comparable to the Newton-Raphson method. The mole fraction of arsenic in the liquid phase and the vapor phase is shown equations 6.1 and 6.2.

$$x_{As} = \frac{\frac{Wt. \%_{As}^{PROD}}{M_{As}}}{\frac{Wt. \%_{As}^{PROD}}{M_{As}} + \frac{Wt. \%_{Pb}^{PROD}}{M_{Pb}}} \quad (6.1)$$

$$y_{As} = \frac{\frac{Wt. \%_{As}^{DIST}}{M_{As}}}{\frac{Wt. \%_{As}^{DIST}}{M_{As}} + \frac{Wt. \%_{Pb}^{DIST}}{M_{Pb}}} \quad (6.2)$$

The saturated vapor pressure is calculated using the Clausius-Clapeyron equation (eq. 6.3) for which the coefficients are provided in table 3.2.

$$\log_{10} P^0 (mmHg) = \frac{A}{T (K)} + B * \log_{10} T (K) + C * T (K) + D \quad (6.2)$$

Rearranging equation 3.3, we obtain equation 6.3 as shown below:

$$\gamma_{As} = \frac{y_{As} * P}{x_{As} * P_{As}^0} \quad (6.3)$$

One thing to remember is that the binary parameters calculated from equation 6.3 are specific to the temperature of the experiment; it is therefore necessary to calculate them at the experimental temperature shown in table 3.6 before comparison and adjustment is done.

6.2 The Pb-Sb Binary System

6.2.1 Lead-Antimony Binary Alloys

For the Pb-Sb binary system, the first batch of samples were prepared with a target of 3.0 wt. % following the procedure mentioned in section 6.1.1. A total of 17 samples were cast from this batch and put together they weighed 2669.1 gram after casting from a 2741.6 gram starting point. The weight loss incurred was 2.64 wt. %. Representative samples were obtained from each sample and they were submitted for analysis using ICP-MS and AAS. The samples' composition is shown in table 6.12. The second "batch" of Pb-Sb samples was prepared by varying the

composition of antimony from 0.3 to 3.8 wt. %. Batch 2 analysis is shown in table 6.13. The experimental matrix for the Pb-Sb system is shown in table 6.14.

Table 6.12 Chemical analysis of batch 1 of Pb-Sb feed samples

Sample ID	Analyte Concentration (wt. %)			
	Sb	Sn	As	Pb
Sample # 1	2.38	0.007	0.151	97.46
Sample # 2	2.26	0.004	0.083	97.65
Sample # 3	2.28	0.003	0.112	97.60
Sample # 4	2.27	0.002	0.056	97.68
Sample # 5	2.75	0.003	0.075	97.17
Sample # 6	2.98	0.001	0.057	96.96
Sample # 7	3.48	0.003	0.034	96.49
Sample # 8	2.26	0.006	0.024	97.71
Sample # 9	2.28	0.002	0.077	97.64
Sample # 10	2.01	0.027	0.195	97.77
Sample # 11	2.35	0.002	0.112	97.54
Sample # 12	2.33	0.006	0.093	97.57
Sample # 13	2.22	0.002	0.240	97.54
Sample # 14	2.42	0.002	0.063	97.52
Sample # 15	2.69	0.001	0.093	97.21
Sample # 16	2.42	0.001	0.081	97.50
Sample # 17	2.51	0.010	0.074	97.41

Table 6.13 Chemical analysis of batch 2 of Pb-Sb samples

Sample ID	Analyte Concentration (wt. %)			
	Sb	Sn	As	Pb
Sample #1	0.32	0.001	0.006	99.67
Sample #2	0.90	0.001	0.005	99.10
Sample #3	1.37	0.002	0.003	98.62
Sample #4	2.34	0.000	0.004	97.65
Sample #5	3.81	0.001	0.019	96.17

Table 6.14 Experimental matrix for Pb-Sb binary system

Test No	Pressure (Pa)	Temperature (° C)	Time (minutes)
1	5	550	30
2	5	600	30
3	5	650	30
4	5	700	30
5	5	750	30
6	5	700	45
7	5	700	60
8	5	700	90
9	10	700	30
10	15	700	30
11	20	700	30
12	5	700	45
13	5	700	45
14	5	700	45
15	5	700	45
16	5	700	45

6.2.2 Effect of Time

Table 6.15 shows the results for the effect of distillation time on antimony removal for experiments conducted at 5 Pa, and 700°C; the concentration of the feed samples were 2.38, 2.22, 2.01, and 3.48 wt. %. As distillation time increased, the distillation fraction weight also increased. While the weight increase was gradual from 30 to 45 minutes, it was significant when time was increased from 60 to 90 minutes reaction time.

Table 6.15 Effect of distillation time on the removal of antimony

Test No	Time (minutes)	Feed weight (g)	Distillate Weight (g)	Product weight (g)	Weight loss (wt. %)	Calculated Distillate Weight (g)
4	30	150.84	0.161	149.65	0.68	1.19
6	45	153.01	1.301	151.12	0.38	1.89
7	60	153.11	0.646	150.94	1.00	2.17
8	90	154.63	1.216	151.62	1.16	3.01

Figure 6. 16 shows the effect of distillation time on the antimony content in the distillate fraction. According to these results the antimony content in the distillation fraction increased with an increase in distillation time. As was shown in figure 3.1, the separation of antimony from lead is based on their difference in volatility. At 700°C, the saturated vapor pressure of pure antimony is 8872 Pa while that of pure lead is 2.39 Pa, Table 6.16 shows the equilibrium vapor pressure of antimony in the concentration range of 2.0 to 4.0 wt. % for a distillation run at 700°C. As can be seen in the table, the equilibrium vapor pressure of antimony is significantly reduced to a range of 14 and 28 Pa; consequently, the driving force for its removal is decreased. Additionally, lead evaporation is favored at 5 Pa system pressure. Given lead’s high activity in the melt, it is evident that it would volatilize readily, while antimony would slowly volatilize, hence the trend observed in the figure.

Table 6.16. Equilibrium partial pressures for distillation at 700 °C

Sb wt. % in Liquid Phase	a_{sb}	a_{pb}	Sb $P_{equilibrium}$ (Pa)	Pb $P_{equilibrium}$ (Pa)
2.0	0.027	0.966	240.4	2.312
2.5	0.034	0.958	300.6	2.292
3.0	0.041	0.949	360.8	2.272
3.5	0.047	0.941	420.9	2.252
4.0	0.054	0.933	481.0	2.233

Figure 6.17 shows the effect of distillation time on the removal extent of antimony. According to the figure, antimony removal increased gradually from 30 to 45 minutes then it sharply increased when the distillation time was increased from 45 to 90 minutes. As the alloy undergoes distillation for longer times, more material is volatilized and report to the distillate fraction. The trends seen in figures 6.16 and 6.17 suggests that at 5 Pa distillation, the alloy needs to react for 60 to 90 minutes to achieve a considerable removal of antimony.

Figure 6.18 shows the effect of distillation time on the content of antimony in the feed and product samples. From this figure it can be seen that the antimony content is not considerably decrease for distillation experiments conducted at 30 and 45 minutes. Longer distillation time improved the removal; distillation at 60 minutes decreased the antimony content from 2.01 to 1.4 wt. %, while antimony was decreased from 3.48 to 2.2 wt. % when distillation was carried out for 90 minutes. Figure 6.19 shows the effect of distillation time on the lead content in the feed and product samples; according to the results shown in the figure, lead refining does occur for all distillation times; however, longer distillation time achieve higher refining. At 90 minutes, lead was refined from 96.5 to 97.8 wt. %.

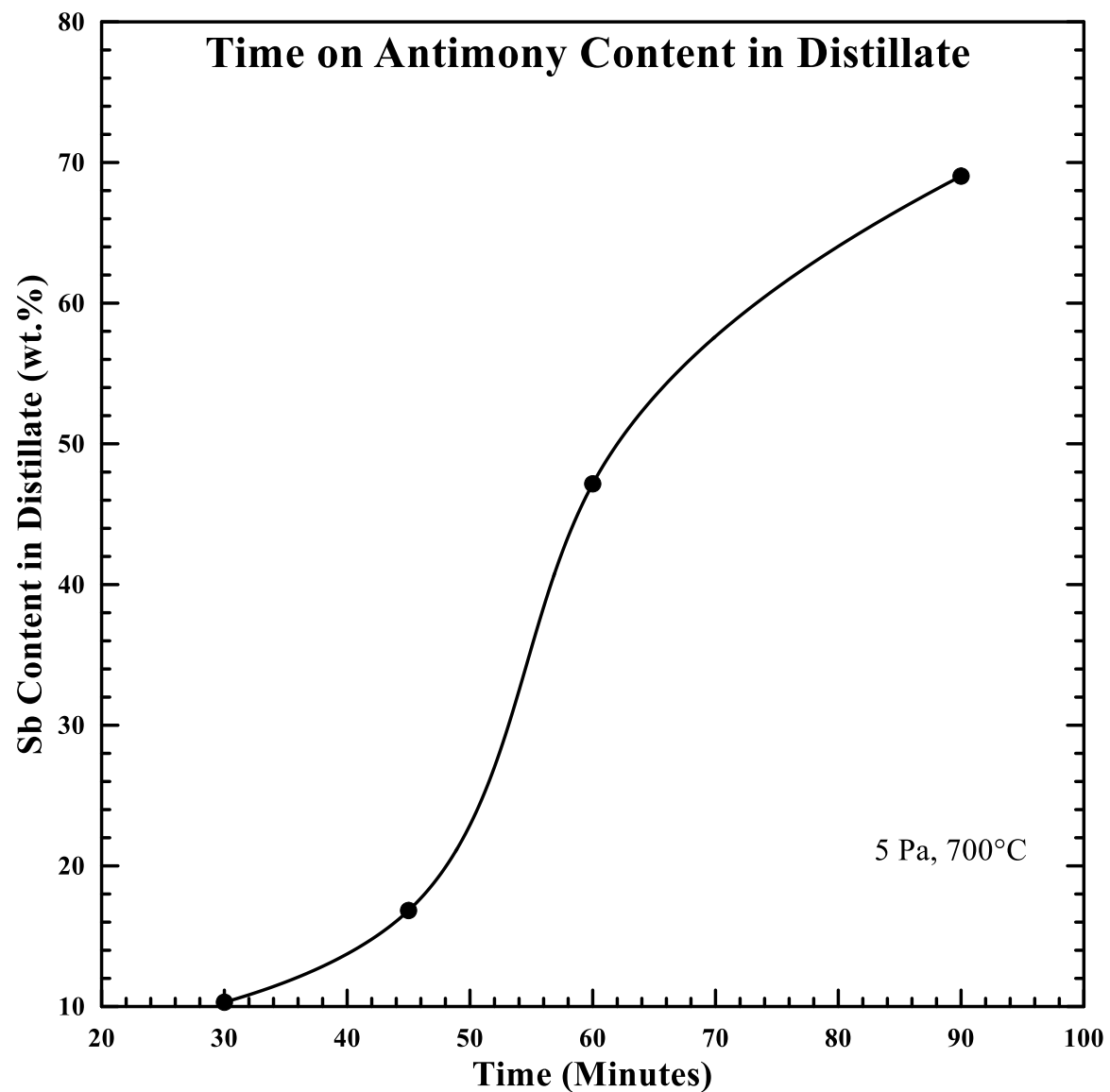


Figure 6.16 Effect of distillation time on the antimony content in the distillate fraction, experiments conducted at 5 Pa and 550°C

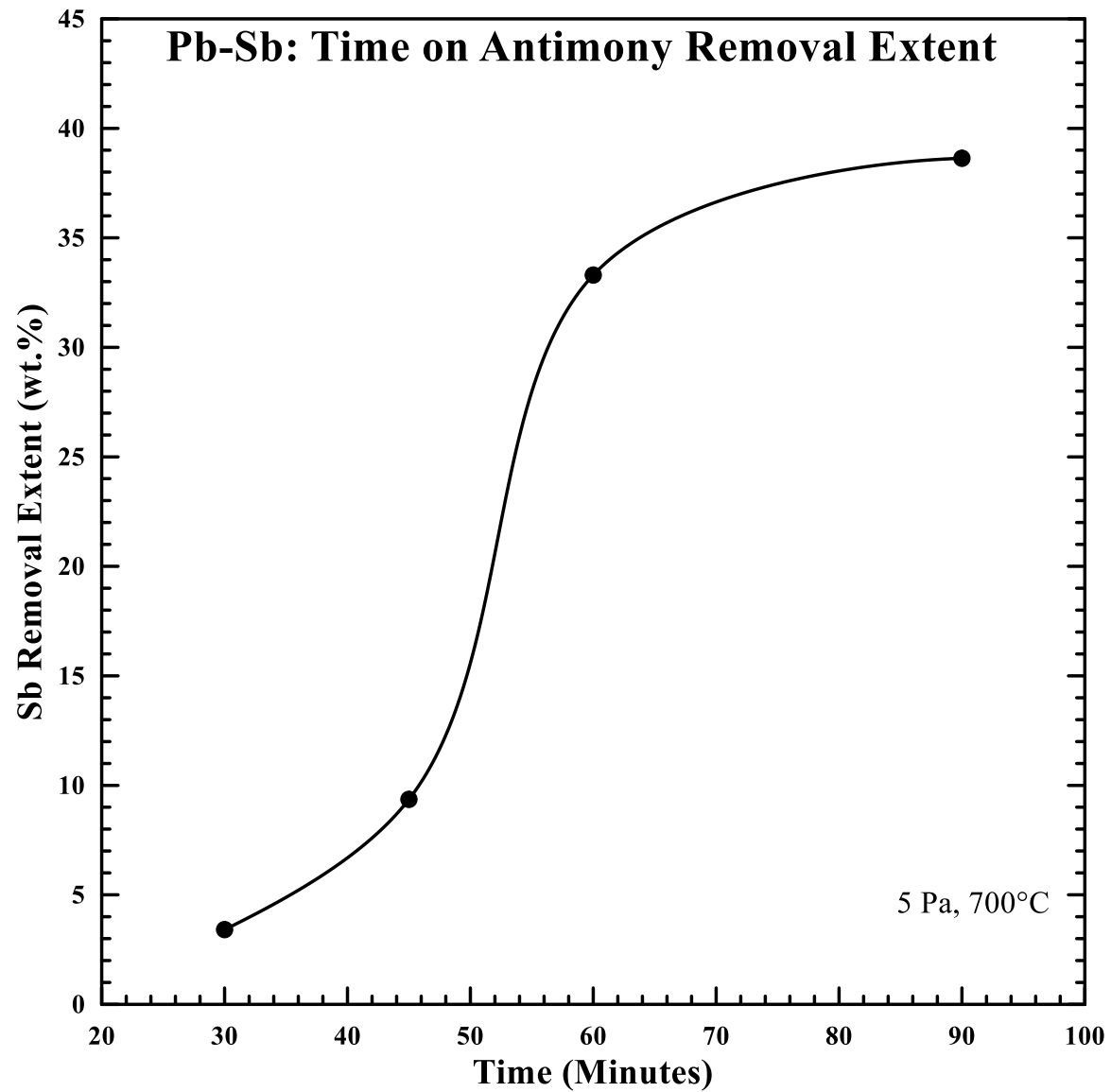


Figure 6.17 Effect of distillation time on the removal extent of antimony, experiments conducted at 5Pa and 700°C

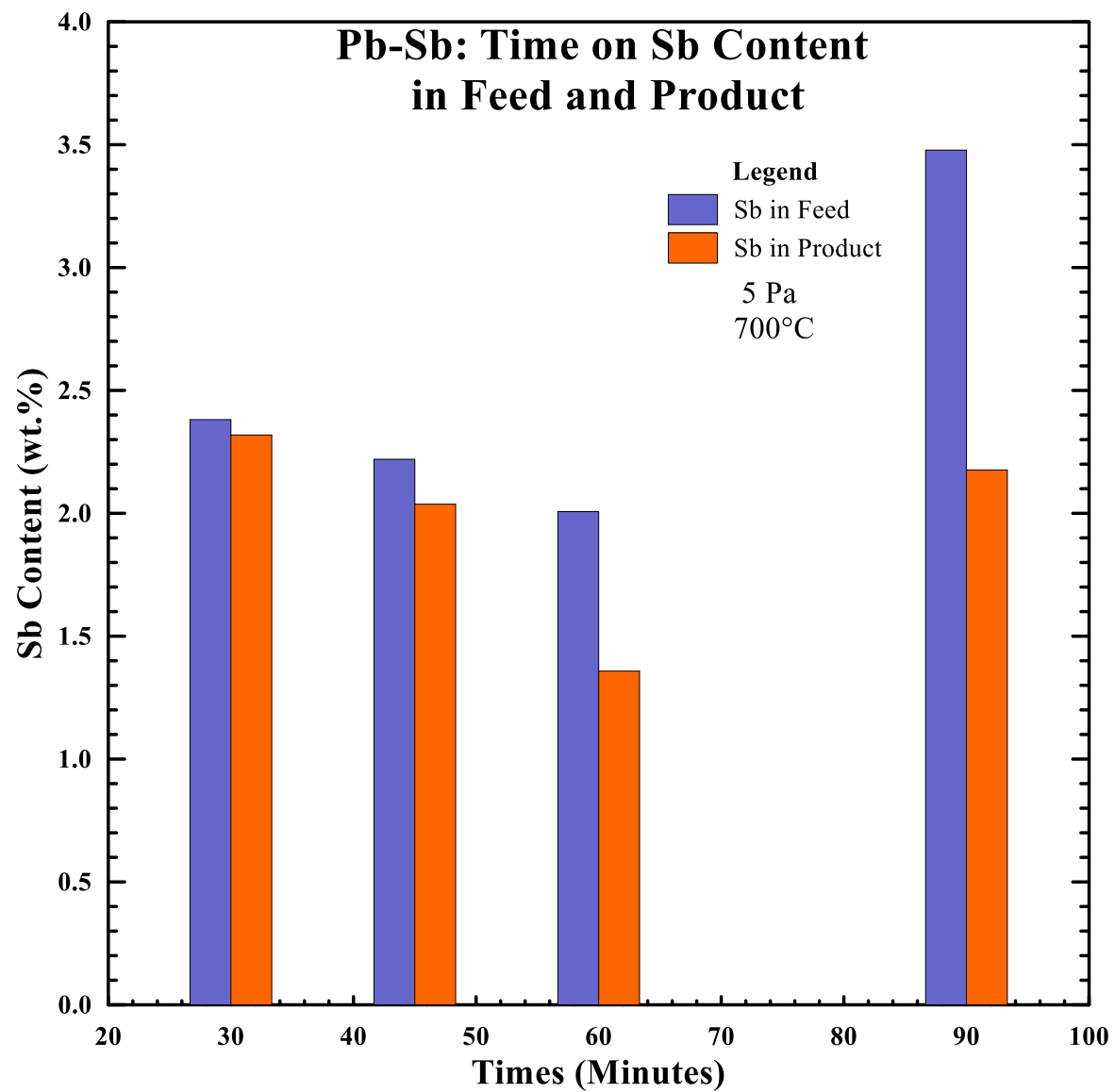


Figure 6.18 Effect of distillation time on the antimony content in both the feed and product samples, experiments conducted at 5 Pa and 700°C

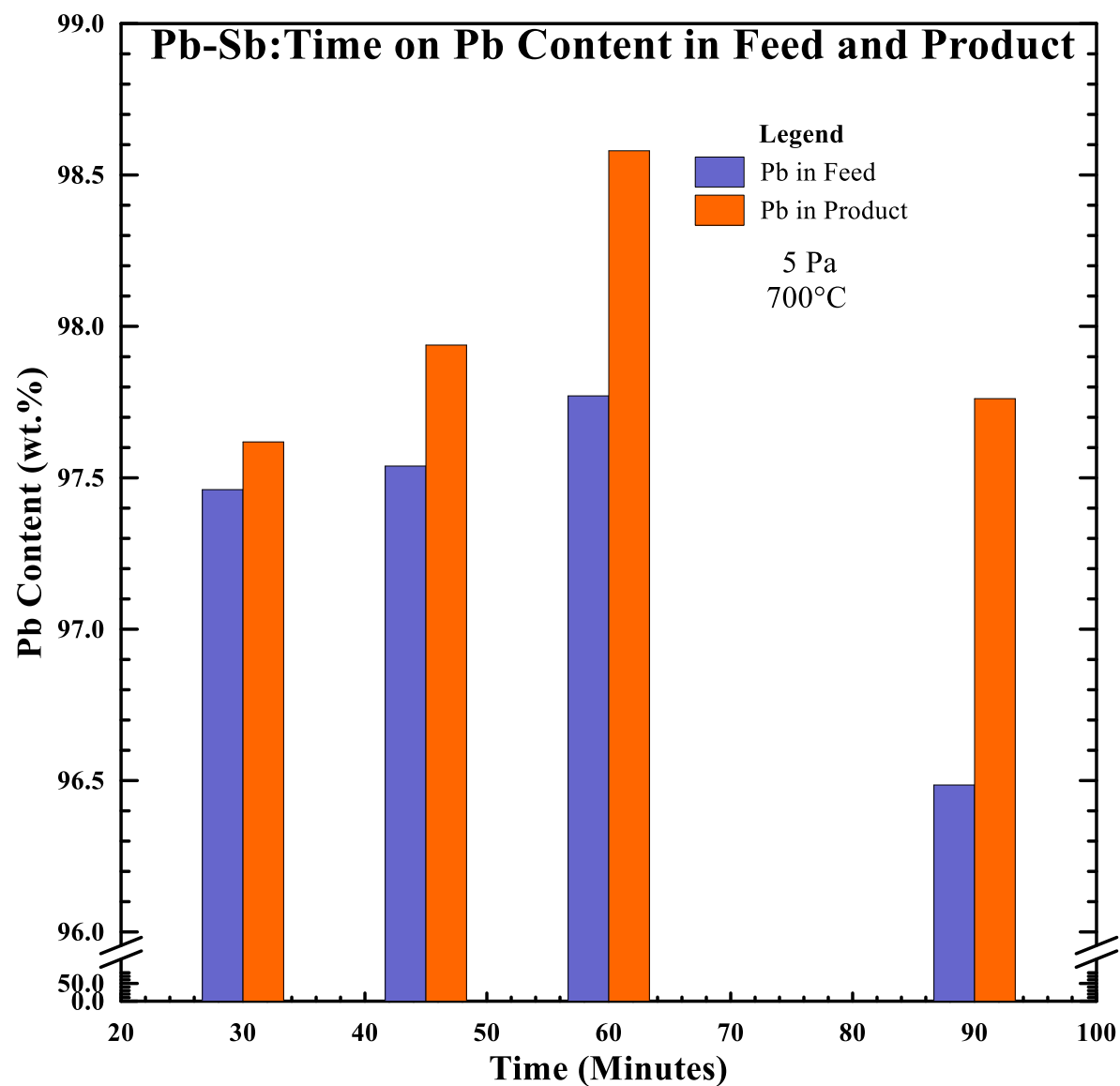


Figure 6.19 Effect of distillation time on lead content in both the feed and the product sample, experiments conducted at 5 Pa and 700°C

6.2.3 Effect of Pressure

Table 6.17 shows the results of the effect of distillation pressure for experiments conducted at 700°C for 30 minutes. The antimony content in the feed samples were 2.38, 2.69, 2.33, and 2.75 wt. %. As expected, the amount of material evaporated increased with a decrease in distillation pressure. Unlike the case of Pb-As system, the distillation pressure has a reasonably high effect on the weight of distillation, hence antimony removal.

Table 6.17 effect of distillation pressure on the removal of antimony

Test No	Pressure (Pa)	Feed weight (g)	Distillate Weight (g)	Product weight (g)	Weight loss (wt. %)	Calculated Distillate Weight (g)
4	5	150.84	0.161	149.65	0.68	1.19
9	10	156.10	1.126	155.35	0.24	0.75
10	15	156.63	1.024	156.07	-0.30	0.56
11	20	157.42	0.746	156.98	0.19	0.44

Figure 6.20 shows the effect of distillation pressure on the antimony content in the distillate fraction. Antimony content steadily decreased from 87.6 wt. % to about 11 wt. % when the pressure was decreased from 20 to 5 Pa. As was shown in table 6.16, distillation at 5 Pa favored lead volatilization, especially due to its high activity in the melt. By increasing the distillation pressure, lead's volatilization is less favored and the driving force for the separation of antimony from lead increases, hence antimony's content increased as well.

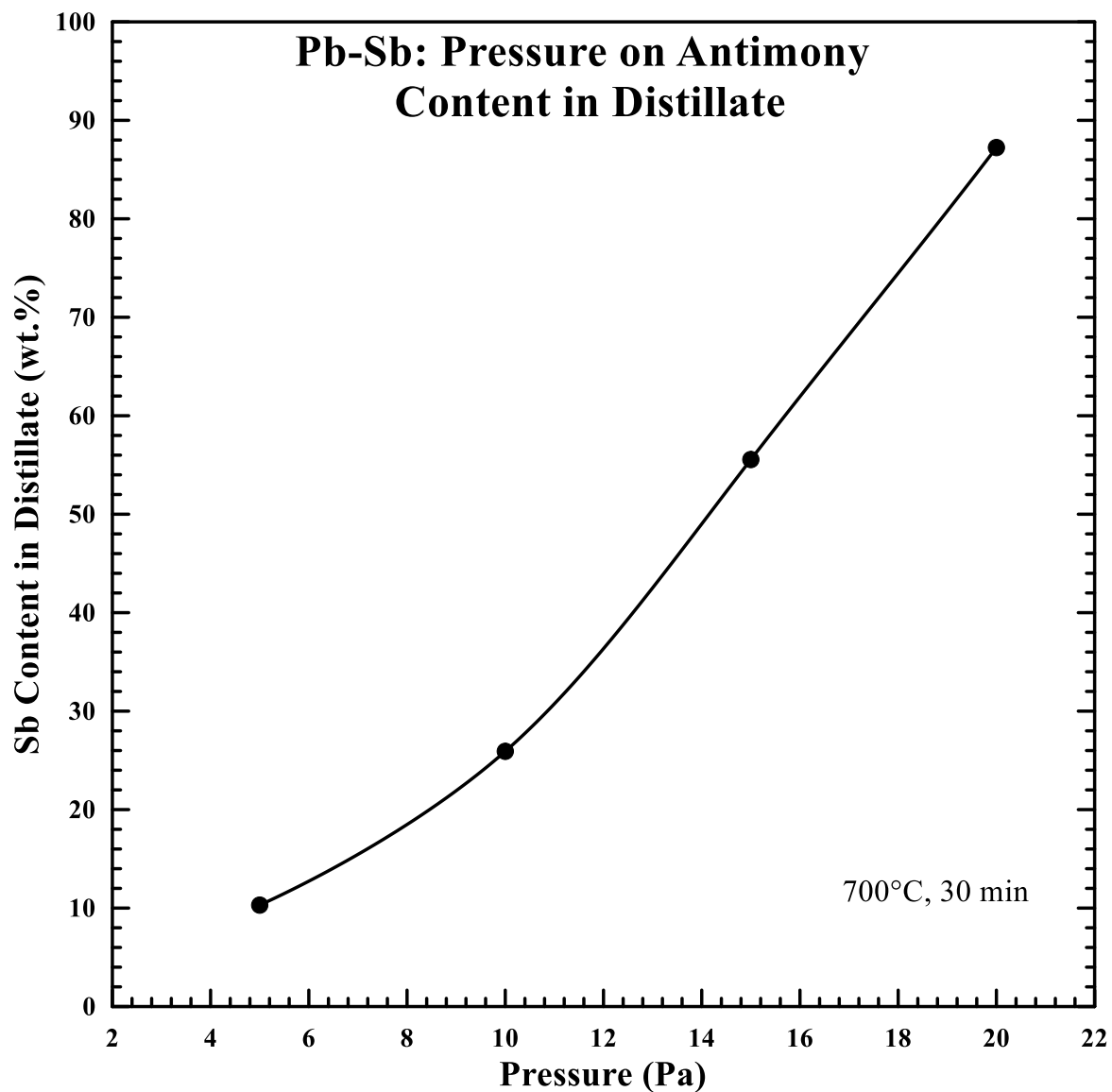


Figure 6.20 Effect of distillation pressure on antimony content in the distillate fraction, experiments conducted at 700° for 30 minutes

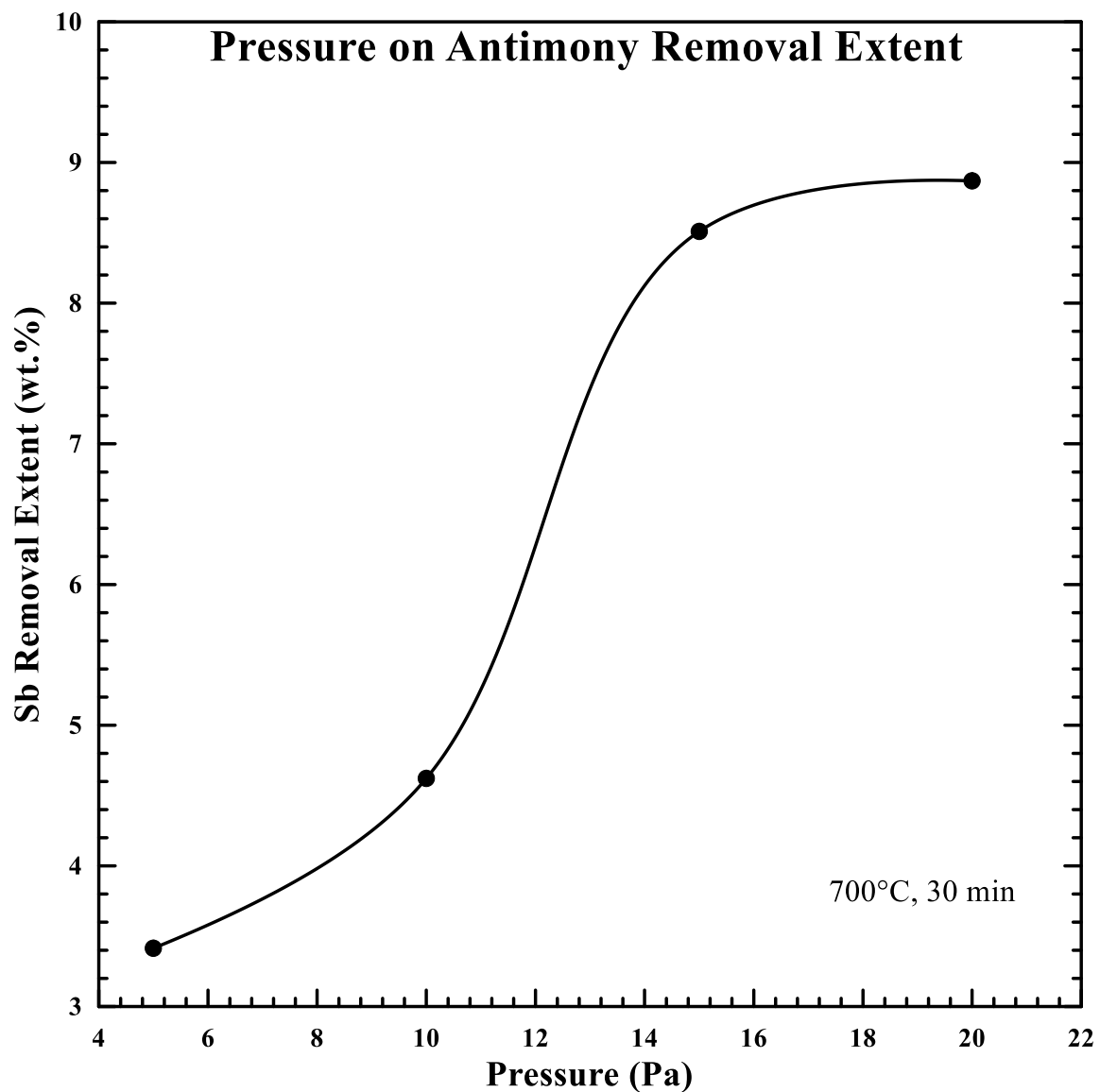


Figure 6.21 Effect of distillation pressure on antimony removal extent, experiments conducted at 700°C for 30 minutes

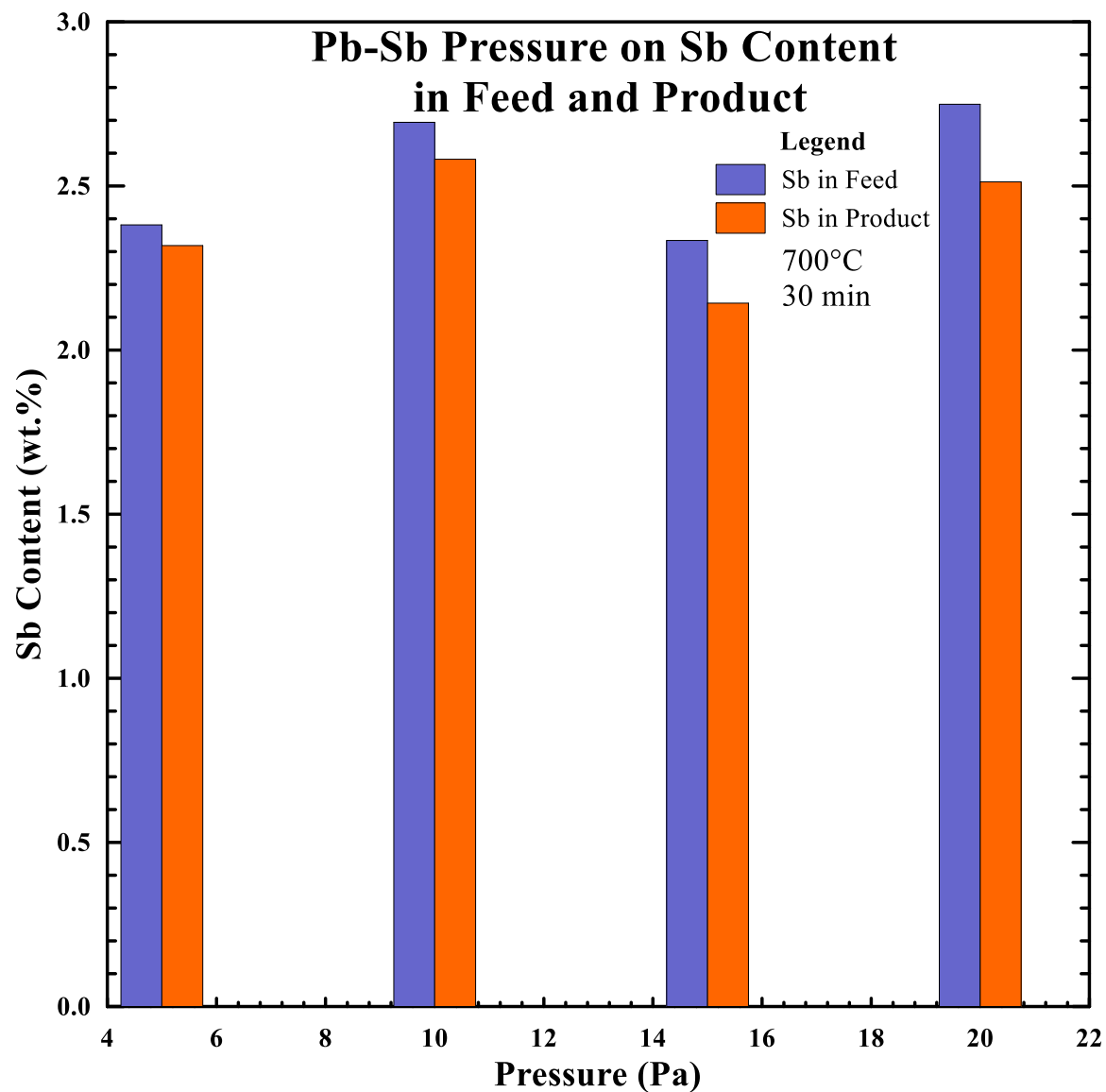


Figure 6.22 Effect of distillation pressure on antimony content in both the feed and product fraction, experiments conducted at 700°C for 45 minutes

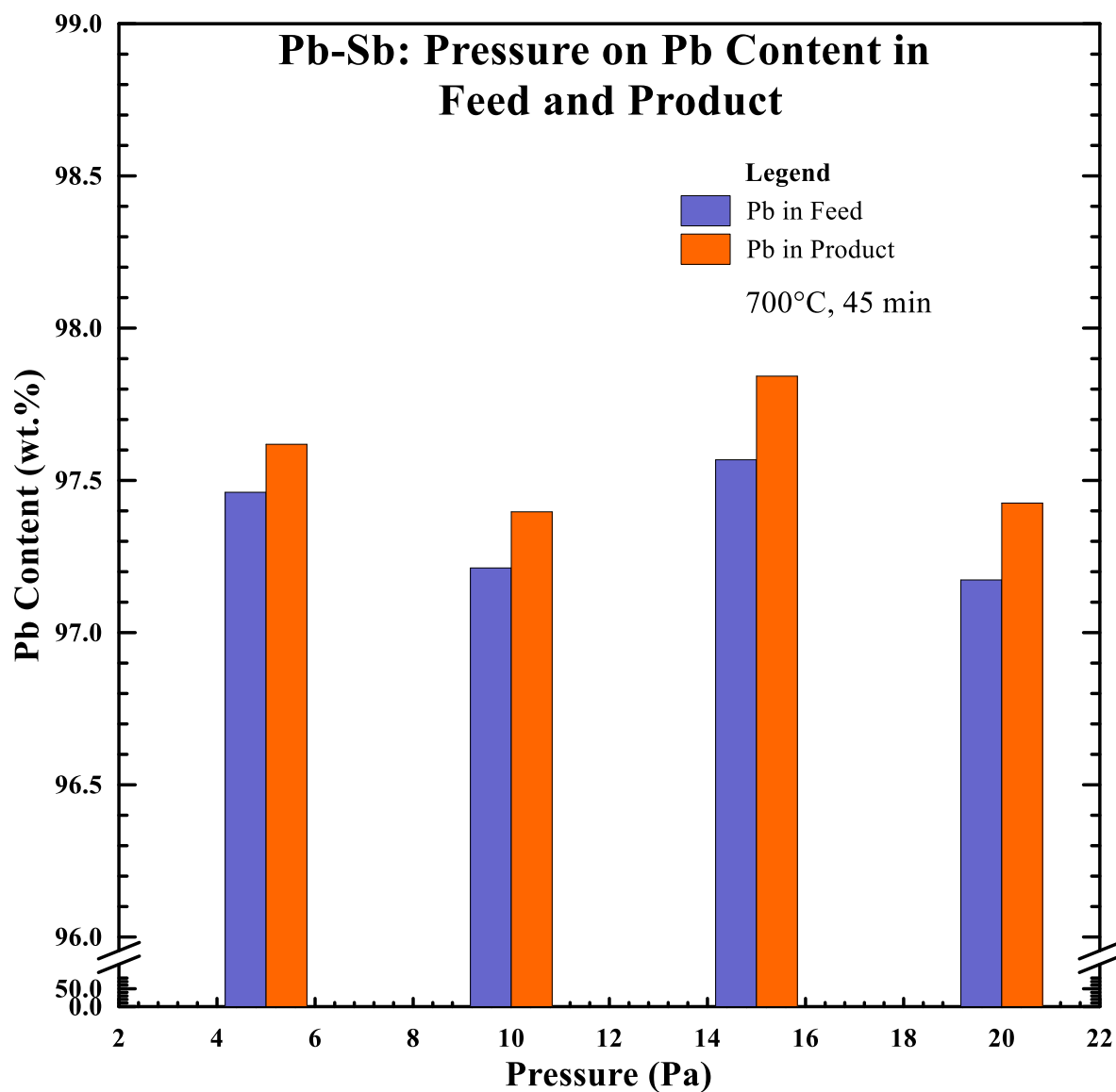


Figure 6.23 Effect of distillation pressure on lead content in both the feed and the product fractions, experiments conducted at 700°C for 45 minutes

Figure 6.21 shows the effect of distillation pressure on antimony removal. From figure 6.17, it was shown that in the 30-45 minutes range, antimony is still slowly happening; consequently, even at 20 Pa lead still volatilizes readily while antimony volatilizes slowly. Increasing the distillation pressure, enhances antimony removal; however, the removal extent does not increase significantly at 30 minutes since it increased from 3.4 to 9.8 wt. % from 5 to 20 Pa.

Distillation pressure does not significantly affect the removal at a fixed time and temperature. Figure 6.22 shows the effect of distillation pressure on antimony content in both the feed and product samples. According the results shown in the figure, no significant decrease in antimony content was achieved by decreasing the distillation pressure; antimony content decrease by 0.1 to 0.2 wt. % only. As can be seen in figure 6.23, it can be seen that only a minute level of refining was achieved for by decreasing the distillation pressure for an experiment of 30 minutes.

6.2.4 Effect of Temperature

Table 6.18 shows the results for the effect of distillation temperature for experiments conducted at 5 Pa for 30 minutes; the antimony concentration of the feed samples were 2.42, 2.28, 2.42, 2.38, and 2.51 wt. %. As shown in the table an increase in distillation temperature sharply increased the amount of material vaporized from the alloy. Because distillate fraction of experiments 1 and 2 were very small to obtain an accurate analysis, they were excluded from the study of the effect.

Table 6.18 Effect of distillation temperature on the removal of antimony

Test No	Temperature (°C)	Feed weight (g)	Distillate Weight (g)	Product weight (g)	Weight loss (wt. %)	Calculated Distillate Weight (g)
*1	550	149.21	0.045	149.16	0.0064	0.05
*2	600	149.2	0.050	149.15	0.0002	0.05
3	650	150.81	0.138	150.52	0.10	0.29
4	700	150.84	0.161	149.65	0.68	1.19
5	750	151.13	2.448	146.81	1.24	4.32

*Experiments excluded from effect analysis because of inconclusive analysis

Figure 6.24 shows the effect of distillation temperature on the antimony content in the distillate fraction. According to results shown in the figure, the antimony content in the distillate fraction sharply decreased from 20.3 to 8.5 wt. % when the distillation temperature was increased from 650°C to 750 °C. An increase in distillation temperature above 650 °C results in a significant decrease in antimony content in the distillate fraction. Not only antimony, but also lead volatilization is greatly enhanced with an increase in temperature; lead content in the distillate fraction increased from 56 to 91 wt. % (see figure B-7 in appendix B).

As shown in figure 6.25, the increase in distillation temperature increased antimony removal extent from 1.6 to 9.8 wt. %. While the increase in temperature increases antimony removal, lead entrainment to the distillate fraction is significant enough that the distillate can be viewed as a hard lead product for experiments conducted at 750°C and 30 minutes. Referring to results shown in figure 6.17, this effect would be even stronger as distillation time increases. Therefore, it is not ideal to run the experiments at temperatures equal to or above 750°C to separate antimony from lead.

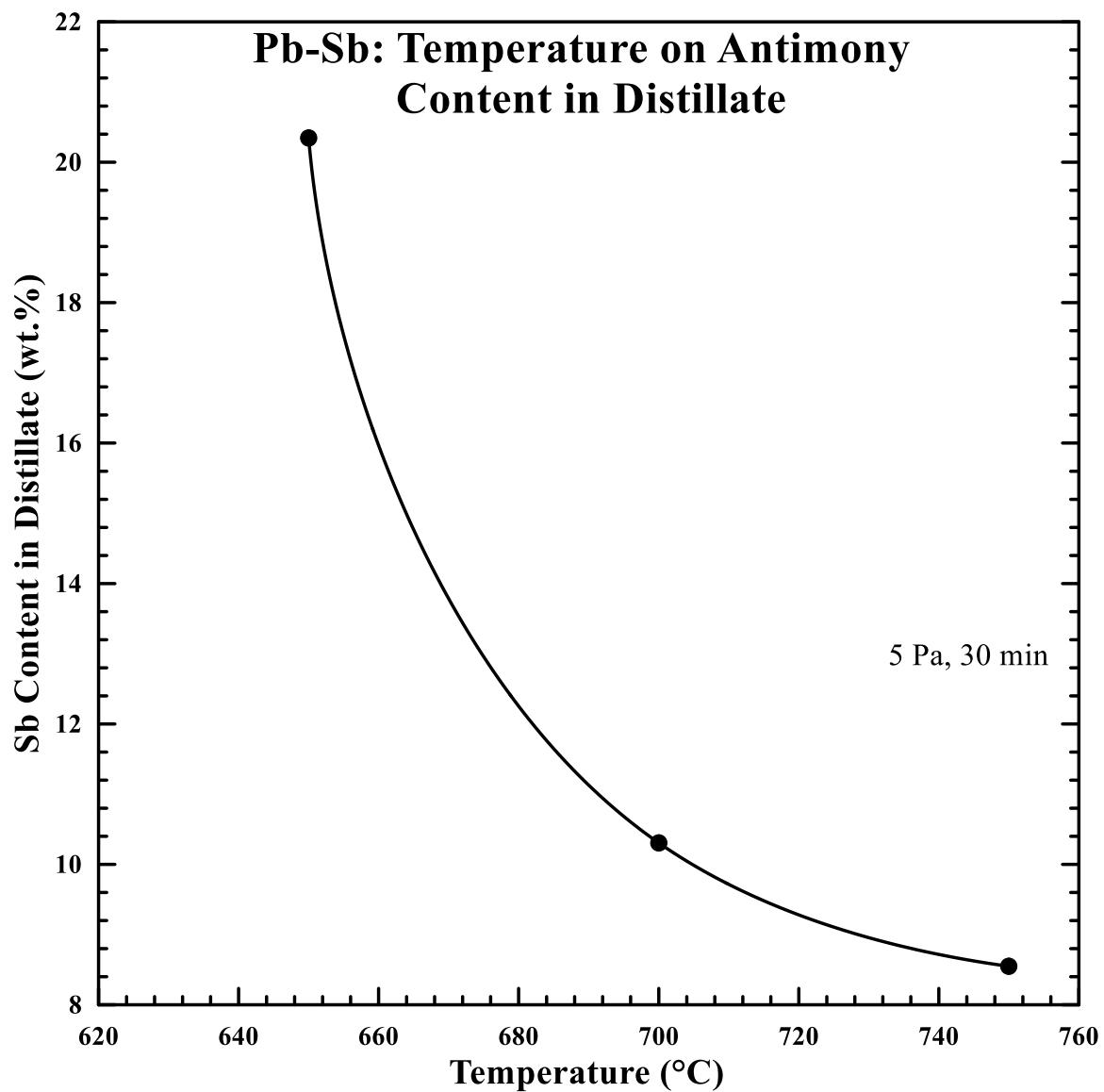


Figure 6.24 Effect of distillation temperature on antimony content in the distillate fraction, experiments conducted at 5 Pa for 30 minutes

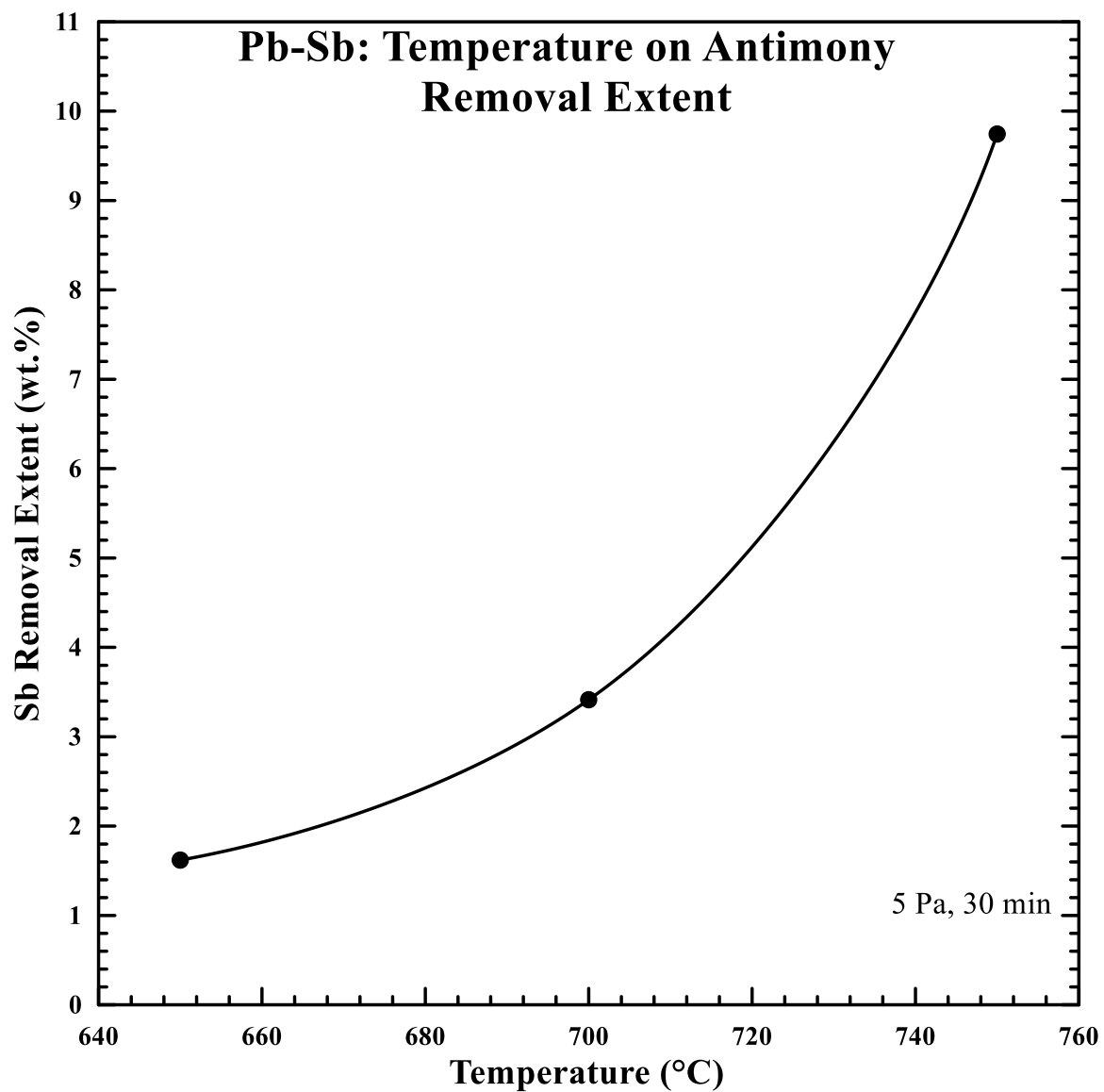


Figure 6.25 Effect of distillation temperature on the removal extent of antimony, experiments conducted at 5 Pa for 30 minutes

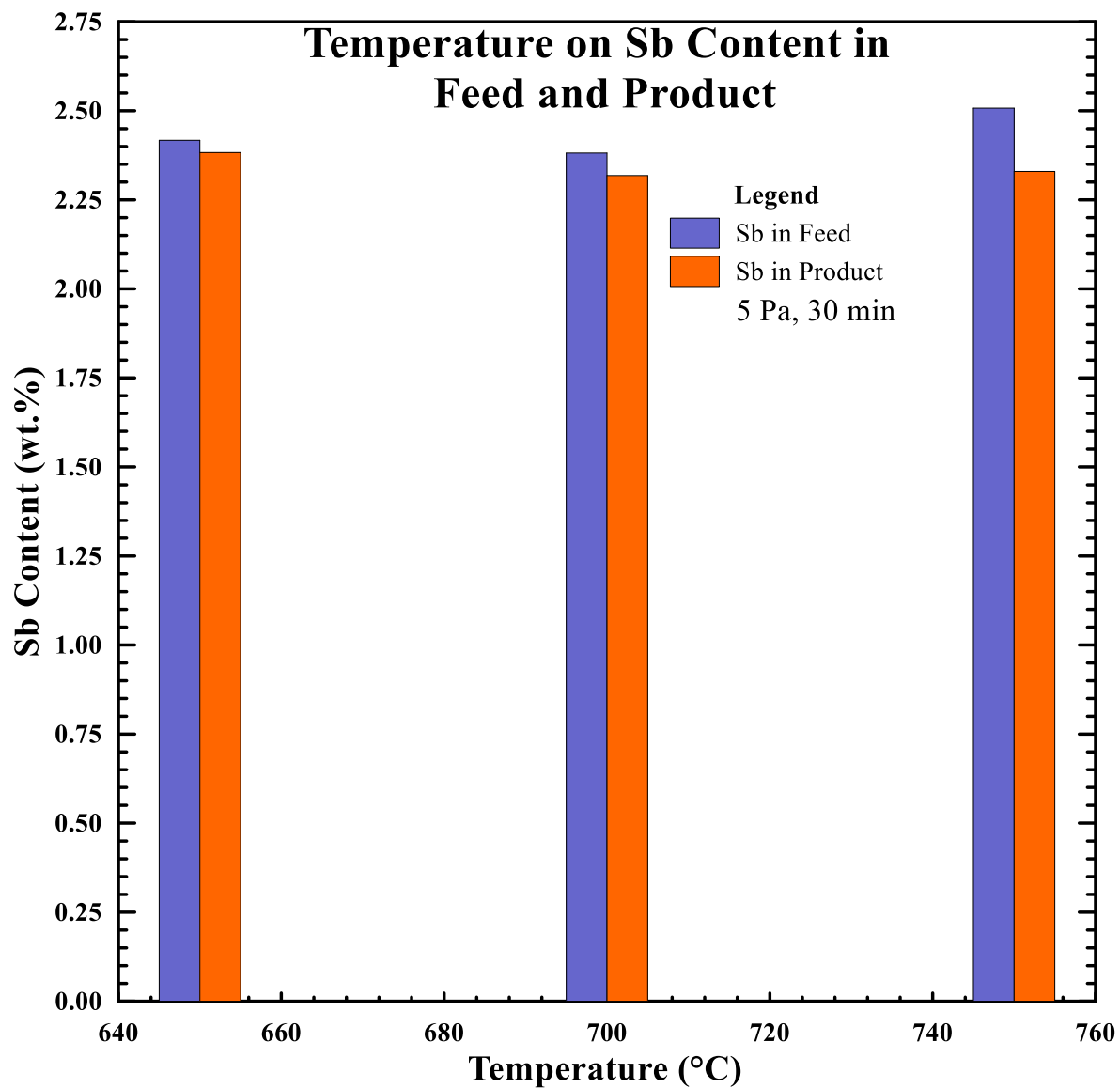


Figure 6.26 Effect of distillation temperature on antimony content in both the feed and product samples, experiments conducted at 5 Pa for 30 minutes

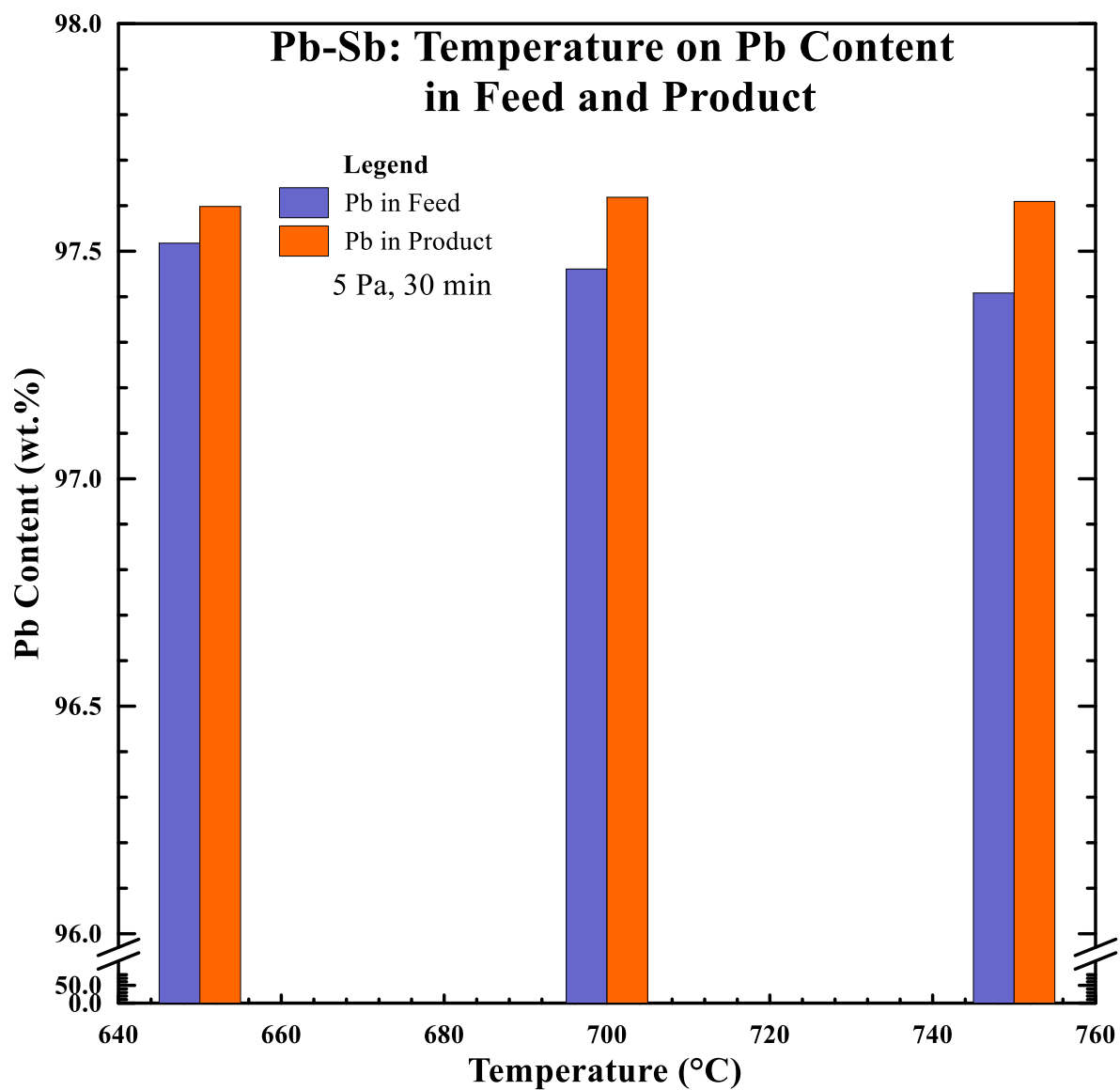


Figure 6.27 Effect of distillation temperature on lead content in both the feed and product samples, experiments conducted at 5 Pa for 30 minutes

Figures 6.26 and 6.27 show the effect of distillation temperature on antimony and content in both the feed and product samples the increment of increase in lead content and decrease in antimony content in the product sample steadily increased with an increase in distillation temperature. The antimony removal and lead refining itself was not significant; antimony content decreased from 2.5 to 2.33 wt. % while lead was refined from 97.4 to 97.6 wt. %.

Results shown here are based on single tests; therefore, no error bars are shown; nonetheless, this kind these results, cannot be considered per say as an improvement in refining. Propagation of error in calculating the antimony and lead content could be comparable to the 0.2 wt. % increment. Replicate testing need be conducted to confirm, or dispute results presented here. Also, longer distillation time should be investigated to assess the temperature effect above 45 minutes.

6.2.5 Effect of Initial Arsenic Content in the Feed

Table 6.19 shows the results of the effect of antimony initial composition for experiment conducted at 5 Pa, 700 °C, and 45 minutes; the antimony content in the feed sample are those shown in table 6.13. The amount of material vaporized was relatively constant in this case. It was however slightly higher than the distillate fraction that from experiment 4.

Table 6.19 Effect of initial antimony content on the removal of antimony

Test No	Sb Grade in Feed (wt. %)	Feed weight (g)	Distillate Weight (g)	Product weight (g)	Weight loss (wt. %)	Calculated Distillate Weight (g)
12	0.32	196.42	0.423	194.40	0.81	2.02
13	0.63	198.52	1.022	196.70	0.40	1.82
14	1.37	195.72	1.241	193.63	0.43	2.09
15	2.34	193.78	1.575	191.95	0.13	1.83
16	3.81	195.20	0.939	193.73	0.27	1.47

Figure 6.28 shows the effect of initial antimony content in the feed sample on its content in the product sample. According to the results, antimony content in the distillate phase increases with an increase with its initial concentration. The removal of impurities is a function of their activity in the melt; as the antimony content is increased, so is its activity, in turn its equilibrium partial pressure. Consequently, an increase in antimony content in the distillate fraction is expected, hence the trend observed in figure 6.28.

Table 6.19 shows that the distillate weight is relatively constant as the initial antimony content increases; meanwhile, figure 6.28 shows that antimony content in the distillate fraction increases with the same effect. This suggests that lead volatilization is favored compared to that of antimony. This observation strengthens the author's claim for the trend seen in figure 6.16 and 6.20. Lead is in fact vaporizing readily from the alloy at 5 Pa; its content in the distillation fraction decreases from 91.5 to 52 wt. % in the distillate fraction (see figure B-8 in appendix B).

Figure 6.29 shows the effect of initial antimony concentration on antimony removal extent. According to the results, antimony removal decreased significantly with an increase in initial concentration. An increase in initial content of antimony means that there is more of it in the alloy that is available for removal. Meanwhile, the distillation takes place at 45 minutes which results in the same distillate weight. Even though its activity in the melt is increased, antimony still volatilizes slowly compared to lead. It makes sense that the removal extent decreases significantly as seen in the figure because antimony is barely volatilized after 45 minutes distillation time.

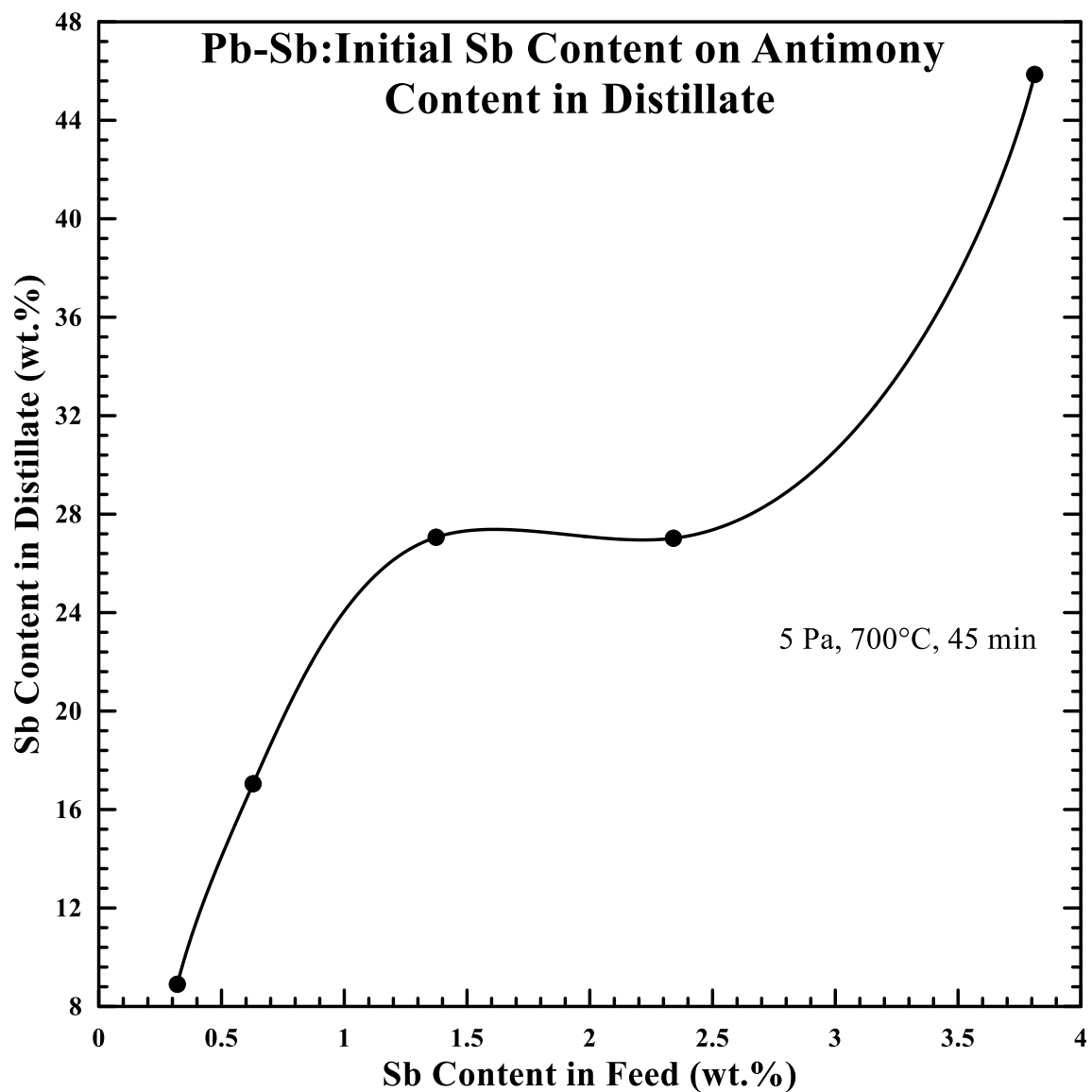


Figure 6.28 Effect of initial antimony content in the feed sample on antimony content in the distillate fraction, experiments conducted at 5 Pa, 700°, and for 45 minutes

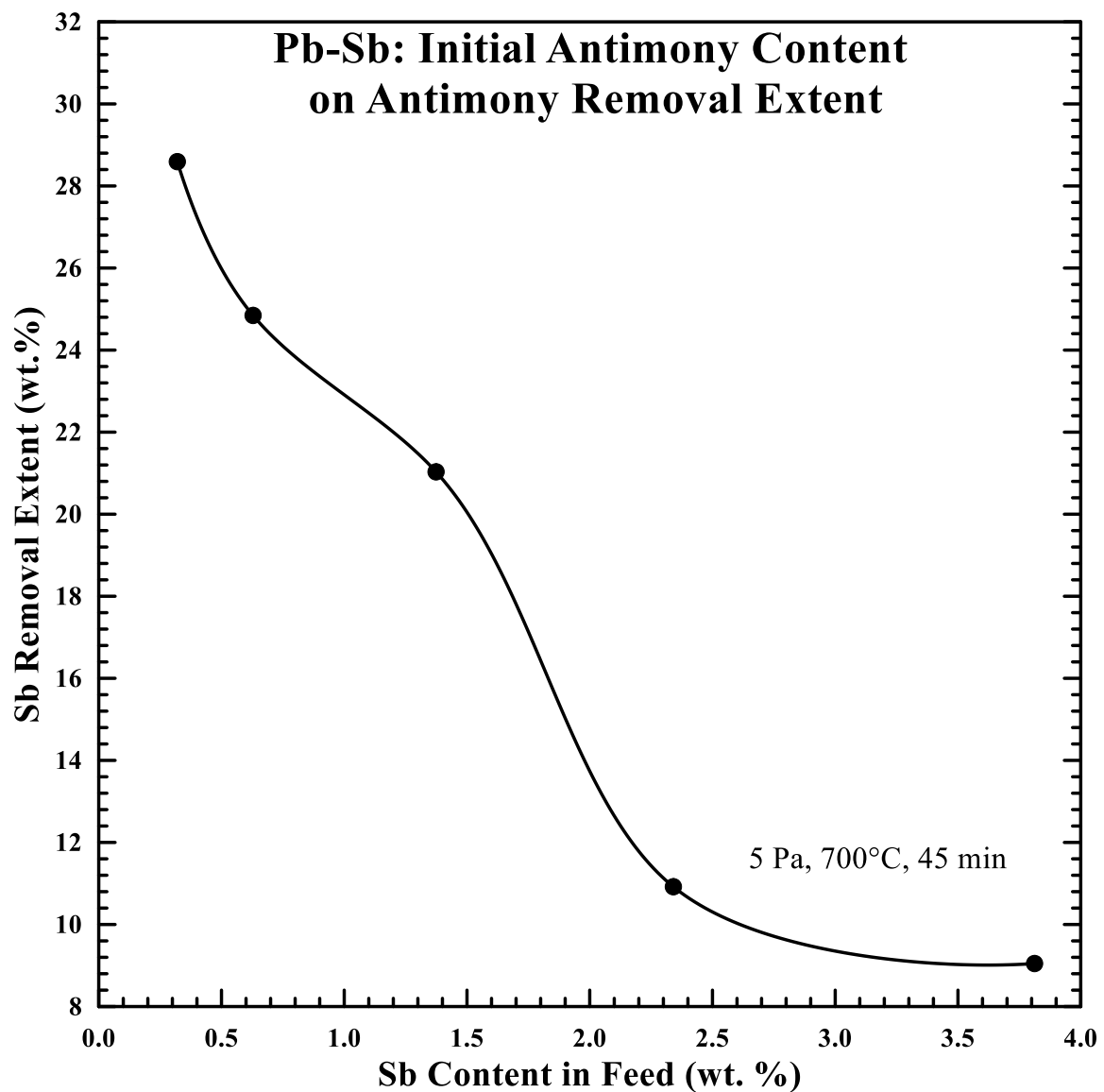


Figure 6.29 Effect of initial antimony concentration in the feed sample on antimony removal extent, experiments conducted at 5 Pa, 700°C and for 45 minutes.

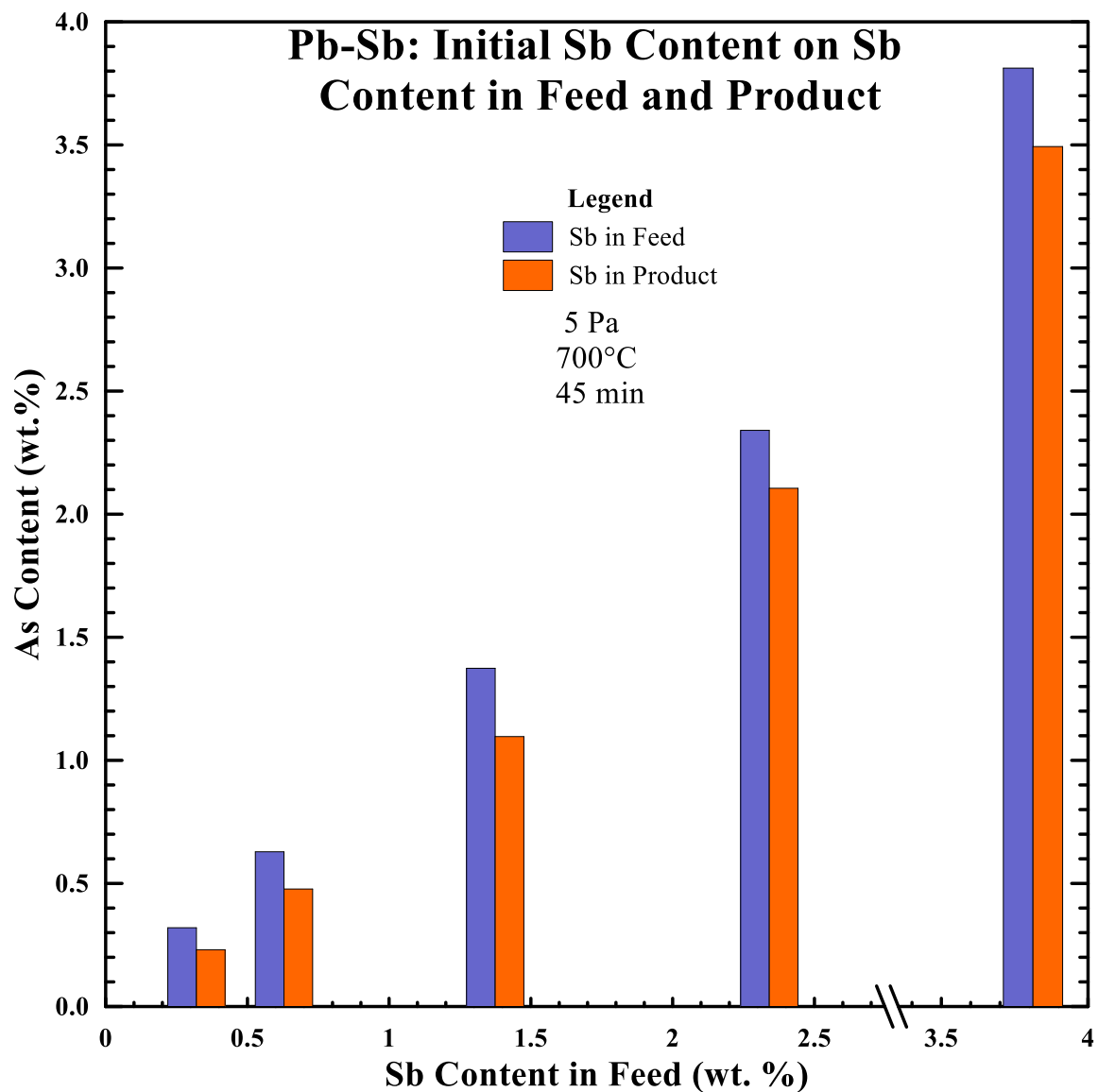


Figure 6.30 Effect of initial antimony initial concentration on antimony content in both the feed and product sample, experiments conducted at 5 Pa, 700°C, and for 45 minutes

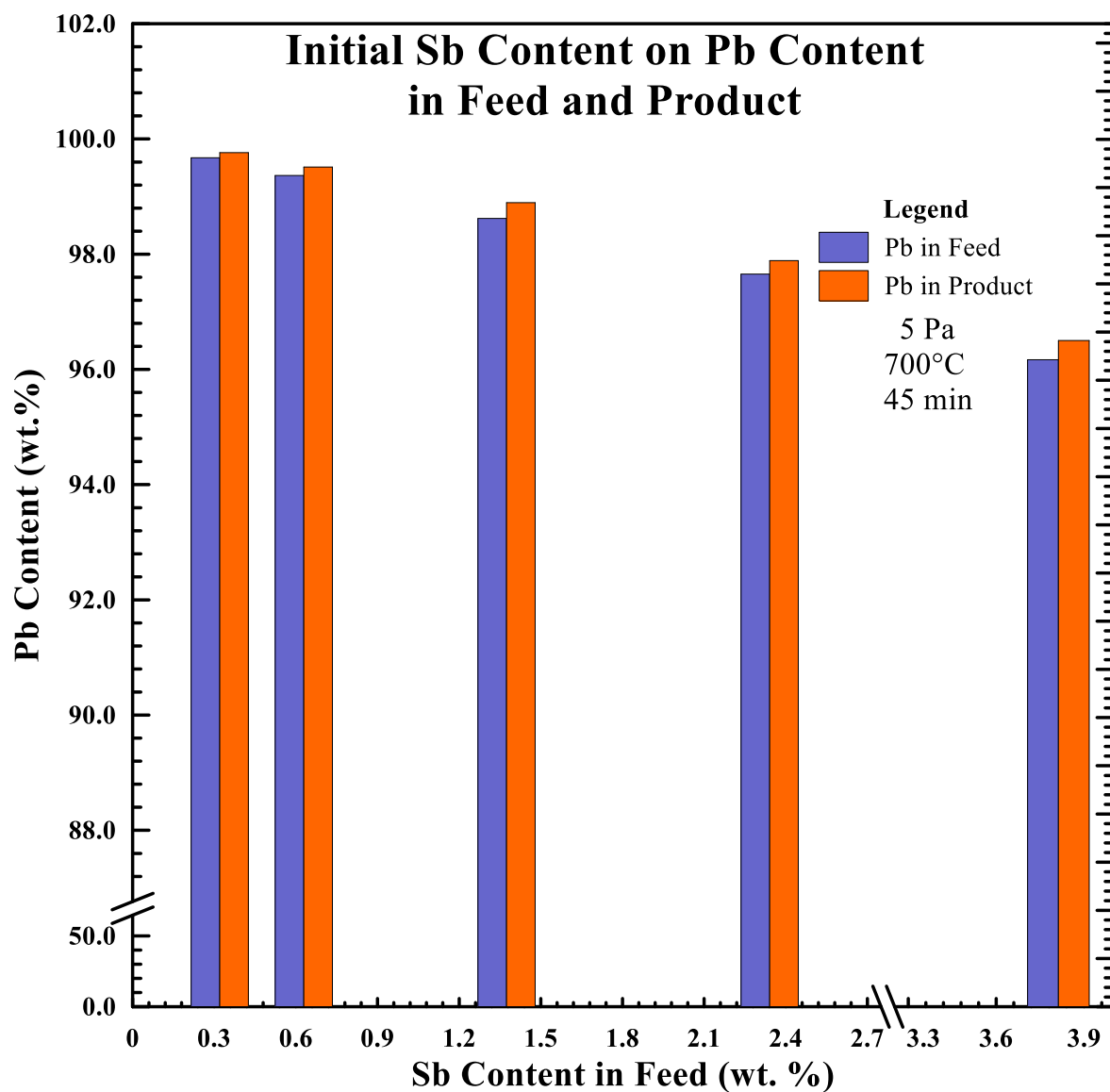


Figure 6.31 Effect of initial antimony initial concentration on lead content in both the feed and product sample, experiments conducted at 5 Pa, 700°C, and for 45 minutes

Figures 6.30 and 6.31 show the effect of initial antimony concentration on antimony and lead content in both the feed and the product samples. According to these results, the decrease in antimony content, and eventually the refining of lead is affected by the initial concentration. The increments of increase or decrease in concentration were not significant enough to attribute success to the refining process

An interesting outcome from the study of this effect is that in the first 45 minutes of distillation, lead appears to be the first to vaporize due to its high activity in the melt. This suggests that the onset for lead removal occurs before that of antimony because whether it was .5 or 3.9 wt. % initial concentration, about 1.8 grams of material was collected in the distillate fraction.; the onset of antimony removal was accelerated by an increase in temperature; however an increase in temperature also has the effect of enhancing the kinetics of lead vaporization.

CHAPTER SEVEN

CONCLUSIONS

Predictions of vapor-liquid equilibrium (VLE) were applied to binary systems, and vacuum distillation experiments were conducted for Pb-As and Pb-Sb alloys. Major conclusions drawn from the present study are listed as followed:

1. A literature survey was conducted, and thermochemistry data for the Pb-As are provided
2. The MIVM, Wilson equation, and NRTL model were used to predict binary parameters (henceforth activity coefficient), and the parameters are for the MIVM $B_{AS-Pb} = 0.9248$, $B_{Pb-As} = 1.1754$, for the Wilson equation $A_{AS-Pb} = 0.0199$, $A_{Pb-As} = 3.9968$, and for NRTL ($\tau_{AS-Pb} = -2.3885$, $\tau_{Pb-As} = 4.0669$). VLE predictions, and T-x-y diagram were obtained; since there was no other predictions that have been reported in literature for the Pb-As system, the research team has accepted the diagram as acceptable.
3. Binary parameters were predicted for the Pb-Sb system and they are for the MIVM $B_{Sb-Pb} = 1.0223$, $B_{Pb-Sb} = 1.0224$, for the Wilson equation $A_{Sb-Pb} = 1.1287$, $A_{Pb-Sb} = 1.1287$, and for the NRTL model $\tau_{Sb-Pb} = -1.4718$, $\tau_{Pb-Sb} = 1.7258$. Parameters predicted with MIVM was in general agreement with data reported in literature. The slight difference came from the use of a difference value for the constant D of the Clausius-Clapeyron equation for lead. Parameters determined using the NRTL model was an exact match with data reported in literature. Once again, the different in appearance of the diagram came from the different use of D.

4. Vacuum distillation experiments were conducted for binary Pb-As and Pb-Sb alloys by varying the distillation pressure, temperature, time, and initial composition of the impurity in the alloy. It was determined that the arsenic removal extent increased with a decrease in distillation pressure, and an increase in distillation time and temperature. It was also observed that the removal was a stronger function of distillation temperature than it is of time and pressure. At 5 Pa, 45 minutes, and 650°C, arsenic was reduced from 2.46 wt. % in the feed sample to 0.53 wt. % in the product sample; this was the highest removal that was achieved across all experiments. At this point in the research, it is recommended that distillation be conducted at temperatures between 600 and 650°C, for durations between 45 and 60 minutes.
5. Vacuum distillation experiments conducted on the Pb-Sb binary system showed that no significant evaporation was obtained below 700 °C. It was shown that the removal of antimony was strongly dependent on temperature and time.
6. It was also interestingly observed that lead was vaporized before antimony regardless of the initial antimony content in the feed sample. The onset of antimony vaporization decreased with an increase in temperature; however, high temperature results in enhanced vaporization of lead such that the distillation fraction was just another crude lead alloy. The decrease in distillation pressure did not result in significant increase in antimony removal. At this point in the research, it is recommended that time and temperature be studied further for the removal of antimony from lead as they are stronger functions. While pressure does not significantly increase antimony removal, a higher distillation pressure will decrease lead entrainment in the distillate fraction.

CHAPTER EIGHT

RECOMMENDATIONS AND FUTURE WORK

8.1 Effect of Melt Agitation

As was mentioned in the conclusion chapter, the lowest arsenic content in the product sample (0.53 wt. %) was obtained from a distillation test conducted at 650°C, for 45 minutes, and 5 Pa pressure. Experiments shown in the results section were conducted in the absence of agitation of the melt. The evaporation reaction is assumed to be spontaneous (arsenic is evaporated as soon as it arrives on the surface); the resistance of vapor transport is significantly decreased because at lower pressures, collisions between vapor particles is decrease. Consequently, the transport of the impurity from the bulk to the liquid/vapor interface is determined to the evaporation rate limiting step.

To enhance mass transfer in the liquid phase, the interface should quickly be replenished in arsenic, and one way of doing it is through agitation. In order to control vacuum, the melt can be agitated by bubbling an inert gas (argon gas in this case). For ease of operation, a vertical configuration of the distillation reactor should be considered. With this suggestion, agitation will be most effect around the area close to the bubbling gas contact with the melt; high flow rates of the bubbling gas might be required to achieve uniform mixing of the melt. A remediation to this problem is the use an induction mixing. Another possibility of enhancing mass transfer in the liquid phase is to increase the area to volume ratio. In this scenario, the heated melt would be trickled down in reactor on a plate. In this manner, the area being exposed to low pressure is significantly larger than the volume which can be obtained by the mass trickling down divided

by the melt density. This method will require an intricate design of the reactor such that the pressure and temperature are controlled, while the sample is introduced in the reactor.

8.2 Multicomponent Systems VLE

The presence of multiple impurities the lead bullion will affect the removal of arsenic during distillation. Depending on their content in the melt, their activity might be higher or lower than that of arsenic. The partial pressure for each impurity above can be predicted. One of the reasons the three models studied in the present research were chose was their ability to predict the activity of multicomponent system using only the parameters for the respective binary systems. Prior to the selection of the impurities of interest, the research team proceeded to predict binary parameters for seven impurities which are commonly found in lead bullion and are shown in tables 8.1-4.

Binary parameters for the As-Cu, As-Ag, and Ag-Zn were not calculated because of the lack of activity data through their intermetallic parts of the phase diagram. (C_p data for intermetallic phases could not be located). For the As-Bi, calculations were difficult because the research team had not successfully located experimental activity data, nor even an expression for the excess Gibbs free energy for this system. Consequently, there is still room for research on these particular binary systems. Equations 3.6, 3.22 and 3.32 can be used to calculate the multicomponent activity coefficient for each component, then the partial pressure can still be calculated using equation 3.3.

Table 8.1 MIVM Binary parameters for lead and seven of its most common impurities.

MIVM						
Temp (K)	i	j	B_{ij}	B_{ji}	RMSD a_i	RMSD a_j
913	Pb	As	1.1754	0.9248	0.0114	0.0210
923	Pb	Zn	0.8621	0.6009	0.0596	0.0699
905	Pb	Sb	1.0224	1.0223	0.0004	0.0004
700	Pb	Bi	1.0889	1.0629	0.0041	0.0037
1273	Pb	Ag	0.6310	1.2999	0.0074	0.0101
1050	Pb	Sn	0.5310	1.2639	0.0042	0.0044
1473	Pb	Cu	0.8699	0.7864	0.0099	0.0076
1423	As	Zn				
1373	As	Sb	0.7971	1.4150	0.0217	0.0255
913	As	Bi				
1423	As	Ag				
913	As	Sn	1.4670	0.5649	0.1036	0.0585
1423	As	Cu				
823.1	Zn	Sb	1.4462	0.8088	0.0632	0.0396

Table 8.1 Continued

MIVM						
Temp (K)	i	j	B_{ij}	B_{ji}	RMSD a_i	RMSD a_j
873	Zn	Bi	0.5119	1.0985	0.0228	0.1821
1023	Zn	Ag	1.2686	1.0893	0.0227	0.0138
750	Zn	Sn	0.9896	0.8247	0.0455	0.0428
1300	Zn	Cu	1.3187	0.9796	0.0236	0.0087
1200	Sb	Bi	1.3689	0.7688	0.0297	0.0499
1250	Sb	Ag	1.2645	0.9246	0.0700	0.0699
905	Sb	Sn	1.3663	0.7768	0.0140	0.0080
1190	Sb	Cu	1.3450	0.9251	0.0769	0.0868
1000	Bi	Ag	1.0187	0.8601	0.0730	0.0871
600	Bi	Sn	1.1605	0.7852	0.0008	0.0003
1200	Bi	Cu	0.9538	0.7290	0.0050	0.0050
1250	Ag	Sn	1.2155	0.9587	0.0759	0.0419
1423	Ag	Cu	0.9763	0.8109	0.0962	0.0098
1400	Sn	Cu	1.5974	0.6006	0.0535	0.0872

Table 8.2 MIVM coordination numbers at experimental activity temperatures

Coordination Number Z								
T (K)	Pb	As	Zn	Sb	Bi	Ag	Sn	Cu
913	9.3149	4.3803	9.4935	8.9583	8.7756	9.8072	9.2171	9.9460
923	9.3216	4.3703	9.4999	8.9485	8.7750	9.8036	9.2177	9.9402
905	9.3097	4.3886	9.4885	8.9665	8.7762	9.8104	9.2168	9.9510
700	9.2133	4.7039	9.4183	9.3217	8.8686	9.9764	9.2587	10.1798
1273	9.6226	4.1714	9.8260	8.8247	8.8763	9.8093	9.3211	9.8937
1050	9.4170	4.2691	9.5974	8.8607	8.7876	9.7794	9.2389	9.8923
1473	9.8388	4.1367	10.0784	8.8748	9.0049	9.8873	9.4275	9.9546
1423	9.7823	4.1419	10.0116	8.8567	8.9692	9.8643	9.3986	9.9353
1373	9.7273	4.1493	9.9472	8.8421	8.9358	9.8435	9.3712	9.9185
913	9.3149	4.3803	9.4935	8.9583	8.7756	9.8072	9.2171	9.9460
1423	9.7823	4.1419	10.0116	8.8567	8.9692	9.8643	9.3986	9.9353
913	9.3149	4.3803	9.4935	8.9583	8.7756	9.8072	9.2171	9.9460
1423	9.7823	4.1419	10.0116	8.8567	8.9692	9.8643	9.3986	9.9353
823.1	9.2617	4.4875	9.4459	9.0710	8.7938	9.8547	9.2205	10.0161
873	9.2897	4.4239	9.4700	9.0027	8.7806	9.8249	9.2165	9.9731
1023	9.3952	4.2871	9.5744	8.8743	8.7822	9.7815	9.2325	9.8988
750	9.2289	4.6038	9.4233	9.2033	8.8297	9.9173	9.2375	10.1017
1300	9.6502	4.1644	9.8577	8.8278	8.8913	9.8175	9.3339	9.8992
1200	9.5507	4.1949	9.7443	8.8237	8.8398	9.7916	9.2892	9.8839
1250	9.5995	4.1780	9.7996	8.8233	8.8641	9.8030	9.3106	9.8897
905	9.3097	4.3886	9.4885	8.9665	8.7762	9.8104	9.2168	9.9510
1190	9.5412	4.1987	9.7336	8.8244	8.8353	9.7897	9.2852	9.8832
1000	9.3772	4.3038	9.5557	8.8878	8.7786	9.7844	9.2278	9.9058
600	9.2044	4.9764	9.4425	9.6554	8.9943	10.1499	9.3332	10.4030
1200	9.5507	4.1949	9.7443	8.8237	8.8398	9.7916	9.2892	9.8839
1250	9.5995	4.1780	9.7996	8.8233	8.8641	9.8030	9.3106	9.8897
1423	9.7823	4.1419	10.0116	8.8567	8.9692	9.8643	9.3986	9.9353
1400	9.7568	4.1450	9.9817	8.8495	8.9536	9.8545	9.3858	9.9273

Table 8.3 Wilson Equation Binary parameters for lead and seven of its common impurities

Wilson						
Temp (K)	i	j	A_{ij}	A_{ji}	RMSD a_i	RMSD a_j
913	Pb	As	3.9968	0.0199	0.0124	0.0339
923	Pb	Zn	0.0087	0.1908	0.0321	0.0548
905	Pb	Sb	1.1287	1.1287	0.0003	0.0003
700	Pb	Bi	1.4731	1.4485	0.0046	0.0038
1273	Pb	Ag	1.8940	0.0998	0.0227	0.0184
1050	Pb	Sn	1.0691	0.0990	0.0095	0.0116
1473	Pb	Cu	0.2828	0.3397	0.0195	0.0156
1423	As	Zn				
1373	As	Sb	0.3881	2.0806	0.0456	0.0257
913	As	Bi				
1423	As	Ag				
913	As	Sn	1.1640	2.4853	0.1002	0.0768
1423	As	Cu				
823.1	Zn	Sb	1.5723	2.0877	0.0654	0.0359

Table 8.3 Continued

Wilson						
Temp (K)	i	j	A_{ij}	A_{ji}	RMSD a_i	RMSD a_j
873	Zn	Bi	0.9299	0.0327	0.0327	0.1852
1023	Zn	Ag	1.8705	2.8240	0.0232	0.0198
750	Zn	Sn	0.7482	0.3992	0.0274	0.0266
1300	Zn	Cu	2.2573	2.2573	0.0036	0.0036
1200	Sb	Bi	2.4794	0.4744	0.0362	0.0462
1250	Sb	Ag	0.3420	4.7462	0.0483	0.0377
905	Sb	Sn	1.4988	1.4988	0.0005	0.0005
1190	Sb	Cu	0.0991	8.7119	0.0409	0.0455
1000	Bi	Ag	0.2345	1.8545	0.0982	0.0883
600	Bi	Sn	0.4359	1.4913	0.0008	0.0016
1200	Bi	Cu	0.4737	0.4982	0.0113	0.0312
1250	Ag	Sn	0.2954	3.1622	0.0492	0.0490
1423	Ag	Cu	0.4799	0.4899	0.0031	0.0029
1400	Sn	Cu	0.0888	7.9744	0.0301	0.0351

Table 8.4 NRTL Binary parameters for lead and seven of its common impurities

NRTL $\alpha_{ij} = 0.2$; $\alpha_{ji} = \alpha_{ij}$								
Temp (K)	i	j	Tau _{ij}	Tau _{ji}	G _{ij}	G _{ji}	RMSD a _i	RMSD a _j
913	Pb	As	4.0669	-2.3885	0.4434	1.6124	0.0249	0.0163
923	Pb	Zn	0.3872	3.1885	0.9255	0.5285	0.0493	0.0080
905	Pb	Sb	1.7258	-1.4718	0.7081	1.3423	0.0007	0.0006
700	Pb	Bi	-2.3693	3.0442	1.6062	0.5440	0.0068	0.0045
1273	Pb	Ag	1.9863	-0.9771	0.6722	1.2158	0.0060	0.0095
1050	Pb	Sn	2.8341	-0.8281	0.5673	1.1801	0.0086	0.0095
1473	Pb	Cu	0.5464	1.3661	0.8965	0.7609	0.0093	0.0060
1423	As	Zn						
1373	As	Sb	-2.2890	3.9908	1.5806	0.4502	0.0103	0.0142
913	As	Bi						
1423	As	Ag						
913	As	Sn	-2.2189	1.4489	1.5586	0.7484	0.0954	0.0985
1423	As	Cu						
823.1	Zn	Sb	6.9083	-3.2857	0.2512	1.9293	0.0239	0.0251

Table 8.4 Continued

NTRL $\alpha_{ij} = 0.2$; $\alpha_{ji} = \alpha_{ij}$								
Temp (K)	i	j	Tau_{ij}	Tau_{ji}	G_{ij}	G_{ji}	RMSD a_i	RMSD a_j
873	Zn	Bi	3.9939	-0.9966	0.4499	1.2206	0.0180	0.1707
1023	Zn	Ag	-1.9300	0.3619	1.4711	0.9302	0.0258	0.0241
750	Zn	Sn	1.2470	-0.0983	0.7793	1.0199	0.0271	0.0267
1300	Zn	Cu	-0.9073	-0.9073	1.1990	1.1990	0.0007	0.0007
1200	Sb	Bi	-2.7899	4.9412	1.7471	0.3722	0.0160	0.0199
1250	Sb	Ag	6.2394	-3.0586	0.2871	1.8436	0.0565	0.0773
905	Sb	Sn	-0.4257	-0.4257	1.0889	1.0889	0.0003	0.0003
1190	Sb	Cu	-1.6783	-0.0658	1.3989	1.0133	0.0831	0.0998
1000	Bi	Ag	4.4787	-1.9125	0.4083	1.4659	0.0394	0.0389
600	Bi	Sn	-0.8898	1.3794	1.1948	0.7589	0.0006	0.0010
1200	Bi	Cu	0.0099	1.4956	0.9980	0.7415	0.0074	0.0066
1250	Ag	Sn	6.6266	-2.8051	0.2657	1.7525	0.0363	0.0305
1423	Ag	Cu	0.5549	0.7099	0.8950	0.8676	0.0998	0.0019
1400	Sn	Cu	7.7389	-3.4604	0.2127	1.9979	0.0788	0.1068

8.3 Kinetics Vacuum Distillation

Aside from thermodynamic, the study of kinetic of vacuum distillation is important in order to determine the rate limiting steps of the process. Using the kinetic theory of gases, and assuming that vapor molecules follow a Maxwell-Boltzmann velocity distribution, Langmuir determined that the rate of evaporation of a volatile component from a surface was proportional to its pressure and molecular weight. For a vapor-liquid equilibrium (VLE), he determined the maximum rate of evaporation w_i (g/cm²-sec) as shown in equation 8.1.

$$w_i = P_i \sqrt{\frac{M_i}{2\pi RT}} \quad (8.1)$$

Evaporation based on equation 3 is only possible under perfect vacuum at a point where the rate of evaporation is small such that the mean-free path of the vapor is larger than the distance between the evaporation and condensation surfaces. The net evaporation rate is the difference between the rate at which gas molecules leave the surface and that at which they return to the melt surface; this relationship is illustrated in equation 4. Should there be a multicomponent system, the vapor pressure dependence upon activity of the component must be accounted for, leading to equation 8.3.

$$w_i = (P_{i,o} - P_1) \sqrt{\frac{M_i}{2\pi RT}} \quad (8.2)$$

$$w_i = (P_i^0 - P_i') \gamma_i x_i \sqrt{\frac{M_i}{2\pi RT}} \quad (8.3)$$

Where $P_{i,o}$ is the saturation pressure of component i ,

P_1 is the pressure of the vapor at the evaporating surface,

M_i is the molecular weight of component i;

P_i^0 is the equilibrium partial pressure of pure component i;

P_i' is the effective partial pressure of component i in the vapor phase;

R is the universal gas constant;

T is temperature in K;

Based on equation 5, the mole fraction of the impurities in the melt and therefore their weight in the vapor phase can be calculated as a function of distillation time as shown in equation 8.4.

$$\log_{10} \left(\frac{x_i^{t=0}}{x_i^t} \right) = \frac{S}{2.303 V \rho} P_i^0 \gamma_i \sqrt{\frac{M}{2\pi RT}} t \quad (8.4)$$

Where V is the melt volume,

S is the surface area of the melt (cm²),

ρ is the density of the melt at the distillation temperature.

Equation 8.4 is only valid if the evaporation is controlled by the evaporation reaction. In many cases of metallurgical processes, diffusion-controlled reactions are predominant. In that case equation 8.4 can be rewritten as shown in equation 3.51 where K_i is the overall mass transfer coefficient. Equation 3.51 is valid only if the evaporation of solute i is of first order with respect to its concentration; equation 8.5 is the Knudsen-Langmuir equation.

$$\log_{10} \left(\frac{x_i^{t=0}}{x_i^t} \right) = \frac{S}{V} K_i t \quad (8.5)$$

The complete study of kinetics requires experiments to be conducted at different time and temperature ranges. From the effect of time, the reaction order, and the overall coefficient of mass transfer can be determined. Plotting the coefficient of mass transfer as a function of the inverse of temperature will provide information of the apparent activation energy for the removal of impurity *i*. The extensive literature review that was conducted from this thesis produced by McGill University showed the development of kinetic study for an inductively stirred melt. The experiment conducted in the present study were carried out in the absence of mixing. Two publications were located in which was related to kinetic study for laboratory scale, no mixing melts. Zhao and coworkers (Zhao *et al.*, 2017) studied the kinetic of removal of lead from a crude tin sample; they used the MIVM to predict the activity coefficient. They demonstrated that for their experiments, the removal of lead followed a first order of reaction. Korolev and coworkers (Korolev, Krayukhin and Maltsev, 2018) (paper in Russian) inspected the kinetics of removal of antimony and tin from a ternary Pb-Sn-Sb alloy. They determined the apparent activation energy of removal of each component as well as their overall coefficient of mass transfer. Another aspect of the removal of arsenic which was not studied in the present research is the effect of mixing. Mixing is known to enhance the kinetics of removal of impurities because it continuously provides impurities moles to the liquid/vapor interface where they are promptly evaporated provided adequate vacuum conditions. It is in the author's opinion that these sources will provide information and tools to the researcher to investigate the kinetics of vacuum refining.

REFERENCES

- Allaire, A. (1986) *Vacuum Refining of Copper Matte*. McGill University.
- Allaire, A. (1991) *Copper Matte Vacuum Purification*. McGill University.
- Bagshaw, N. E. (1991) 'Grid alloys for maintenance-free deep-cycling batteries', *Journal of Power Sources*, 33(1–4), pp. 3–11. doi: 10.1016/0378-7753(91)85043-V.
- Chai, T. and Draxler, R. R. (2014) 'Root mean square error (RMSE) or mean absolute error (MAE)? -Arguments against avoiding RMSE in the literature', *Geoscientific Model Development*, 7(3), pp. 1247–1250. doi: 10.5194/gmd-7-1247-2014.
- Danovitch, D. (1982) *Vacuum Refining of Copper Melts*. McGill University.
- Dimayuga, F. C. (1986) *Vacuum Refining of Molten Aluminum*. McGill University.
- Frost, P. C. (1999) 'Developments in lead – acid batteries : a lead producer ' s perspective', *Journal of Power Sources*, 78(1–2), pp. 256–266.
- Gokcen, N. A. (1990) 'The As-Pb (Arsenic-Lead) System', *Bulletin of Alloy Phase Diagrams*, 11(2), pp. 120–124.
- Grant, R. M. (2003) 'Lead Production', in Buschow, K. H. J. et al. (eds) *Encyclopedia of Materials: Science and Technology*. 2nd edn. Elsevier Ltd, pp. 4439–4442.
- Guberman, D. E. (2017) *2015 Minerals Yearbook- Lead*.
- Harris, R. and Davenport, W. G. (1982) 'Vacuum Distillation of Liquid Metals : Part I . Theory and Experimental Study', *Metallurgical Transactions B*, 13(December), pp. 581–588.
- Harris, R. and Davenport, W. G. (1984) 'Vacuum Purification of Liquid Metals'. US.
- Harris, R. L. (1980) *Vacuum Refining of Molten Steel*. McGill University. doi: 10.1017/CBO9781107415324.004.
- Hayes, P. C. et al. (2010) 'Lead Smelter Survey', in *Lead-Zinc 2010 Symposium, Held in Conjunction with COM 2010*. Vancouver, BC: Wiley, pp. 345–414.
- Jiang, W. et al. (2016) 'Experimental investigation and modelling of phase equilibria for the Ag-Cu-Pb system in vacuum distillation', *Fluid Phase Equilibria*, 417, pp. 19–24. doi: 10.1016/j.fluid.2016.02.026.

- JJ (2016) ‘MAE and RMSE — Which Metric is Better ? Mean Absolute Error versus Root Mean Squared Error’, *Medium- Human in a Machine World*, March, p. 5. Available at: <https://medium.com/human-in-a-machine-world/mae-and-rmse-which-metric-is-better-e60ac3bde13d>.
- Kelly, T. D. and Matos, G. R. (2005) *Historical statistics for mineral and material commodities in the United States: Lead End-Use Statistics*.
- Korolev, A., Krayukhin, S. and Maltsev, G. (2018) ‘Kinetics of Evaporation of Metals From Sb-Pb-Sn Alloy in Vacuum Distillation’, *PNIPU Bulletin. The mechanical engineering, materials science.*, (4), pp. 61–74. doi: 10.15593/2224-9877/2017.4.04.
- Ozberk, E. (1980) *Vacuum Refining of Copper*. McGill University.
- Renon, H. and Pruasnitz, J. M. (1968) ‘Local compositions in thermodynamics excess functions for liquids mixtures’, *AIChE J.*, 14(1), pp. 116–128.
- Rice, D. M. and Manders, J. E. (1997) ‘A Review of soft-lead Specifications in the light of the requirements of valve-regulated lead/acid batteries’, *Journal of Power Sources*, 67(1–2), pp. 251–255.
- SGTE (2006) ‘As – Sb (Arsenic – Antimony)’, in *Landolt-Börnstein - Group IV Physical Chemistry-Volume 12A 2006*. Springer, pp. 254–258.
- Sibley, S. F. (2004) *Flow Studies for Recycling Metal Commodities in the United States.pdf*.
- Sinclair, R. J. (2010) *The extractive metallurgy of lead*. 1st edn, *Mineral Processing and Extractive Metallurgy*. 1st edn. Carlton Victoria, Australia: The Australian Institute of Mining and Metallurgy. doi: 10.1179/037195510x12804985731362.
- Tao, D. P. (2000) ‘A new model of thermodynamics of liquid mixtures and its application to liquid alloys’, *Thermochimica Acta*, 363(1–2), pp. 105–113. doi: 10.1016/S0040-6031(00)00603-1.
- Tao, D. P. (2002) ‘Prediction of the thermodynamic properties of solutes in Pb-based dilute solutions’, *Metallurgical and Materials Transactions B*, 33(3), pp. 502–506. doi: 10.1007/s11663-002-0061-y.
- Tao, D. P. (2005) ‘Prediction of the coordination numbers of liquid metals’, *Metallurgical and Materials Transactions A*, 36(12), pp. 3495–3497. doi: 10.1007/s11661-005-0023-5.
- Thornton, I., Rautiu, R. and Brush, S. M. (2001) *Lead: the Facts*. Hersham, Surrey, UK: Ian Allan printing.
- US-DOE (2002) *Mining Industry of the Future: Energy and Environmental Profile of the U. S. Mining Industry*.

- USGS (2019) '2019 Mineral Commodity Summaries -Lead'. United States Geological Survey, pp. 94–95.
- Westerheide, D. E. (1963) *Separation of cadmium from the lead-bismuth eutectic by high vacuum single stage distillation*. Iowa State University of Science and Technology.
- Wilson, G. M. (1958) *Vapor-liquid equilibria from measurements of pressure temperature and overall composition: The system water- 2Butoxy ethanol*. Massachusetts Institute of Technology.
- Wilson, G. M. (1964) 'Vapor-Liquid Equilibrium. XI. A New Expression for the Excess Free Energy of Mixing', *Journal of the American Chemical Society*, 86(2), pp. 127–130. doi: 10.1021/ja01056a002.
- Xu, J. *et al.* (2016) '(Vapor + Liquid) Equilibrium (VLE) for Binary Lead-Antimony System in Vacuum Distillation: New Data and Modeling Using Nonrandom Two-Liquid (NRTL) Model', *Metallurgical and Materials Transactions A*, 47(9), pp. 4494–4501. doi: 10.1007/s11661-016-3636-y.
- Yang, X. *et al.* (2016) 'Prediction of vapor-liquid equilibria for the Pb-X (X=Ag, Cu and Sn) systems in vacuum distillation using ab initio methods and Wilson equation', *Fluid Phase Equilibria*. Elsevier Ltd, 417, pp. 25–28. doi: 10.1016/j.fluid.2016.02.024.
- Zhang, C. *et al.* (2015) 'Experimental investigation and calculation of vapor-liquid equilibria for Cu-Pb binary alloy in vacuum distillation', *Fluid Phase Equilibria*. Elsevier B.V., 405, pp. 68–72. doi: 10.1016/j.fluid.2015.07.043.
- Zhao, J. *et al.* (2017) 'Kinetics of Pb Evaporation from Pb-Sn Liquid Alloy in Vacuum Distillation', *Vacuum*, 141, pp. 10–14.

APPENDIX A

SAMPLE BOAT VOLUME CALCULATIONS

The density of lead is 11.3 g/cm^3 ; therefore 100, 200, 300, 400, and 500 grams samples would be 8.85, 17.70, 26.55, 35.40, and 44.25 mL respectively. From table B-1, adopting $\frac{1}{4}$ inch wall thickness would result in an available 30.382 mL in the sample boat. At the same time $\frac{1}{4}$ inch thickness would allow to ease of machining. Working with 200 grams samples would allow for the melt to be well contained on the boat while avoiding splashing during experimentation; therefore, the boat was designed at $\frac{1}{4}$ inch thickness.

Table A.1 Calculations for the vacuum distillation sample boat

1 / 4-inch wall thickness	
$a := 0.412 \text{ in}^2$	$a = (2.658 \cdot 10^{-4}) \text{ m}^2$
$L := 4.5 \text{ in}$	$L := 0.114 \text{ m}$
$V := a \cdot L = 30.382 \text{ mL}$	
1 / 8-inch wall thickness	
$a := 0.6605 \text{ in}^2$	$a = (4.261 \cdot 10^{-4}) \text{ m}^2$
$L := 4.75 \text{ in}$	$L := 0.121 \text{ m}$
$V := a \cdot L = 51.412 \text{ mL}$	
1 / 16-inch wall thickness	
$a := 0.412 \text{ in}^2$	$a = (5.191 \cdot 10^{-4}) \text{ m}^2$
$L := 5.0 \text{ in}$	$L := 0.127 \text{ m}$
$V := a \cdot L = 64.275 \text{ mL}$	

APPENDIX B

SUPPLEMENTAL INFORMATION ON THE RESULTS FOR THE PB-AS

AND PB-SB BINARY SYSTEMS

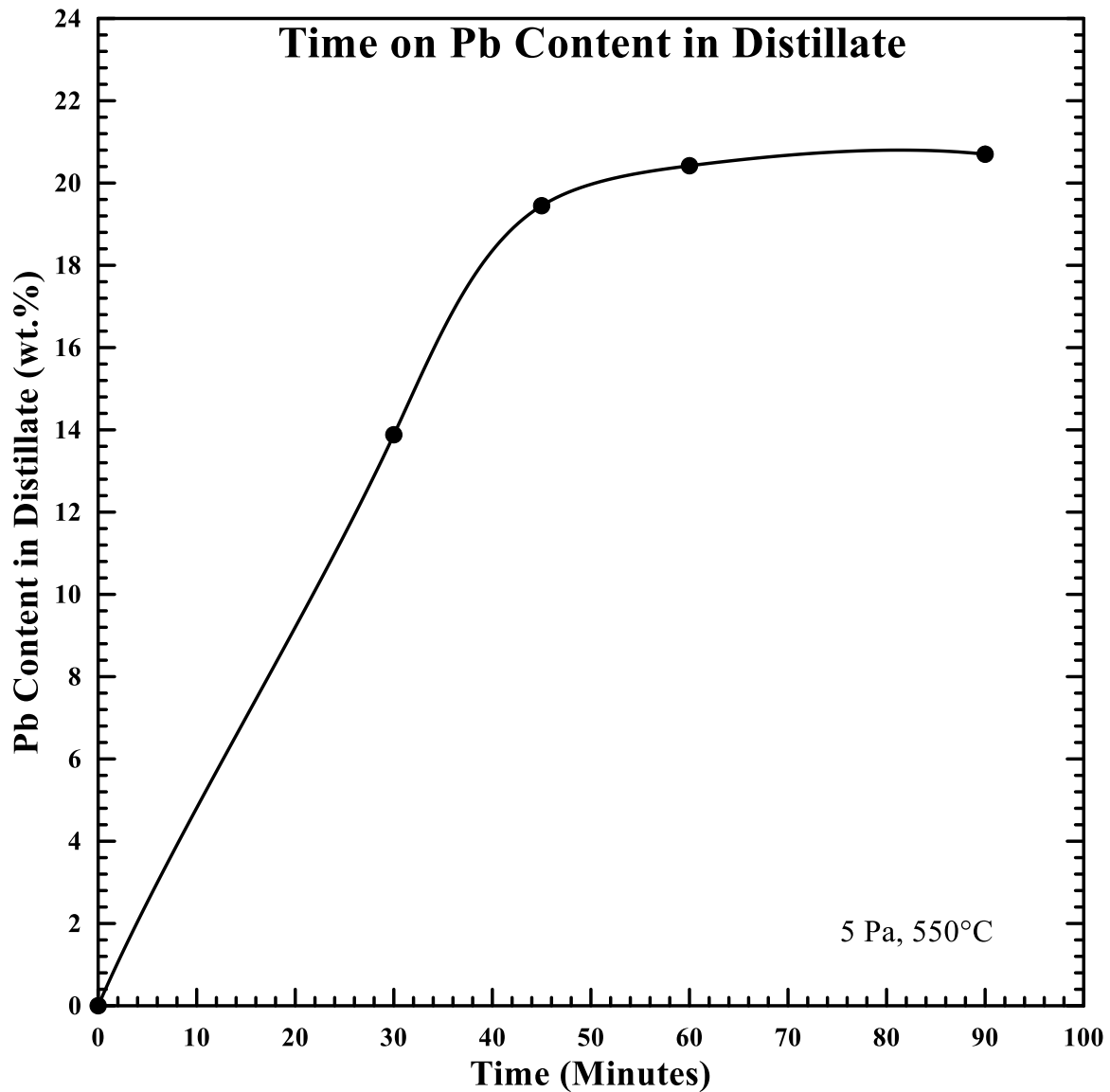


Figure B.1 Effect of distillation time on lead content in the distillate fraction, experiments conducted at 5 Pa and 550 °C

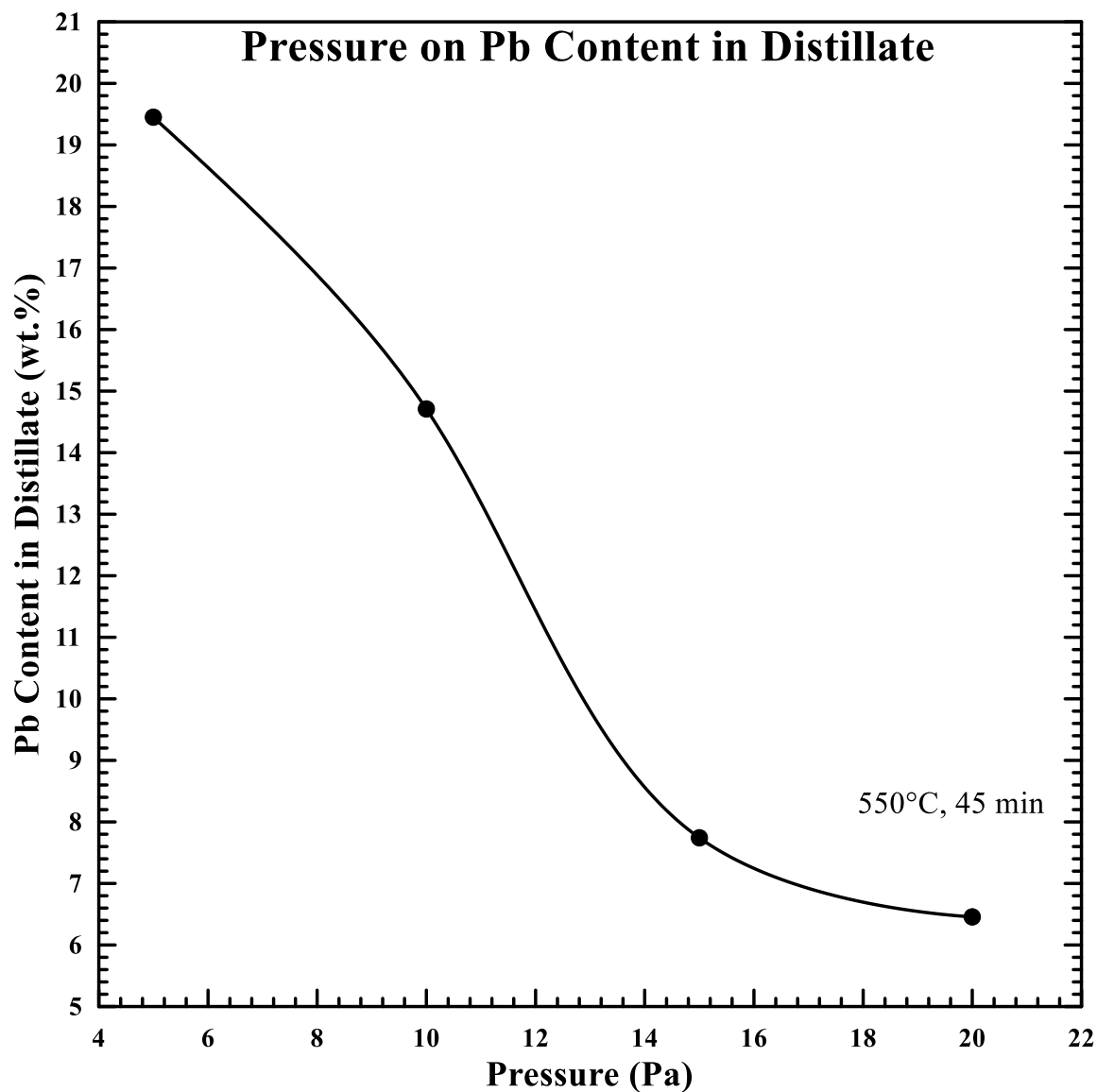


Figure B.2 Effect of distillation pressure on lead content in the distillate fraction experiments conducted at 550°C and for 45 minutes

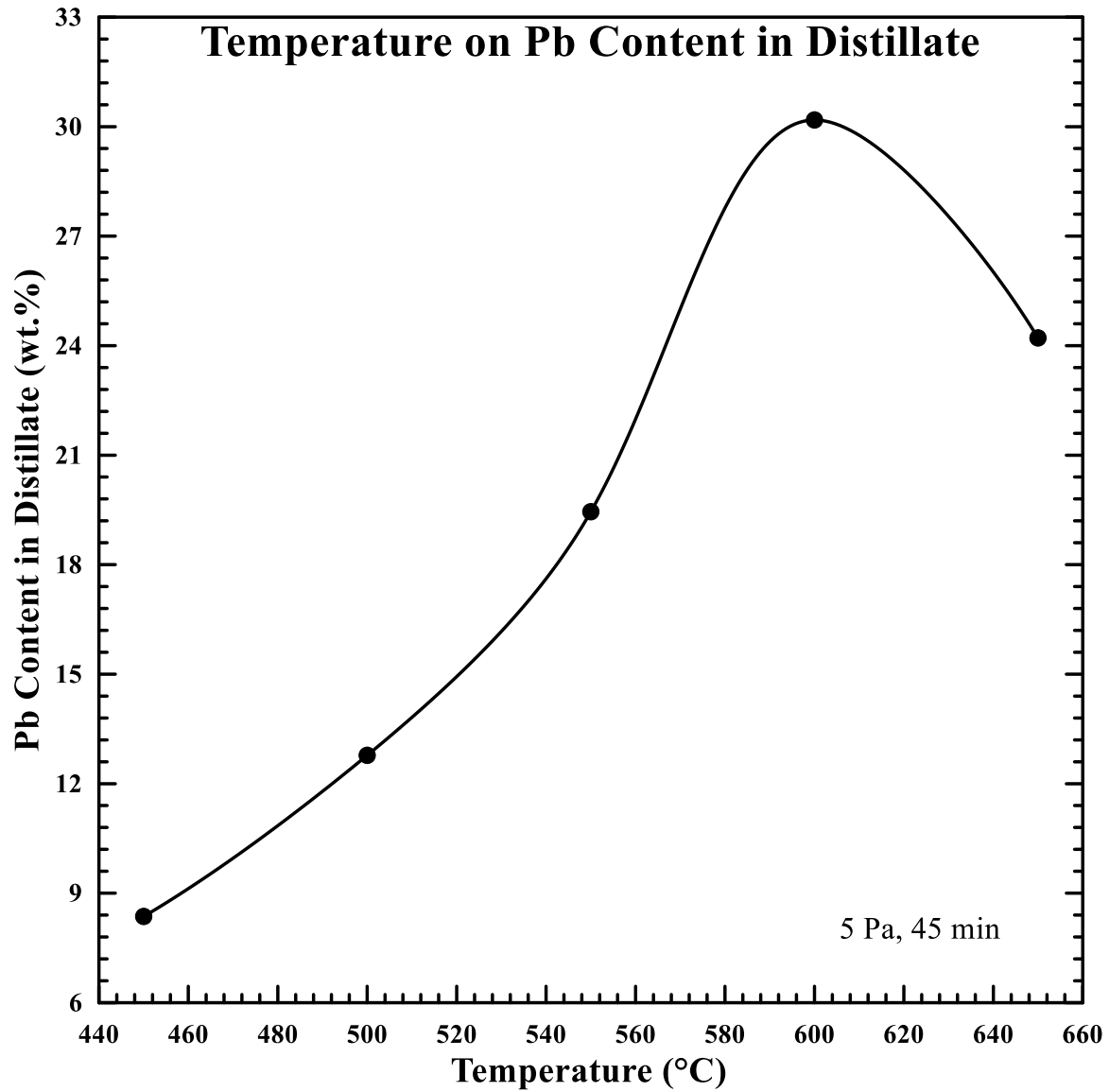


Figure B.3 Effect of distillate temperature on lead content in the distillate fraction; experiments conducted at 5 Pa and for 45 minutes

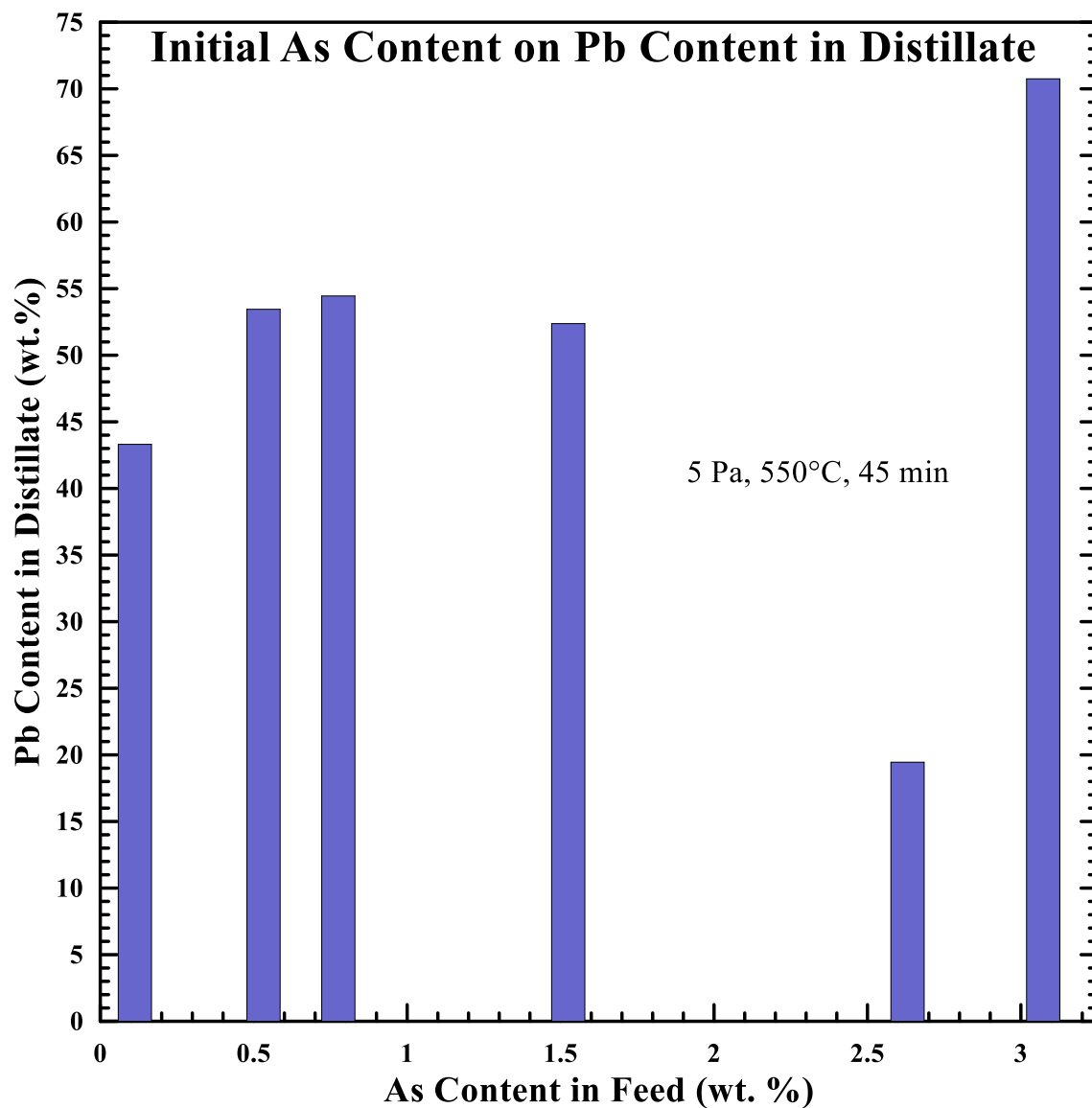


Figure B.4 Effect of initial arsenic content in the feed samples on the lead content in the distillate fraction, experiments conducted at 5 Pa, 550°C, and 45 minutes

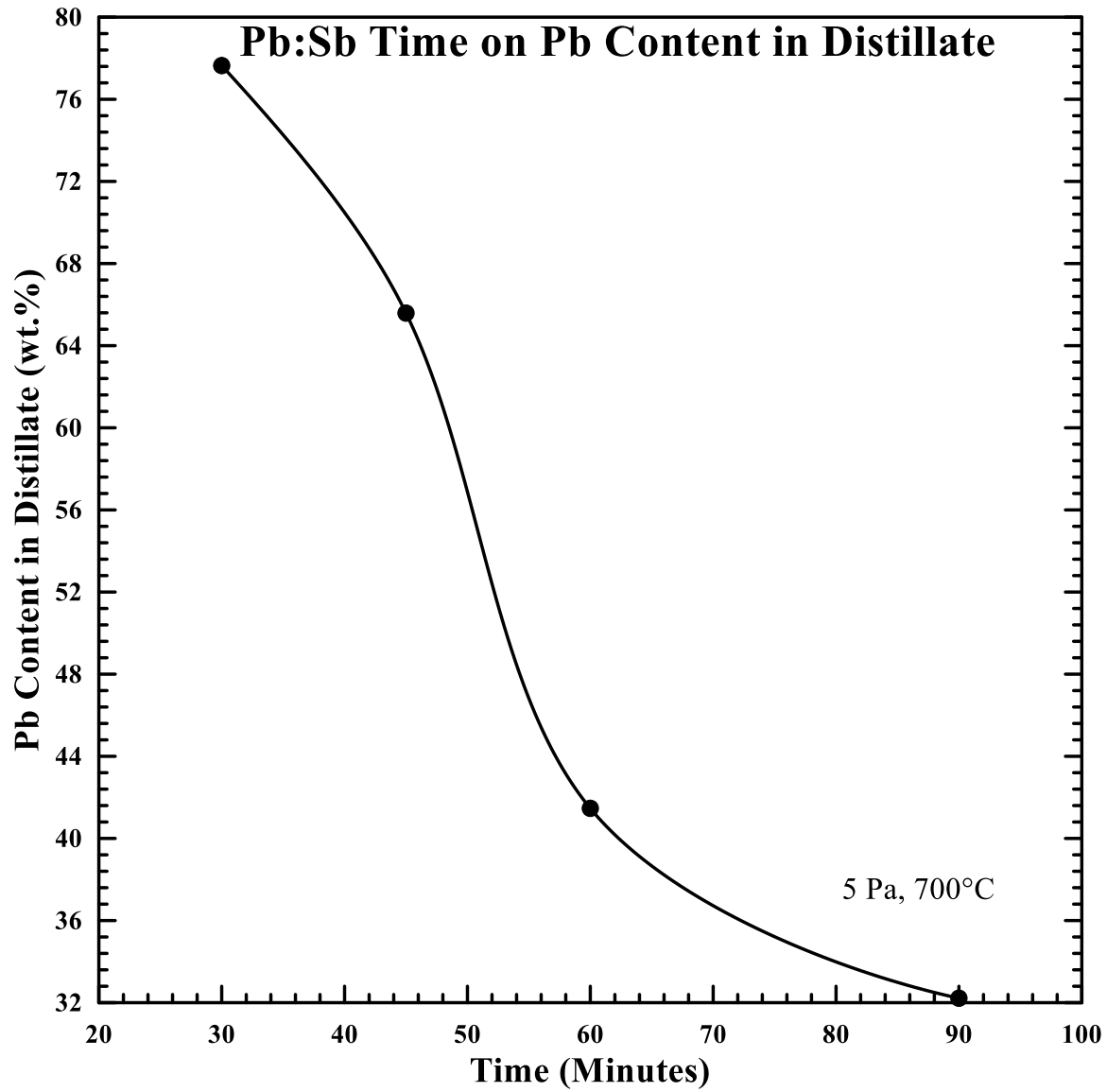


Figure B.5 Effect of distillation time on lead content in the distillation fraction, experiments conducted at 5 Pa and 700 °C

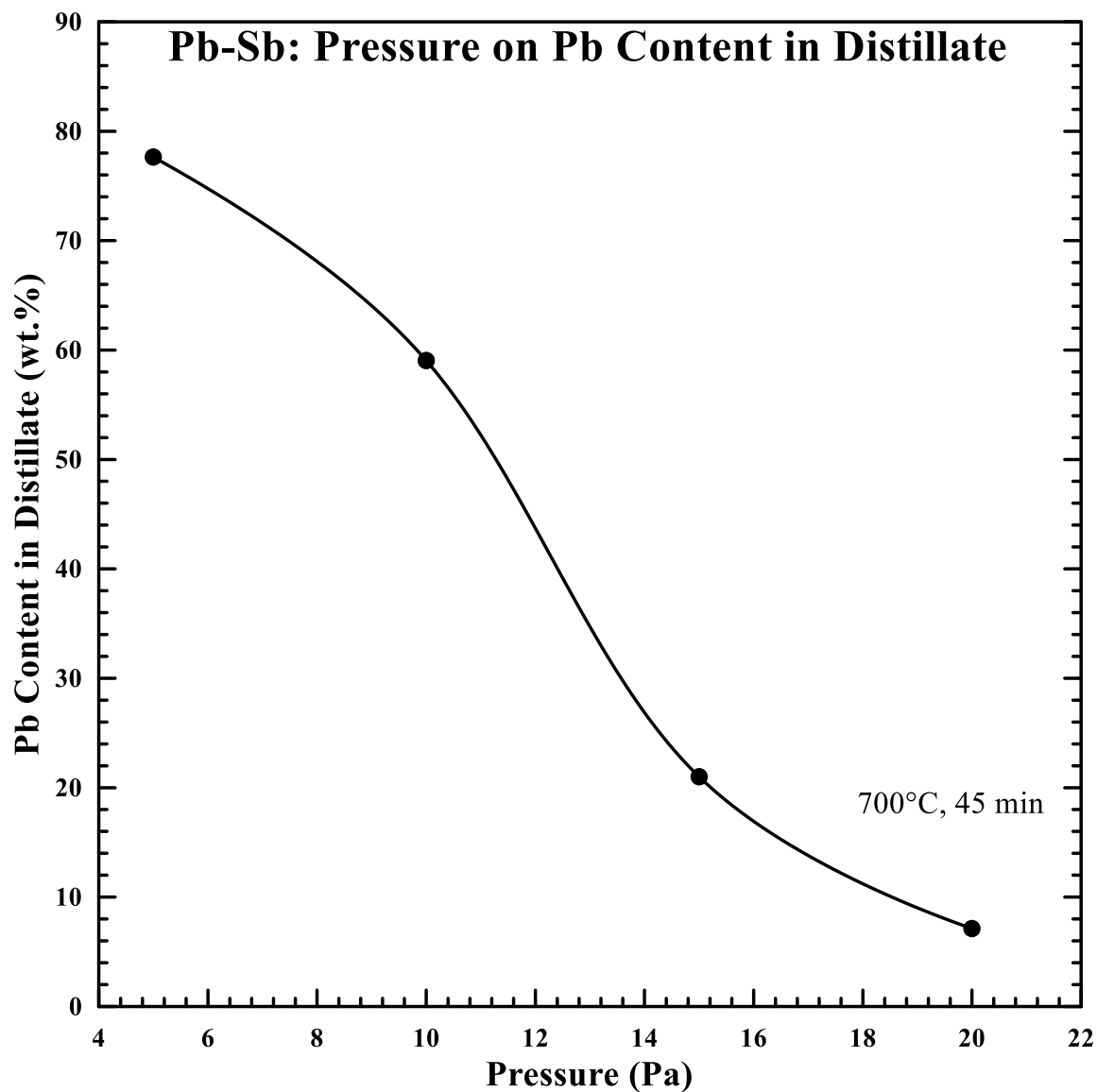


Figure B.6 Effect of distillation pressure on lead content in the distillate fraction, experiments conducted at 700°C for 30 minutes

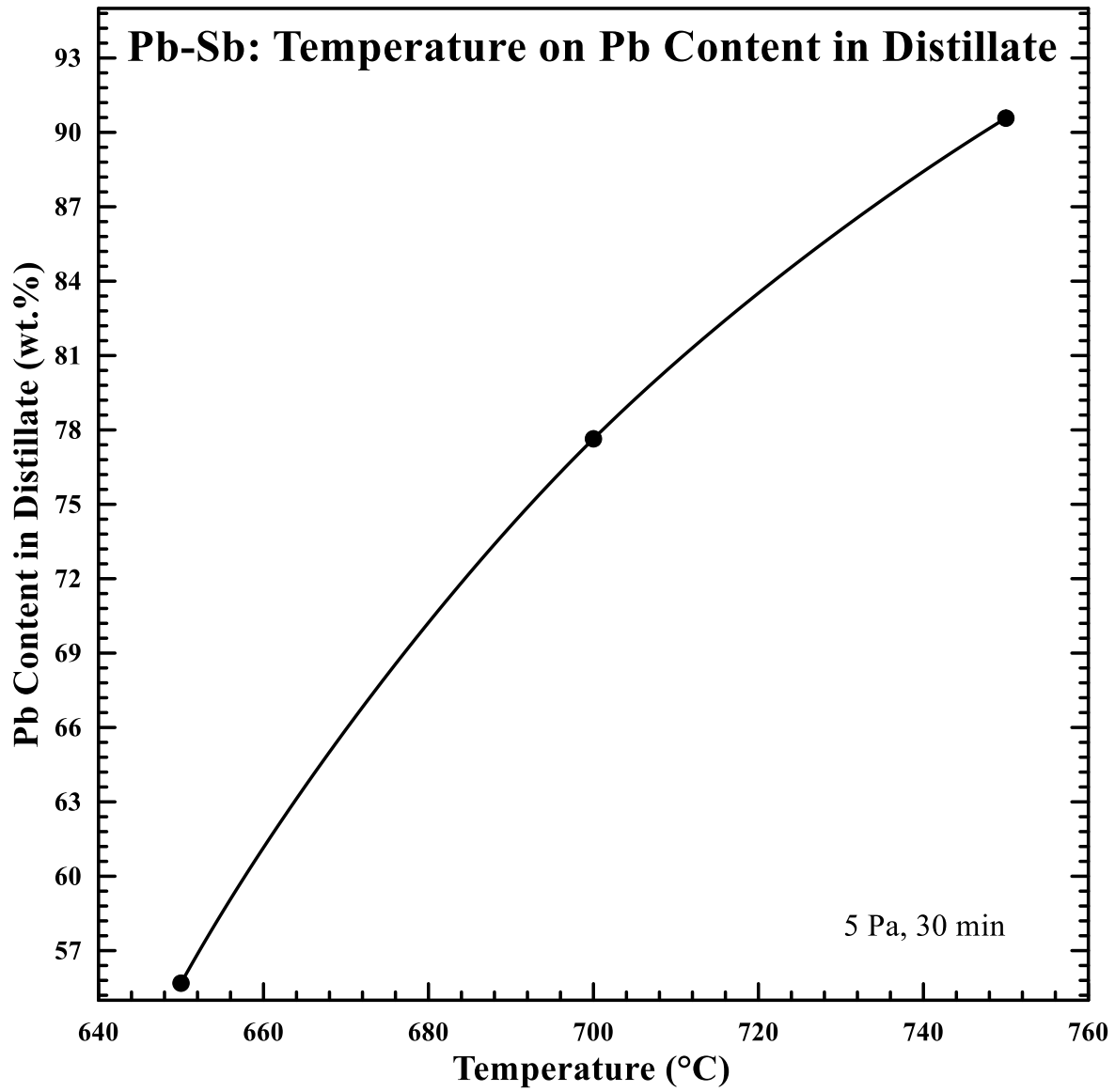


Figure B.7 Effect of distillation temperature on lead content in the distillate fraction, experiments conducted at 5 Pa for 30 minutes

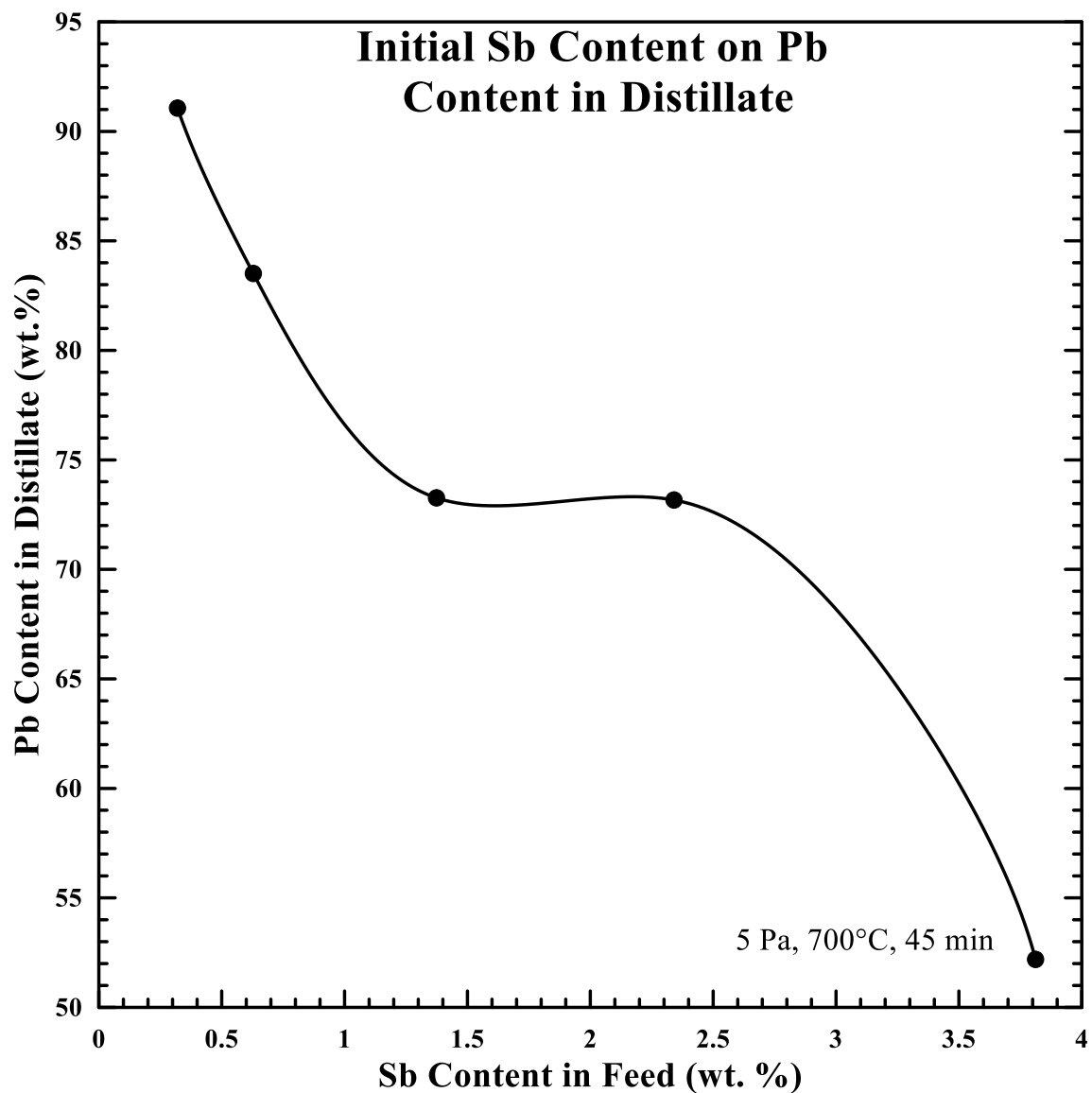


Figure B.8 Effect of initial antimony concentration in the feed sample on lead content in the distillate fraction, experiments conducted at 5 Pa, 700°C, and for 45 minutes